Humanoid robots balance in multi-contact modes settings

Saeid Samadi

THÈSE POUR OBTENIR LE GRADE DE DOCTEUR DE L'UNIVERSITE DE MONTPELLIER

En Systèmes Automatiques et Microélectroniques

École doctorale : Information, Structures, Systèmes

Unité de recherche UMR5506

Humanoid robots balance in multi-contact modes settings

Présentée par Saeid Samadi

Le 22/12/2021

Sous la direction de Abderrahmane Kheddar

Devant le jury composé de

Leonardo Lanari, Professor, Sapienza Università di Roma, Italy	Rapporteur
Wael Suleiman, Professeur, Université de Sherbrooke, Quebec, Canada	Rapporteur
Adrien Escande, Senior Researcher, HdR, AIST, Japan	Examinateur (Président du jury)
Tamim Asfour, Professeur, Karlsruhe Institute of Technology, Germany	Examinateur
Sethu Vijayakumar, Professeur, University of Edinburgh, United Kingdom	Invité
Abderrahmane Kheddar, Directeur de Recherche, CNRS	Directeur de thèse

UNIVERSITÉ DE MONTPELLIER

ACKNOWLEDGEMENTS

Availing from a bright life leader is a magnificent blessing in every individual's life. They show the progress and success road map and bring peace of mind and confidence to step towards the right path. I am sincerely fortunate that I passed in a direction under the supervision of an expert coach named professor Abderrahmane Kheddar, who promoted my challenging journey of academic life with his professional leadership; the valuable strategies, which are enjoyably hard and training your research muscles, and as he always states: "You can not expect incompact and pliant pieces of training from an Olympics athlete coach." He is right! Because finally, the joy of success is for the athlete!

Also, my intellectual dept is to Dr. Stéphane Caron who was my co-supervisor during the first year of my Ph.D. journey. I have had the support and encouragement for carrying out the novel methodologies of the research topic. Without his introductory guidance, my papers would not have materialized.

I am particularly grateful for the assistance given by Dr. Pierre Gergondet and Dr. Arnaud Tanguy regarding the robotic frameworks and technical issues. They made enormous contributions to accomplish the scenarios and practical experiments on the humanoid robot. Moreover, I have greatly benefited from the assistance given by Julien Roux during the experiments and evaluation of the proposed approaches. I would like to express my gratitude to my colleagues in the IDH team, who literally became my true friends and family in Montpellier. Their advice and comments, together with fruitful discussions throughout my research, were an enormous help to me.

Finally, a special thanks to my family and friends for their exceptional supports. Words can not express how grateful I am to my mother, father, and my lovely sister, Helia, for all of the sacrifices that you've made on my behalf. Your prayer for me was what sustained me thus far.

Abstract

In this thesis, we investigate real-time whole-body control of humanoid robots under multi-contact-modes settings. That is to say, under different contact conditions such as a mix of desired fixed contacts and desired (i.e., controlled) sliding ones. Several methods are proposed to maintain the robot's balance and keep the center-of-mass (CoM) within an admissible set. Some of these methods require expensive computations of geometric balance regions. Consequently, the online realization of the balance criteria in multi-contact has been a long-standing challenge. In this thesis, we tackle this challenge in three main steps. First, we present a fast-computing method for the 2D CoM support region in a configuration of multiple fixed and intentionally sliding contacts. To select the most appropriate CoM position within this region, we account for (i) constraints of multiple fixed and sliding contacts, (ii) desired wrench distribution for contacts, and (iii) desired CoM position (eventually dictated by other tasks). These are formulated as quadratic programming (QP) optimization problems. This stage contains computational limitations and can not cover all feasible robot configurations during the scenarios.

Next, we propose a whole-body control strategy for humanoid robots in multi-contact settings that enables switching between fixed and sliding contacts under active balance at will. This approach computes a safe center-of-mass position and wrench distribution of the contact points based on the Chebyshev center in real-time and without any computational limitations. Moreover, this region-free approach does not need the geometric computation of balance regions and *a priori* computation of them. We assess our policy with experiments highlighting switches between fixed and sliding contact modes in multi-contact configurations. A humanoid robot exhibits such contact interchanges from fully-fixed to multi-sliding and also shuffling of the foot. The scenarios represent the execution of our control scheme in realizing the desired forces, CoM position attractor, and planned trajectories while actively maintaining balance.

Finally, we introduce a unified framework for the whole-body dynamic balance controller of humanoid robots in multi-contact as an alternative to controlling the balance in a separate thread (planning). This framework considers the active motion tasks of the robot in real-time within the balance criteria of the robot. We illustrate the applicability of each step by simulations and empirical experiments on the HRP-4 humanoid robot.

Keywords

Humanoid robots, Multi-contact, Dynamic balance, Whole-body control, Contact modes, Chebyshev center.

RÉSUMÉ DE LA THÈSE

Dans cette thèse, nous abordons la commande corps complet de robots humanoïdes dans des configurations de contact multiples multi-modaux. C'est-à-dire, sous différentes conditions de contact telles qu'un mélange de contacts fixes et de contacts glissants désirés (i.e., contrôlés). Plusieurs méthodes sont proposées pour caractériser l'équilibre de robots humanoïdes, comme par exemple, le maintien du centre de masse (CoM) dans un ensemble admissible. Certaines de ces méthodes nécessitent des calculs coûteux des régions d'équilibre géométriques. Par conséquent, l'integration en ligne (c'est-à-dire dans les boucles de commandes) des critères d'équilibre en multi-contact est un défi majeur en robotique humanoïde. Dans cette thèse, nous abordons ce défi en trois étapes principales. Tout d'abord, nous présentons une méthode de calcul rapide pour la région de support en 2D du CoM dans une configuration de contacts multiples fixes et (intentionnellement) glissants. Pour sélectionner la position la plus appropriée du CoM dans cette région, nous tenons compte (i) des contraintes des multiples contacts fixes et glissants, (ii) de la distribution souhaitée du torseur des efforts sur les contacts existants, et (iii) de la position souhaitée du CoM (éventuellement influencée par d'autres tâches). Ces contraintes sont formulées comme des problèmes de programmation quadratique (QP) en optimisation. Cette étape comporte des limitations et notamment, elle ne peut pas couvrir tout les scénarios des configurations multi-contacts possibles du robot humanoïde.

Ensuite, nous étendons l'étude précédente aux configurations multi-contacts dans l'espace 3D en offrant au contrôle corps complet la possibilité d'interchanger en ligne, et à souhaits, des contacts fixes et des contacts glissants. Cette nouvelle approche calcule une position sûre du centre de masse et une distribution du torseur des efforts sur les contacts existants basée sur le centre de Chebyshev. Les calculs se font maintenant en temps-réel et permettent de faire interagir le calcul des régions d'équilibre avec la commande dans l'espace des tâches. De plus, cette approche ne nécessite pas le calcul géométrique explicite des régions d'équilibre. Nous évaluons notre approche à l'aide d'expériences mettant en évidence des commutations entre les modes de contacts fixes et glissants et dans des configurations à contacts multiples non coplanaires. Les scénarios représentent l'exécution de notre schéma de contrôle en réalisant les forces désirées, avec un attracteur de la position du CoM et les trajectoires planifiées tout en maintenant l'équilibre activement.

Enfin, nous introduisons un cadre unifié pour le contrôle de l'équilibre dynamique du corps entier des robots humanoïdes en multi-contact comme une alternative au contrôle de l'équilibre dans un schéma à deux phases. Ce cadre prend en compte les tâches de mouvement actif du robot en temps réel dans le cadre des critères d'équilibre du robot. Nous illustrons l'applicabilité de chaque étape par des simulations et des expériences empiriques sur le robot humanoïde HRP-4.

CONTENTS

INTRODUCTION

The present modern-day is racing towards automation and advancement in technology to achieve *5-P* goals which are productivity, proficiency, preciseness, progress, and most importantly, perseverance! The *5-P* keywords can efficiently express the reason why humans need to rely on robots and accept them in the real-life. Robotic science accelerates the progression and succession in the race of technology. Furthermore, by leaning toward an advanced world, there is a substantial need to minimize humans' presence in difficult and hazardous circumstances. Assisting the human and alleviating the risks of workplaces are foremost goals of robotics. However, there are still issues to address and enhance, which are the main focus of up-to-date researches as the current study.

Currently, according to some specified roles and applications of robots, many robotic manipulators operate in the industries. Nevertheless, it is not surprising that humanoid robots are the fittest variants for enriching all human-like appearances and capabilities in its territory. However, there exist still major challenges in humanoid robotics, preventing the extensive application of these robots in the real world, which are

- high cost of purchasing, maintenance, and repairment,
- limitations of actuator torques,
- limitations of the energy sources of the robots such as batteries preventing from long-time usage,
- lack of effective controllers for maintaining the robot's balance in every type of workspace during the operation.

The former challenges are related to the design and economic aspects of the robot, which are expected to be improved in the following years. But, the last challenge is the main topic and prevailing direction of the current study.

Some humanoid robots with wheeled structures perform practical scenarios on a limited scale for protected industrial, medical, and social environments. Therefore, they do not have the balance challenge as mentioned above. Yet, there exist some restrictions which prevent them from the vast majority of motions. The most serious limitation of wheeled humanoid robots is the inability to cross the environment's regular terrains (essentially stairs, slopes, narrow spaces,...) to access specified localities, highlighting the necessity of employing legged robots.

Humanoid robots are designed to reproduce all sorts of motion skills and physical activities that a human does during his daily life such as running, flipping, jumping, crawling, etc. In theory, state-of-the-art humanoid robot technology could provide hardware capability to achieve –to some extended and relative performances, some of these complex behaviors. Yet, they lack efficient control strategies with robust equilibrium conditions.

Several solutions for the balance challenge of humanoid robots during the locomotion phase have been introduced in the literature. But, naturally, for a robot's maneuver in the environment, we need to investigate the states in which the robot has more contacts than feet with its surrounding, namely multi-contact configuration. These additional contacts enable the robot to benefit from the surrounding objects to balance and even cross the terrains. Additionally, it reduces the probability of losing balance while performing the tasks. Consequently, the robot will be able to perform various scenarios such as multi-contact locomotion, loco-manipulation, grasping, etc.

The balance of the humanoid robot in multi-contact conditions is still a topic of interest and known as one of the open-ended challenges of this trend. Because, unlike the existing methods for the balance of the robot while stance locomotion, evaluating the balance criteria in the multi-contact condition is time-consuming due to the complex computational process. Therefore, most of the proposed methods for multi-contact balancing contain an offline pre-computational phase according to the pre-planned scenarios. The online implementation of the multi-contact balance controller on the robot is a primary challenge that we will discuss explicitly throughout this thesis.

We can classify the humanoid activities as fully-static, quasi-static, semi-dynamic, and fully-dynamic motions from the control perspective. Each category can retain a particular sort of configuration and scenario. A fully-static multi-contact system holds zero CoM acceleration and, respectively, no contact movement. On the other hand, the quasi-static motions contain small quantities of CoM acceleration so that the whole body can move by keeping fixed contact with the environment. The other designs for humanoid control in multi-contact configurations are fully-dynamic patterns. There is a need for planning the CoM motions in these cases as the CoM acceleration is non-zero. Moreover, this category covers the switching between contact modes.

There is a bridge between the quasi-static and fully-dynamic motions, which is counted as semi-dynamic motions. In this category, we can control the movement and switching of contact modes. The controller can be designed to explore different contact modes such as sliding, soft, rolling, etc. However, the motion of the CoM does not need any planning as we consider small quantities for CoM acceleration. Throughout this thesis, we are going to explore semi-dynamic scenarios.

In addition to the balance concern of the multi-contact, the balancing controller should be able to perform and cover the tasks involving different contact modes, such as fixed, sliding, rolling, etc., to master the human-like behaviors on the robot. Besides, the exploration of contact modes increases the complexity of the evaluation of the multi-contact balance criterion. In this thesis, we will investigate and explore different contact modes of the robot and environment, on top of them, the sliding contact mode. The proposed methods in this study enable the online implementation of the

balance controller with a low computational cost which was the challenge for decades. These methods also cover the presence of multiple contact modes, i.e. the multi-modal condition.

The first chapter presents background on balance criteria in humanoid robots and recent studies on multi-contact motion generation methods. The balance criteria in multi-contact settings are essential due to the necessity of exploring challenging scenarios such as accessing narrow spaces, reaching objects and spots, loco-manipulation, ladder climbing, etc. In order to employ different contact modes throughout the plans, we investigate the relevant contact and force models. Finally, for realizing the models and balancing methods on the robot, the whole-body control schemes together with the preliminaries of its implementation are introduced.

In the second chapter, we tackle the online implementation of the balance control strategies in multi-contact conditions in the presence of sliding contacts. We construct the balance region in 2D using an analytical solution. The developed area is computationally cheap due to the simplifying assumptions in the analytical calculations. However, it enables the evaluation of the balance criteria in real-time with proper force tracking. The proposed QP formulation generates the position of the CoM and the wrench distribution for the planned scenario. Experiments show that the advanced methodology guarantees equilibrium criteria for fixed contacts and keeps the robot's balance in the presence of intentionally sliding contacts.

In the third chapter, we tackle the computational limitations addressed by the analytical solution and aim to execute the multi-contact scenarios without any restrictions mentioned above. In this chapter, the multi-sliding and fixed contacts are considered. The framework is formulated based on Chebyshev's optimization method, which guarantees the balance online but is conservative. We implemented an online friction estimation to adjust the accurate coefficient of friction during sliding. The output reference CoM position and contact wrench distribution are achieved using task-space whole-body admittance control. In the experiments, we also assess our approach through complex scenarios involving switching between contact modes under active dynamic balance and force control.

The fourth chapter takes one step further towards the balance control of humanoids. By considering the robot's balance within the planner, we are keeping the full range of the motion features, essentially real-time motion tasks and configurations beyond the scene. In simple terms, the planner is not aware of this motion until the robot contacts the environment. Therefore, we aim to blend a balancing strategy within the controller rather than the planner. So, the whole-body controller of the robot also accounts for the balance of the robot. The capability of the proposed unified framework is evaluated through pushing and wiping scenarios on simulated HRP-4 robot.

CHAPTER 1

BACKGROUND AND PRELIMINARIES

In this chapter, I will present the primary notions which are commonplace in humanoid robotics. These notions include the control aspects, contact modes, configuration, scenarios, applications, and features associated with the robot's appearance. Each of these concepts plays a meaningful role in controlling the motion and performing successful scenarios.

Controlling humanoid robots has numerous hurdles, and each one of these challenges carries separate themes and topics of interest. For instance, the robot's balance can be studied in standing or multi-contact configurations. These configurations result in varying balance control strategies, which can be linked to the ZMP concept for the standing condition or CoM-related methods in multi-contact. Besides, the robot's motion should be considered dynamic or static according to the applications and capabilities of the real-time implementations.

The robot is in contact with its environment. In order to accomplish the motions and desired scenarios with the robot, the contact modes should be adequately investigated. For different contact modes such as fixed, sliding, rolling, etc., numerous models are presented in the literature that we will be discussed in this section.

Humanoid robots utilize their degrees of freedom to accomplish various scenarios. Executing such actions needs meticulous planning of the contact placements and the corresponding consistent motion of the whole-body. To realize the robot's motion according to the designed scenarios, we need to implement a whole-body control strategy in standing or multi-contact conditions. For this purpose, we will introduce the relevant control strategies for the position or torque-controlled robots in the following.

Applying the methods and strategies mentioned above and executing them on the humanoid robot (wheeled or biped robots) can cover a wide range of scenarios and human-like activities. So far, humanoid robots demonstrate several applications and generate motions. Still, there are several unsolved challenges that can influence human life. The main objective of humanoid robotics is to accomplish all activities which human does in his routine life. The current and future applications of humanoid robots will also be discussed in this section. Finally, this section will introduce the tools we used to implement the controllers, such as the control framework, computational method of the planner, and solvers, following the presented chapter's conclusion.

1.1 Multi-contact motions in humanoids

The main characteristic of humanoid robots is their ability to reproduce human-like motions and replacing them with humans in haphazard and unexpected conditions, as highlighted in DARPA Robotics Challenge (DRC) [1]. There exist many leading lines of research on the locomotion of humanoids as well as their manipulation capabilities. However, the combination of locomotion and manipulation techniques for generation of humans routine activities is inevitable. The robot should be capable of executing these tasks in disaster scenarios and interacting with humans. Successful completion of such physically demanding tasks requires exploring multi-contact applications where all possible end-effectors may contact various surfaces through specific contact modes.

As signified in the previous paragraph, the term "multi-contact" in robotics refers to the robot's status with more than one limb interacting with its environment. For a humanoid robot, the feet and hands of the robot are often considered as interacting contacts as shown in Fig. 1.1(a). So, in general, the contact is defined by the interaction of these parts with the environment, but in complex cases, one can choose other contacting points, such as knees, elbows, etc. However, considering a single contact point or a set of points for the contacts has been a topic of interest in robotics and will be discussed further on.

The multi-contact applications in humanoid robots are primarily associated with locomotion, and it has been studied since Frank (1968). The ZMP was the main criterion to assess the locomotion. Vukobratović and Borovac (2004) extended this concept for the multi-contact condition. Still, in his study, the contacts are assumed to be co-planar. Later, the Generalized-ZMP (GZMP) concept was introduced in Harada et al. (2003), which enables the participation of the multiple contacting limbs in the calculation of the supporting region with the projection methods. As a continuation of the multi-contact applications, Hyon et al. (2007) investigated the balance strategy by distributing contact wrenches.

Unlike the robot's locomotion, which considers the ZMP with the assumption of co-planar surface contacts, real-world applications mainly deviate from this assumption. Contact points may not be co-planar for stepping on terrains, grabbing and carrying the objects, ladder climbing by holding a handrail, etc. Therefore, the multi-contact applications of the robot are more challenging than the locomotion because of:

1. need for taking additional contacts into account in the scenario and balance in contrary to simply regarding feet and ground contacts,

1. The Defense Advanced Research Projects Agency (DARPA) is a research and development agency of the United States Department of Defense responsible for the development of emerging technologies for use by the military. The DRC is a competition of robot systems and software teams vying to develop robots capable of assisting humans in responding to natural and artificial disasters. Participating teams, representing some of the most advanced robotics research and development organizations in the world, are collaborating and innovating on a concise timeline to develop the hardware, software, sensors, and human-machine control interfaces that will enable their robots to complete a series of challenge tasks selected by DARPA for their relevance to disaster response Defense Advanced Research Projects Agency (2018).

2. consideration of *acyclic* motions rather than the repeated motion of stepping as a constant pattern for locomotion.

As first investigations on contact interaction of robotic manipulators, Khatib (1980); Raibert and Craig (1981) were considered as primary studies of this topic over dynamics and force control aspects. However, in the context of multi-contact motion generations for humanoids, the virtual linkage model is introduced to continue the multi-finger Joh and Lipkin (1991); Kumar and Waldron (1988); Sinha and Abel (1992) and multi-arm Yun (1991); Zheng and S. Luh (1986) grasping and manipulation interests. This model characterizes the internal wrenches by considering the manipulation process as a closed chain mechanism and physically representing the interior and gravito-inertial forces.

As a general statement, Sentis (2010) adopts the virtual linkage strategy for *multi-contact* interaction of the robot with the environment (Fig. 1.1(b)) considering the balance criterion by retaining the CoM inside a cloud of achievable CoM static positions. In the following, we focus more specifically on the multi-contact planning features of recent investigations and developed methodologies in this domain.

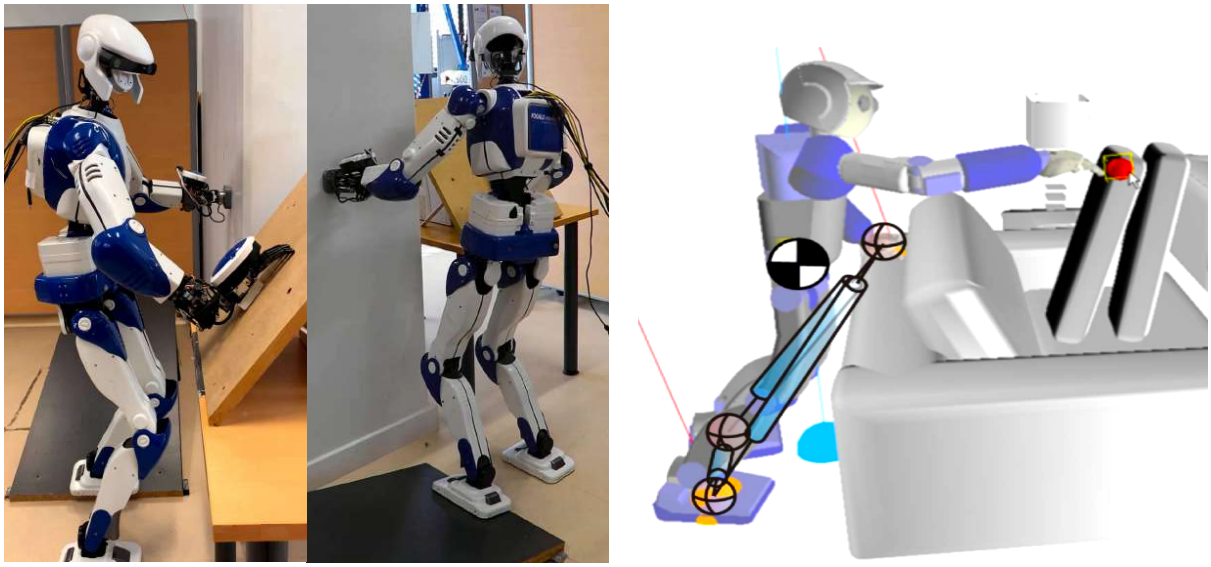

(a) (b)

FIGURE 1.1 – *Multi-contact motions of humanoids robots. (a) illustrates the HRP-4 robot with four non-co-planar contacting limbs Samadi et al. (2021), and (b) is the demonstration of the multi-contact posture assessed by the virtual-linkage model presented in Sentis (2010).*

1.1.1 Multi-contact motion planning

In order to plan a multi-contact motion, the robot needs to choose the contact points and their contact modes, the respective body configurations, a proper strategy to switch between the contacts and configurations (as a smooth trajectory) and take into account the constraints of the motion. These constraints also need to include the collision (in

case of obstacles) Kanajar et al. (2017); Merkt et al. (2019) and self-collision avoidance conditions Quiroz-Omaña and Adorno (2019); Koptev et al. (2021).

Multi-contact planning surpasses the locomotion problem and is crucial for increasing humanoid robots' loco-manipulation abilities in confined and narrow spaces Kheddar et al. (2019). The most common procedure to execute this hybrid motion is to dedicate the feet contacts for the balance problem while standing Kuffner et al. (2002); Yamane et al. (2004) or during the locomotion phase Kuffner et al. (2001); Chestnutt et al. (2003), along with manipulating with the remaining limbs. As a result, the problem can be decoupled for dual-arm robots with the locomotion capability Yoshida et al. (2008).

On the other hand, there exist conditions in which the decoupling of locomotion and manipulation motions is not considered as an efficient strategy; such as ladder climbing Vaillant et al. (2016), accessing/crawling under the table Escande et al. (2013) or box pushing Harada et al. (2007). The control of locomotion and manipulation problems have the actuated torques and contacting forces (involving the contact friction) in common. So, the hybrid motion (loco-manipulation) can be considered as the same problem.

Complex multi-contact motions are found in non-gaited or acyclic locomotion Reher et al. (2020); Kumagai et al. (2019) in complex and cumbersome scenes Chung and Khatib (2015), grasping Collette et al. (2008), manipulation Garcia-Haro et al. (2019), balancing in cramped spaces Henze et al. (2017), heavy-object pushing Murooka et al. (2015), etc. Such skills shall be achieved under active balance of the humanoid robot Kajita et al. (2010); Caron et al. (2019); Morisawa et al. (2018, 2019). In what follows, we explore some of the most common applications of humanoid robots in multi-contact scenarios.

Multi-contact Reaching Tasks

One of the most essential and basic motions that multi-contact conditions can carry out is contacting the planned spots (namely, reaching). The reaching motion accompanies numerous intentions such as grasping and manipulating different objects, maintaining the balance with additional contact points with the environment, pushing or holding things, performing industrial tasks such as pressing a button or placing particles into their place, etc.

Designing the algorithm of reaching a target in scenarios is the foremost step of the multi-contact planner. After accomplishing the reaching motion, the robot can perform the next states, such as pushing heavy objects. Mirjalili et al. (2018) designed a reaching algorithm on top of the proposed method by Mason et al. (2018) for multi-contact locomotion in the presence of perturbations and illustrated the reaching capability through a kid-sized humanoid robot as shown in Fig. 1.2(a).

In another study, Ruscelli et al. (2020) leverages the contact reaching for executing the static balance of the robot in confined spaces. It places the feet on non-coplanar surfaces and reaches the wall located beyond the robot. Also, Hiraoka et al. (2021)

demonstrated multiple scenarios such as crossing over rough terrains and reaching objects (see Fig. 1.2(b)) through a multi-contact online motion generator and prioritized inverse kinematics for realizing the targets from the planner. Moreover, Fig. 1.2(c) displays the reaching and placing of the particle in multi-contact condition inside the Airbus civilian airliner manufacturing plant Kheddar et al. (2019).

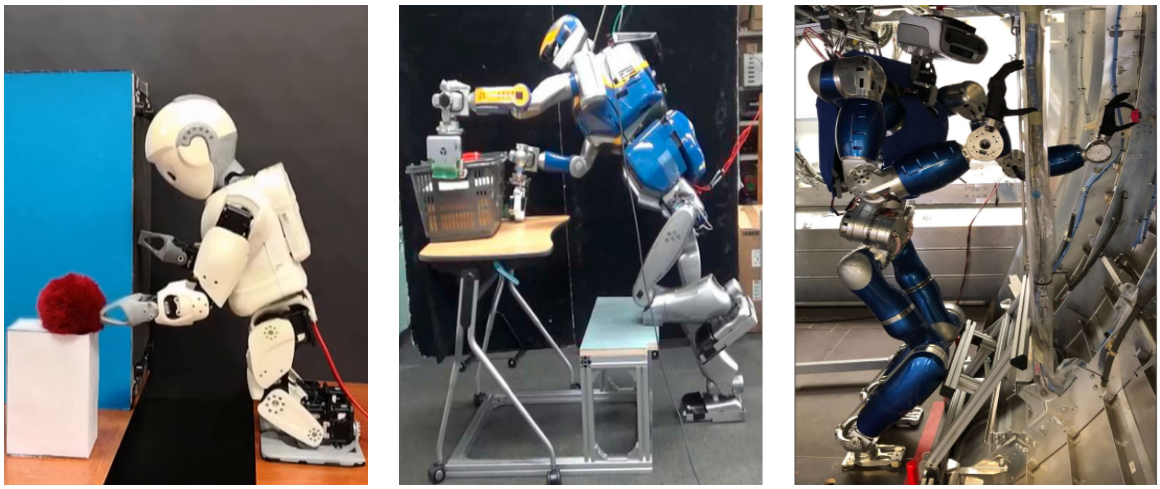

(a) (b) (c)

FIGURE 1.2 – *Multi-contact reaching maneuvers humanoid robots. The figure illustrates the generated multi-contact motions for (a) object-reaching of kid-sized SURENA-mini Mirjalili et al. (2018), (b) HRP-2 robot reaching a basket with establishing knee contact Hiraoka et al. (2021), and (c) particle-placing of TORO in the airbus manufacturing site Kheddar et al. (2019).*

Loco-manipulation and Multi-contact Locomotion

Moving different sizes and weights of objects by humanoid robots highlights the necessity of investigations and execution of loco-manipulation tasks while maintaining the robot's balance. For the balance of the robot, the recent studies are focused on motion generation Audren et al. (2014); Morisawa et al. (2019) and stabilization Farnioli et al. (2015) of multi-contact motions during the pushing motion Polverini et al. (2020); Hiraoka et al. (2021).

There are relevant studies on this scope which are proposing the controllers for pushing or pulling of objects Nishiwaki et al. (2006); Stilman et al. (2008) as well as pivoting Yoshida et al. (2010); Murooka et al. (2014) (see Fig. 1.3(a)) the massive objects. The other manipulation application of the humanoids would be opening the doors, which is an inevitable task for the robot working in the real world. Recently, Murooka et al. (2021) introduced a multi-contact control approach for loco-manipulation, which deals with the external perturbances and handles the rolling contacts as demonstrated in Fig. 1.3(b).

On the other hand, multi-contact locomotion is the additional capability that a humanoid should master if it wants to perform scenarios in large-scale manufacturing sites. The robot needs to traverse the pathways which are designed for humans and get

assistance from the environment for the locomotion Morisawa et al. (2018); Kumagai et al. (2020) and stair climbing Kumagai et al. (2021). The importance of multi-contact locomotion is in expanding the support region and decreasing the probability of losing the balance. Fig. 1.3(c) shows the humanoid robot passing through an industrial corridor using designed handrails.

(a) (b) (c)

FIGURE 1.3 – *Loco-manipulation and Multi-contact Locomotion of humanoid robots. (a) illustrates the HRP-2 humanoid robot, pivoting the heavy and large object Murooka et al. (2014) and (b) demonstrates the loco-manipulation of the HRP-5P robot with an industrial rolling bobbin Murooka et al. (2021). Additionally, (c) displays the multi-contact locomotion capability of this robot in a simulated industrial corridor Kumagai et al. (2020).*

Multi-contact Ladder Climbing

The most outstanding demonstrations on ladder climbing have been performed in the DARPA challenge. The champion team (SHAFT) was able to escalate the ladder using its feet only. The next group, HUBO+, was able to climb until the last rung. They demonstrated multi-contact climbing scenarios based on the approach introduced in Zhang et al. (2013). This team employed the multi-limbed locomotion planner stated in Luo et al. (2014) that generates the ladder-climbing trajectory based on the ladder model. Fig. 1.4(a) shows a stair climbing scenario that is reproduced to be close to the DARPA's conditions. Other than these two teams, the other participants were not able to climb.

However, ladder climbing is not a new challenge to tackle, and it has been the focus of interest since the 80th. To this end, the Toshiba company designed a robot with four limbs with grippers Iida et al. (1989). afterwards, there had been a majority of designs for climbing purposes such as LIBRA as a three-legged climbing robot Bevly et al. (2000), a metamorphic robot with deformable limbs Nakai et al. (2002), ASTERISK robot Fujii et al. (2008) with six legs, and Gorilla III Yoneda et al. (2008) which executed three demos of transverse, pace with constant velocity and trot with acceleration.

Recently, Noda et al. (2014) introduced a humanoid motion planner which enables the robot to climb the ladder or a car as shown in Fig. 1.4(b). Vaillant et al. (2016) also proposes a multi-contact planner by considering the pre-planned set of contacts for the

climbing motion. He demonstrated the scenario with an HRP-2 humanoid robot and a vertical ladder. The foot places in this approach can be placed on any rung at the will of the planner. Fig. 1.4(c) displays this vertical ladder climbing.

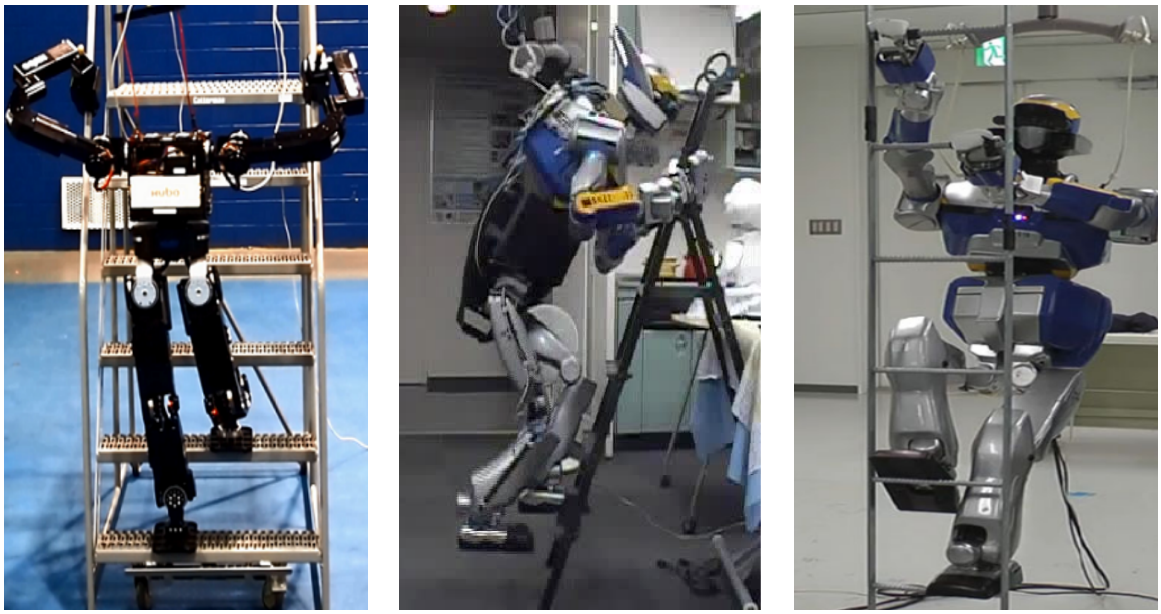

(a) (b) (c)

FIGURE 1.4 – *Multi-contact stair climbing of (a) a DRC-Hubo robot on an industrial ship ladder Luo et al. (2014) which is a simulated environment of DARPA robotic challenge, (b) climbing a sloped Noda et al. (2014) and (c) vertical ladder Vaillant et al. (2016) with HRP-2 humanoid robot.*

Accessing Narrow Spaces

When it comes to locomotion in an obstacle-free zone, the humanoids can only move forward by attachment/detachment of the feet' contacts with the ground. However, in the case of obstacles and pathways with terrains, the planner suggests adding interactions with the surroundings. There are situations in which the robot is asked to pass through unexpected routes with barriers Verrelst et al. (2006); Yokoi et al. (2009). Crawling motions (considering elbow and knee contacts) are needed to execute these crossing scenarios from narrow spaces Escande et al. (2013) as Fig. 1.5(a). Furthermore, Lu et al. (2010) demonstrates the transformation of movements from walking to crawling, highlighting the need for multiple contacting links with the environment.

One way of pathing through the terrains and obstacles is climbing over, crawling under, or shuffling around them, primarily narrow spaces. Kanehiro et al. (2005) introduces an online motion planner based on the produced 3D model of the environment, which enables the robot to move under narrow spaces such as tables or tunnels to arrive at a specified spot as shown in Fig. 1.5(b). Furthermore, Kanajar et al. (2017) tackles the challenge of climbing over the enormous barriers for making use of objects in the environment instead of bypassing them (see Fig. 1.5(c)).

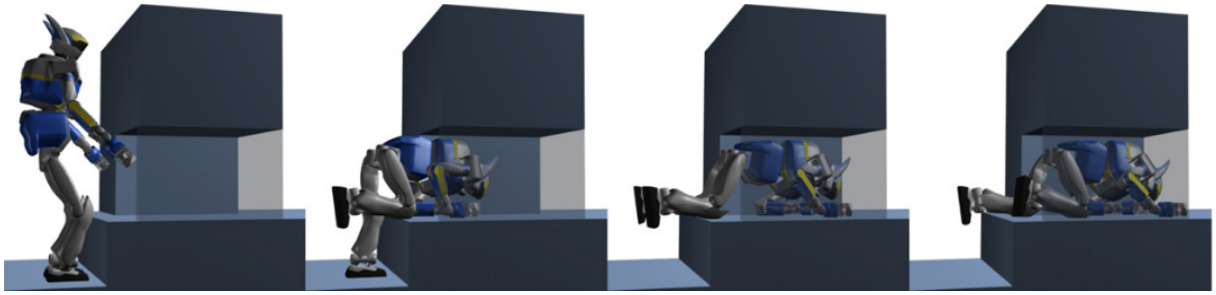

(a)

(b)

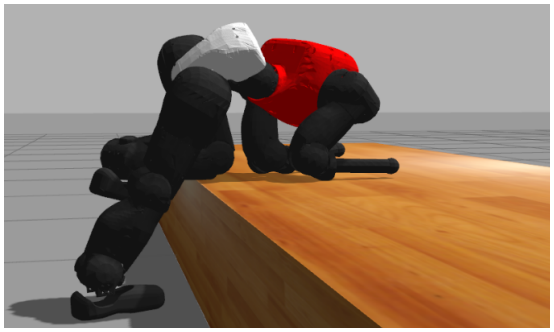

(c)

FIGURE 1.5 – *Multi-contact motion generation of humanoid robots for passing through the narrow spaces and crossing the obstacles by (a) crawling through tight tunnel Escande et al. (2013), (b) moving under the table Kanehiro et al. (2005) and (c) climbing over the large barrier Kanajar et al. (2017).*

1.1.2 Humanoids execuing sliding motions

The state-of-the-art multi-contact planning and control considers only creating and breaking contacts to support the motion Bouyarmane et al. (2019a). In many situations, however, switching contacts through releasing one of the established ones is not possible. This is the case, for example, in narrow or cumbersome spaces where free space is limited. Another example is when balance cannot be kept by breaking any of the existing contacts. In such cases, using sliding contacts to support the motion and the balance is an alternative. There are other contexts where tasks require sliding to be controlled (e.g. sanding or surface smoothing).

The sliding motion is one of the actions that individuals master in performing several tasks in their daily lives. Sliding contacts have been studied on several robots by considering dynamic friction forces and planning and controlling objects by pushing, see a recent example in Shi et al. (2017). In this thesis, we will focus on sliding contact modes included in multi-contact scenarios and address whole-body humanoid multi-contact task-space control allowing interchangeable multi-contact transitions between fixed (creating and removing) and sliding ones.

1.2 Contact modeling

Contact is the state of physical touching. Contact modeling aims to determine the interaction force between the contacts and identify the corresponding produced motion based on the contact forces. This model essentially depends on the geometry and physics of contacts and their material properties, which are employed to calculate the surfaces' deformation and friction. In the following, we describe the fundamental definitions of contact physics and dynamics.

1.2.1 Interaction features

To study the robot's interaction with the surrounding environment, some definitions are established that promote characterizing and formulizing the contact sorts. In this section, we perceive these principal notions.

Contact mode

When an end-effector of the robot is in contact with the environment, the kinematic transform comprises six degrees of freedom (DOF) which correspond to linear and angular DoF. Establishing contact is equivalent to restraining some of DoF in the form of equality constraints. Constraining the linear and angular DoF result in the generation of contact forces and torques, respectively. The *contact mode* is a compound of these constraints under a point or surface contact.

As mentioned, the contact mode is characterized by DoF, which constrains the contact among all DoF. A fixed contact mode is provided by six constrained DoF, restricting the contacting link from any movements. However, two DoF is set to be free for generating a sliding motion on a 2D tangential surface. Still, numerous methods assume keeping the fixed contact mode during the scenarios and excluding the possibility of experiencing other modes Balkcom and Trinkle (2002).

The term *contact swithcing* refers to the transition between the contact modes, and this switching happens when the force conditions reach the limits of the constraints. Therefore, we need to acquire these boundary conditions for controlling the motion of the end-effectors. The following definition is *contact stability* which comprises the stated conditions.

Contact stability

During the scenario, if all contacts of the robot with the environment stay in the same contact mode, the motion is known to be contact stable. So, this is a term contrary to contact switching. It is also important to mention that the application of the term "stable" is different from the standard definition of stability in control theory.

Pang and Trinkle (2000) introduced the contact stability criterion in terms of contacting forces which is commonly used in the literature Caron (2015). He indicated that for a fixed contact, there exists a solution for the equations of motion satisfying the contact mode for all contacting links and fulfill the following conditions:

- there occurs no relative motion of the contacting links (kinematic constraint),
- satisfies the joint torque limits,
- the contact forces do not exceed the limitation for fixed contact mode.

1.2.2 Contact models based on applications

Choosing the correct model of the contact depends instantly on the application and purpose of the main scenario. Employing the proper analytical contact model helps meet the setup's functionality expectations, which can be enhanced through manipulation or dexterous motions. There are two classifications of models developed for unilateral constraints based on smooth and non-smooth contact dynamics accordingly.

Rigid-Body Models

This model incorporates the vast majority of manipulation and grasping purposes. In this model, penetration and deformation of the interacting surfaces are not taken into account. Thus, the contact forces are the direct consequence of the frictional and rigidity property of the surfaces. The Rigid-body models are efficient due to their straightforward and linear formulation, leading to an efficient computational process in the algorithms.

Notwithstanding, there are some significant deficiencies beyond this model. When it comes to manipulating multiple objects, the model is not capable of resolving the static indeterminacy problem Bicchi (1994); Harada et al. (2000). Therefore, the model is not able to determine the force of the multiple grasping points. Furthermore, the deformation of manipulated objects is not always neglegible Lin et al. (2000).

Nevertheless, consideration of this deformation is out of the scope of the rigid-body model. Based on researches such as Lötstedt (1982); Wang et al. (1991), applying the Coulomb friction model can result in a lack or variety of solutions for mechanical problems. So, the compliant models would be advantageous for accurate and industrial applications.

Compliant Models

The compliant model takes into account the deformation of the objects under interacting forces. So, the contact force can be obtained by the stiffness model. Realizing these models are more complicated than the rigid-body models. However, they resolve

the static indeterminacy problem without neglecting the deformation of the contacting regions under loads.

The exact model for stiff material and contacts is complex to use within the schemes. Therefore, a reduced model with fewer variables is often favored to be used as a quasi-rigid-body approach instead of the detailed one. In order to model the local deformation of the fixtures, 3D finite-element methods (FEM) Dandekar and Srinivasan (1995); Xydas et al. (2000) or similar approaches Komvopoulos and Choi (1992); Tenek and Argyris (1997) can be applied.

1.2.3 Contact kinematics

Contact kinematics refers to the kinematic study of links for generating the motion with desired contact modes. In other words, contact dynamics take care of the motion of linked bodies while maintaining the end-effector's contact mode.

Assume two rigid-bodies in a workspace and the distance of their end-effectors noted by $\mathbf{d}$ as a function of bodies' configuration. According to this notion, $\mathbf{d} \geqslant 0$ indicates the detaching of end-effectors, and no contacts exist under this condition. Also, $\mathbf{d} \leqslant 0$ can be the condition of penetration which is not reflected under the rigid-body assumption. So, we concentrate on the contacting condition which is $\mathbf{d} = 0$. According to the kinematic chain, we calculate the derivation of distance in order to determine and predict the contact while tracking a configuration trajectory with bodies. As indicated, the distance term is a function of body configuration ($\mathbf{q}$). So, the derivation of distance can be calculated as follows:

$$\dot{\mathbf{d}} = (\frac{\partial \mathbf{d}}{\partial \mathbf{q}})\dot{\mathbf{q}}. \tag{1.1}$$

In this regard, we can leverage the Jacobian matrix expression for distance application as $\mathbf{J}_d = \frac{\partial \mathbf{d}}{\partial \mathbf{q}}$. Therefore, we have the derivations of distance function as:

$$\dot{\mathbf{d}} = \mathbf{J}_d\dot{\mathbf{q}} \tag{1.2}$$

$$\ddot{\mathbf{d}} = \dot{\mathbf{J}}_d\dot{\mathbf{q}} + \mathbf{J}_d\ddot{\mathbf{q}}. \tag{1.3}$$

Table 1.1 shows the interaction possibilities for two rigid-bodies.

1.2.4 Friction and forces

Assume that a rigid-body, with the mass of m, has a set of points in unilateral contact with the environment. The vector $\mathbf{n}$ is a unit vector normal to the contacting surface. The interaction (contact) force is noted by $\mathbf{f}^c$, and there can be the external forces acting on the rigid body, which we name as $\mathbf{f}^{ext}$. Fig. 1.6(a) illustrates the mentioned setup. According to rigid-body dynamics, the normal (f^z) and tangential ($\mathbf{f}^t = [f^x \;\; f^y]^T$) components of the contact force are represented as:

$$f^z \stackrel{\text{def}}{=} \mathbf{n}.\mathbf{f}^c \tag{1.4}$$

$$\mathbf{f}^t \stackrel{\text{def}}{=} \mathbf{f}^c - (\mathbf{n}.\mathbf{f}^c)\mathbf{z} \tag{1.5}$$

TABLE 1.1 – *Conditions of contact establishment*

d	$\dot{d}$	$\ddot{d}$	Explanation
> 0	$-$	$-$	complete detachment (no contact)
$= 0$	$-$	$-$	penetration (not considered in rigid-body model)
$= 0$	> 0	$-$	beginning of contact breaking
$= 0$	< 0	$-$	beginning of penetration (not considered)
$= 0$	$= 0$	> 0	beginning of contact breaking
$= 0$	$= 0$	< 0	beginning of penetration (not considered)
$= 0$	$= 0$	$= 0$	complete contact

where $\mathbf{n} = [0\ 0\ 1]^T$ is the unit normal vector (along z axis).

Coulomb's friction model describes the limits in which the contact mode switching happens due to exerted forces. Assuming the object presented in Fig. 1.6(a), this friction model indicates that there will be no movement if the contact force $\mathbf{f}^c = [f^x,\ f^y,\ f^z]^T$ lays inside the friction cone or equivalently, the inequality $|f^x| \leqslant \mu f^z$ is satisfied for the static friction coefficient μ. Note that the frames shown in Fig. 1.6 are local, and the constraints need to be expressed in the lab frame using rotation matrices.

When the contact force reaches the boundaries of the inequality, the box will start to slide with a different governing formula as $f^x = \mu^d f^z$ where μ^d indicates the dynamic (kinetic) friction coefficient. In general, the complementary Coulomb condition is in the following form:

$$\mathbf{f}^c.\mathbf{n} > 0 \tag{1.6}$$

$$\|\mathbf{n} \times \mathbf{f}^c \times \mathbf{n}\|_2 \leqslant \mu(\mathbf{f}^c.\mathbf{n}). \tag{1.7}$$

Eq. (1.7) contains the Euclidean norm $\|\circ\|_2$ which results in the friction cones with circle sections. This representation is the exact assumption of the friction cones; however, to employ the friction condition in the approaches, it is more convenient to use the linearized cones Hauser (2014); Del Prete et al. (2016). Regarding the $\mathbf{x}$ and $\mathbf{y}$ as tangential unit vectors (normal to vector $\mathbf{n}$), the linearized Coulomb condition in the complementary form becomes:

$$\mathbf{f}^c.\mathbf{n} > 0 \tag{1.8}$$

$$|\mathbf{f}^c.\mathbf{x}| \leqslant \mu(\mathbf{f}^c.\mathbf{n}) \tag{1.9}$$

$$|\mathbf{f}^c.\mathbf{y}| \leqslant \mu(\mathbf{f}^c.\mathbf{n}) \tag{1.10}$$

The Fig. 1.6(b) demonstrates the exact and linearized Coulomb friction cones.

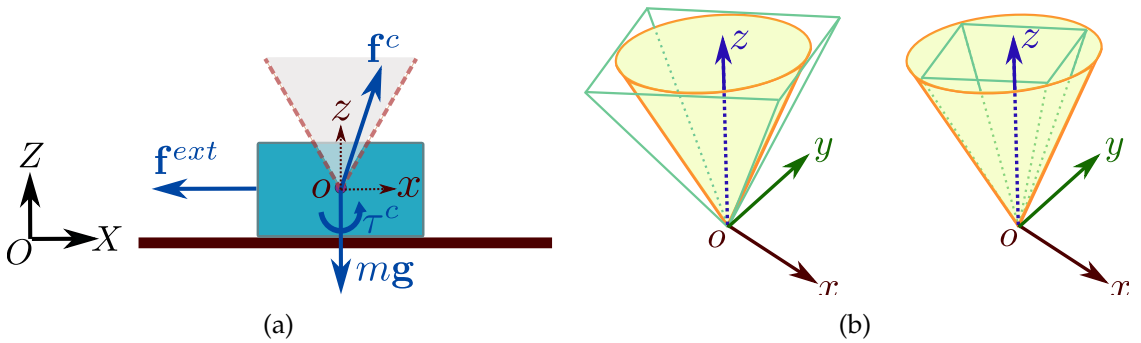

FIGURE 1.6 – *Representation of forces and frictional contact cones (a) acting on a box as a rigid-body in 2D and (b) linearization of the corresponding friction cones by inner and outer approximations in 3D. The xyz frame with the origin of o represents the local contact frame, and XYZ are coordinates of the lab (global) frame with center O.*

1.3 Whole-body multi-contact control

The planned motions and scenarios need to be implemented and executed on the robot. For this purpose, a controller needs to be employed that controls all robot joints based on the desired tasks. However, most of the time, multiple tasks need to be executed simultaneously on the robot (e.g., locomotion of the robot and manipulation of objects). Approaching various tasks is also the responsibility of the whole-body controller.

The multi-contact condition helps the humanoids to maintain balance in cumbersome circumstances by using additional interactions with the environment. There are several strategies introduced for controlling the robot in multi-contact conditions. As the first implication, Samson and Espiau (1990) introduced the usage of task functions for sensor-based control schemes and proposed a general model of interaction task. This work discussed the definition of task functions, control stability criteria, and task redundancy. Since then, there have been significant studies on task-space kinematic and inverse dynamic control of the robots Mansard et al. (2009), particularly redundant ones Siciliano and Slotine (1991).

The recent studies aim for formalizing the task-space controllers into a QP problem. The execution of these tasks is based on their prioritization hierarchy. This order-based scheme can be held either as a strict, weighted, or hybrid priority. Within the QP formulation Kanoun et al. (2011); Escande et al. (2014); Kuindersma et al. (2014), the tasks can be formulated as cost functions or constraints of the problem.

Saab et al. (2013) expressed the controller, which advises multiple objectives in task-space with a strict hierarchy. In this work, they extend inverse kinematics to the full dynamics of the robot for generating whole-body motions. A similar strict prioritization is implemented in Sentis (2010) to illustrate the complex interactions between contact forces and CoM behavior. Recently Kim et al. (2018) proposed a multi-objective whole-body control approach that delivers robustness and efficiency to the computations.

The study of Sentis (2010) deals with the internal forces in multi-contact as also practised by Righetti et al. (2013) which is employed in the form of constraints inside

the whole-body controller. As mentioned in the previous chapter, they use the virtual-linkage model, which describes the internal and gravitio-inertial wrenches, to obtain the optimal solution for the balancing problem. This optimization problem can further include the regulation of the Center-of-Pressure (CoP) Wensing et al. (2013) of feet or minimizing the contact wrenches Righetti et al. (2013) resulting in equal wrench distribution between contacts.

Del Prete et al. (2014) provides a strict-prioritized optimization problem including the linearized system dynamics. They indicated that using a strict hierarchy strategy bypasses the diverse weight-tunings, which becomes critical in the existence of numerous tasks. Some research studies the situations where the control forces exerted from specific end-effectors are of much importance. For instance, assume the manipulation of a fragile object where the grasping pressure should not exceed a certain value. Considering these situations, Sherikov et al. (2015) proposed a strict prioritization framework for the force distribution of optional contacts in multi-contact settings.

The primary deficiency of strict hierarchy is the incompatibility of their formulation with the addition of inequality constraints to the problem. One of the constraints that should be considered in the whole-body controller framework is the contact stability criteria that need to be implemented as inequality constraints.

To overcome this shortcoming, Saab et al. (2011); Escande et al. (2014) addressed the hierarchical quadratic programming (HQP) algorithm. This approach categorizes the tasks into higher and lower priority tasks. The algorithm can solve multiple QPs in the order of priority. Consequently, the low priority tasks will be solved in the null-space of high priority ones under constraints.

The major concern of solving two-level task categories is the smooth transition of task hierarchies in their sudden rearrangement. In simple words, for a dynamic system acting in the environment, some tasks need to be activated and deactivated through the time steps with their corresponding priority and Keith et al. (2011); Petrič and Žlajpah (2013) proposed the method for achieving a smooth rearrangement of hierarchies. Also, this smooth transition has been carefully investigated in Liu et al. (2016). This study introduces a semi-dynamic control structure with switchable strict and non-strict priorities and dynamic transition of task hierarchy.

On the contrary, there is the term weighted prioritized task-space controllers Abe et al. (2007). Optimization methods accompany these control structures with non-strict task hierarchies. They are mostly solved as tasks and constraints in QP forms Liu et al. (2011); Bouyarmane and Kheddar (2011a) with the implementation of different weights. In this approach, strict priority can not be accomplished by assigning weights for tasks.

Collette et al. (2007) introduced a weighted prioritized QP optimization task-space formulation for performing the complicated scenarios in multi-contact. Consecutively, Salini et al. (2010) argued the priorities between the tasks in a multi-contact balancing structure. In this study, the linear QP (LQP) cost function is set as the weighted sum of the task functions based on their importance.

The corresponding prioritization idea has been widely used in the literature Modu-

gno et al. (2017); Lee et al. (2021). Bouyarmane et al. (2019b) proposed the whole-body task-space controller based on the multi-robot concept, which is synthesized within a unique optimization problem of the controller rather than the planner Bouyarmane and Kheddar (2011a, 2012). The term multi-robot refers explicitly to modelling the robot's interactions with the environment as a cluster of robots. The weight-prioritization hierarchy is also the basis of this approach.

The whole-body motion of the robot in multi-contact settings is mainly classified in two primary conditions. First, considering all the contacting links in the realization of the balance of the robot and performing the desired tasks such as manipulation, carrying, pushing, etc. The second condition is to discriminate between the balancing and interacting contacts. Balancing contacts are considered contacts in charge of the robot's balance and are not conducting other tasks. However, the remaining contacts aim to realize the desired tasks, excluding the balance of the robot. In the latter form, the computed wrenches of the interacting links should be involved in the computation of the balance regions. Still, the duty of maintaining the balance is for balancing contacts.

As a matter of weighted prioritized controller, weights can be assigned so that the corresponding contact wrenches for interaction are mainly contributed to their related tasks at each control cycle. The rest of the wrenches are given to balancing. For instance, for the execution of a manipulation task, weights are designed to select some specific components of contacting wrenches and assign the rest for other tasks instead of donating the entire contact elements for this purpose. Henze et al. (2014) prefaced this weight-based implementation where the whole-body controller adjusts the hip orientation the same as Ott et al. (2011). In this context, the presented method in Lee and Goswami (2010) is applicable for controlling the whole-body momentum.

Classifying the contacts into balancing and interacting ones decreases the computation time and bypasses the repetition of balance region calculation at each control cycle where a motion occurs. Abi-Farraj et al. (2019) leverages this method to preserve the balance through high-force interaction tasks in multi-contact. Still, this compliant controller suffers from high computational costs. Even with separating the balancing contacts, there is a need for pre-computations of the balance region (more precisely, the distance of the balancing wrench from edges of the balance region).

By considering the whole-body motion of the humanoid, inverse kinematics provides the joint commands needed for realizing the desired trajectory of the CoM and the respective body configuration. For a torque-controlled robot, Stephens and Atkeson (2010) proposes a model-based dynamic balance force controller that commands the joint torques to the whole-body based on the desired CoM and contact forces. This framework employs virtual task forces in order to accomplish regular tasks as manipulation and posture tasks and solves the quadratic optimization problem for calculating the wrench distribution to control the motion of CoM and angular momentum of the robot. As a passivity based whole-body controller, Henze et al. (2016) appropriated the non-strict task hierarchy strategy for balancing the robot in multi-contact conditions. The approach is devised based on the categorization of interacting and balancing contacts.

The centroidal momentum control can be employed for whole-body control strate-

gies Macchietto et al. (2009); De Lasa et al. (2010); Orin et al. (2013). They are known to be more robust in the presence of perturbances than the controllers based on inverse-dynamics Herzog et al. (2014). So far, there have been notable researches on the hybrid dynamics of the humanoids, which incorporate remarkable results as presented in Posa et al. (2014); Neunert et al. (2018). Though, leveraging the mentioned methods is computationally expensive. On the other hand, simplified dynamical models are have been proposed that accelerate the calculations by decreasing the dimensions of the problem Herzog et al. (2016); Winkler et al. (2018), such as centroidal dynamics Orin et al. (2013); Dai et al. (2014).

Primarily, the planners provide the proper wrench distribution according to the centroidal model. The whole-body balance controller takes responsibility for realizing the wrenches on the robot and maintaining the balance. This control layer also operates the mapping of the contact forces into the joint positions Bouyarmane et al. (2019b) or torques Henze et al. (2016) for the position- or torque-controlled robots, respectively. Polverini et al. (2020) exploits the pushing of heavy objects with a torque-controlled platform and tracks the planned contacts through hierarchical inverse kinematics as a multi-contact controller.

1.4 Balancing in multi-contact

Maintaining the robot's balance in standing posture refers to the control of angular and linear momentums. For this purpose, the proper force of the contacting forces should be assigned on the robot holding the support area of the feet Macchietto et al. (2009). However, there is a need for additional contacting limbs in more challenging situations to preserve the balance, leading to the multi-contact condition. The multi-contact condition is not restricted to the hands and feet end-effectors. However, contacting limbs can contain every part of the robot, such as knees and elbows. The major limitation of using these contacts is the absence of sensors in mentioned spots of the robot so that, for instance, the amount of force acting on them can not be measured directly.

The balance controllers are mainly discussed through two categories. First, the controllers which are based on the whole-body inverse dynamics Saab et al. (2013); Posa et al. (2016) which aims for solving the optimal wrench distribution. Second category utilizes an approximation of the introduced methods by inverse dynamics including the pre- Werner et al. (2016) or post-optimization Laurenzi et al. (2018) of contact wrenches.

The robot's motion is considered static, quasi-static, semi-dynamic, or dynamic based on the purposes and capabilities of the scenarios. Ruscelli et al. (2020) implements the centroidal statics model to ensure the balance of the robot while performing multi-contact scenarios with planned contact transition on non-coplanar surfaces. Hiraoka et al. (2021) proposed a multi-contact controller for quasi-static motions including the control of wrench distribution, modeling of error compensation and adaption of actual contact states with the environment.

One of the most significant challenges in the motion of humanoid robots is sustaining the equilibrium in multi-contact settings. Ruscelli et al. (2020) implements the centroidal statics model to ensure the balance of the robot while performing multi-contact scenarios with planned contact transition on non-coplanar surfaces.

The objective of multi-contact planning and control of humanoid robots is applying dynamic balance criteria that account for unilateral contacts Bouyarmane et al. (2019a). Balance in multi-contact conditions was studied theoretically in Collette et al. (2007), Lee et al. (2016), Bouyarmane and Kheddar (2011b), Henze et al. (2014) but restricted to non-sliding contacts. To enforce dynamic balance for multi-legged robots in multi-contact, recent methods suggest computing the Zero-tilting moment points (ZMP), center-of-mass (CoM) support polygons, and gravito-inertial wrench cones (GIWC). In the following, we discuss about the multi-contact balance approaches.

1.4.1 CoM-based methods

The CoM-based approaches are based on the evaluation of the CoM trajectory or its acceleration. This evaluation can be executed through the construction of the balance regions. The balance region contains all feasible solutions for the CoM (or acceleration) of the relevant configurations that maintain the balance. Bretl and Lall (2008) and Audren and Kheddar (2018) proposed static and dynamic multi-contact balance criteria for frictional non-coplanar contacts.

The corresponding balance region is calculated via centroidal dynamics considering the equation of motion and contact stability conditions. In order to construct the balance region, both studies use the ray-shooting algorithm. Bretl and Lall (2008) considers the null CoM acceleration, whereas Audren and Kheddar (2018) holds a bounded set of accelerations in the computation of the corresponding region.

There are other approaches for the construction of balance regions, such as sampling Sentis (2010), approximation Nozawa et al. (2016) or learning Carpentier et al. (2017). These regions are essentially used for CoM trajectory planning purposes Audren and Kheddar (2017); Orsolino et al. (2020). However, Del Prete et al. (2016) uses this region for offline testing the feasibility of CoM positions.

The balancing strategies are associated with the trajectory of the CoM and the distribution of contact wrenches. The main restriction of applying the dynamic equation of motion is the non-linearity concerning the cross-product of CoM and its acceleration. In static mode, the acceleration is set to be zero, and the CoM balance region can be computed directly through the linear relation.

Fernbach et al. (2018) expressed the CoM trajectory as a Bezier curve with only one DoF to handle the cross-product issue. The other linearization technique is proposed by Padois et al. (2017) by setting a fixed normal component of the position of CoM. Concerning the optimal trajectory of CoM and joint configuration, Dai et al. (2014) proposed a method by applying the constraints as a linear relationship between the joint velocity and the momentum Orin et al. (2013).

1.4.2 GIWC-based methods

Caron et al. (2015a) leveraged the GIWC as the general contact stability criteria. This methods needs to be re-compute at each stance configuration switching. A recent study on the interaction of the robot with the environment introduces a passivity-based whole body balancing framework Abi-Farraj et al. (2019). In this latter work, gravito-inertial wrench cone (GIWC) introduced in Caron et al. (2015b) is used to keep the balance in multi-contact by ensuring the feasibility of the balancing wrenches, eventually under moving but not sliding contacts. Also, an independent algorithm is designed based on the end-effectors configuration to shift the weight and forces between the contacts in the absence of the effect of CoM position.

1.4.3 ZMP and MPC-based methods

As an extension of the ZMP criterion for the robot's balance while locomotion, Harada et al. (2006) introduced the term generalized zero-moment point (GZMP) for performing manipulation tasks. The balance region is calculated by considering the displacement and the moment about the edges of the convex hull of supporting points. Caron et al. (2017) evaluated the balance controller based on the generalization of ZMP support areas for multi-contact applications with non-coplanar and frictional contacts. They provide a fast-generating method for the ZMP-support region. This procedure is obtained through null motion constraints (full support area) and imposing the constraints of Linear Pendulum Mode (LPM) for the motion of the robot (pendular support area).

One of the proposed methods for controlling the balance of the humanoid robot is constructing it upon the model predictive control (MPC). As a case in point, Ibanez et al. (2012) proposed a ZMP-based balance controller for the lower body to accomplish the robot's balance. They also implemented a position-based controller to the upper body for manipulation purposes. This framework employs the MPC method together with consideration of the perturbances caused by manipulation tasks.

Ott et al. (2013) also suggested a comparable framework for kinesthetic teaching that detects the disturbances using a momentum-based disturbance observer and uses this information to generate whole-body compliant motions. Also, the balance controller regards the perturbance entries into the preview horizon of the MPC. In other words, the generated wrenches from performing a task is taken into account in the balance controller. Henze et al. (2014) proposes a balance controller which does not distinguish between the upper and lower body limb and contacts. Still, the legs are in charge of stabilizing the pose of the robot.

1.4.4 Balance with motion and contact transitions

Planning of the multi-contact locomotion and loco-manipulation has been widely studied in humanoids robotics for years. The locomotion himself is defined as a se-

quence of contact transitions. Also, the planning of the multi-contact scenarios contains this transition and refers to the same problem.

The feasibility of the contact transition needs to be evaluated at the beginning of each planning cycle. Also, the stability of the contacts and the balance of the robot need to be considered during the motion generation. Random sampling is a solution for finding the sequence of feasible contact and trajectories. However, it has computationally expensive due to the large scale of possibilities.

In this scope, Tonneau et al. (2018) proposed an efficient algorithm for executing the multi-contact locomotion using the reachability model with the convex hull of achievable limb points. However, not all of the resulting robot postures were possible to produce. To bypass the infeasible contacts, Fernbach et al. (2020) introduced an efficient algorithm based on the CoM trajectory with contact transitions. The computation cost of this approach for planning is of concern.

1.4.5 Balance in existence of sliding contacts

Recent works on humanoid robots are mostly focused on avoiding Kajita et al. (2004); Zhou et al. (2018) or recovering Kaneko et al. (2005); Vázquez and Velasco-Villa (2013) slips. A contact model introduced in Azad et al. (2016) for the interaction of a KUKA arm with a compliant environment. Also, physical interactions of the robot with compliant objects have been studied in Leidner (2019) and a distribution model for particles is introduced to plan the wiping motion of the four-wheeled Rollin' Justin humanoid robot.

Keeping the balance while sliding on purpose has been studied for two feet contacts in both rotational and translational directions. Linear contact constraints have been used in Kojima et al. (2017) for the controller to keep the dynamic balance while slipping in rotational directions on the feet. While rotational-slipping, considering the force distribution within the contact surfaces is the most challenging part of the study. Slip-turn motion for the robot is produced in Miura et al. (2013) by minimizing the floor friction power. The works in Hashimoto et al. (2011); Koeda et al. (2011) are about generating quick turning motion by rotational shuffling.

As a motion planning for translational shuffling, Kojima et al. (2015) implemented two-layer controller to satisfy the stability criteria of the robot using Zero-tilting Moment Point (ZMP) and achieve proper force distribution in two feet contacts. Total motion sequence of this method consists of both slide-and-stop phases and CoM trajectory is generated solving a QP and related constraints. Also, keeping the dynamic balance while shuffling is studied in Posa et al. (2014) by formulating complementary constraints into a QP, and in Kim and Park (2011) by uniform force distribution assumption on the sole for single support phase.

Sliding contacts under active balance is challenging in humanoid robots. There are however successful achievements in specific tasks such as foot shuffling Kojima et al. (2015); Or and Ames (2019); slip-turns and maneuvers by two feet contacts Kojima et al. (2017); Miura et al. (2013); Koeda et al. (2011). Sliding contacts forces must be

controlled to be exactly on their friction cone Trinkle et al. (1997). We have addressed this problem in Samadi et al. (2020), where we considered a mix of sliding and fixed multi-contact scenarios. The CoM support area (CSA) is derived analytically when the fixed contacts are coplanar. To overcome this limitation and extend the balance criteria to be used in control, we propose a novel formulation for the computation of the CoM position and the contact wrenches using the Chebyshev center.

The aforementioned methods end up with computing regions (e.g., polytopes, polyhedral cones...) where the CoM position or the wrenches should live. Reducing the cost of such computations is the main challenge to integrate them in control and reactive planning. Especially while considering the tasks with contact switchings and movements, e.g. pushing, sliding, etc. Indeed, they are mostly used in planning. This thesis will mainly focus on enriching the balance criteria with lower computation costs, enabling the online implementation of the control framework.

1.5 Applications

Nowadays, robots are capable of performing complex scenarios. On top of them, the vast majority of variations of animanoids and humanoids are acknowledged. Expanding this technology aims to reach the objectives, such as replacing robots with humans in risky environments like factories and interacting with humans in public, industrial, and medical communities. Thus, in general, the application of these robots covers research and educational purposes, assistant, rescue, healthcare, and manufacturing. However, there are many unsolved challenges that can lead to assessing the human-like activities of the robots, as shown in Fig. 1.7.

New achievements of robotics are confirming considerable growth in humanoid robotics. These robots demonstrated their capabilities in different areas such as walking, running, crossing through terrains, stair, slope and ladder climbing, etc. Nevertheless, there still exist numerous objections to delivering all humanoid abilities on the robot. The first and most crucial step towards profiting from the capabilities of a humanoid robot in complex scenarios is maintaining balance.

On the other hand, some humanoid robots do not have the balance challenge thanks to their wheeled structure. For these robots, interacting and assisting a human is on top of their intentions. Bolotnikova et al. (2020) explored the interaction of the pepper humanoid robot with the human for physical assistance based on an optimized posture generator. The demonstration of the close interaction of the robot with real humans for assistance purposes Bolotnikova et al. (2021) as shown in Fig. 1.8.

Employing wheeled robots, we can primarily concentrate on goal-oriented tasks. The applications such as wiping a board or surface Henze et al. (2016), grasping, and manipulation Vahrenkamp et al. (2009) are of interest. Using the wheeled robots reduces the concern about the robot's balance significantly. Fig. 1.9 illustrates the capacities of the wheeled robot in performing daily human routines.

Despite the balancing challenge of the legged humanoid robots, these robots can

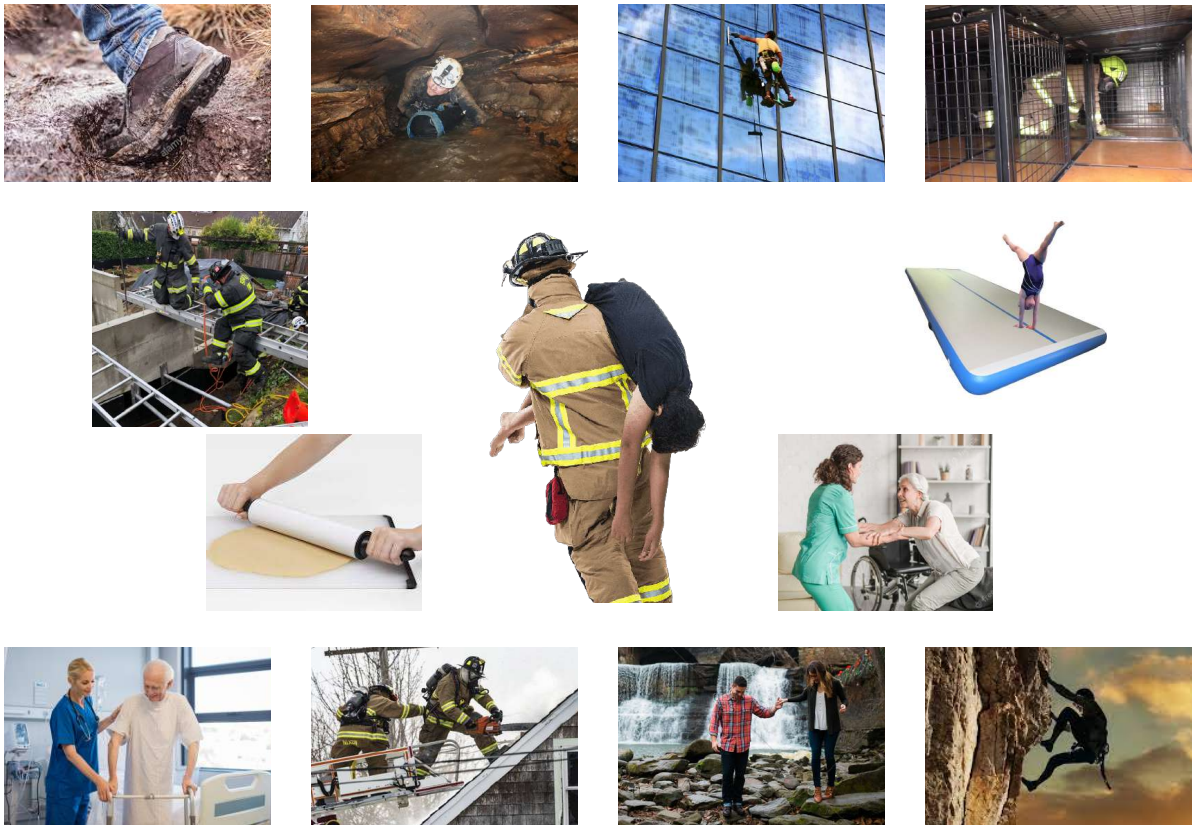

FIGURE 1.7 – *Human routine activities as the intention for humanoid scenarios and applications.*

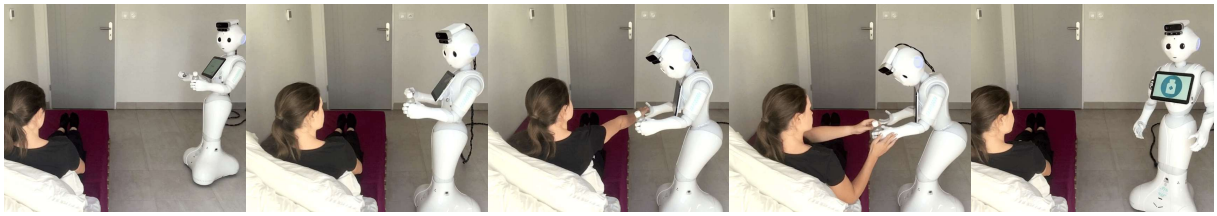

FIGURE 1.8 – *Pepper humanoid robot assisting an individual with close interaction Bolotnikova et al. (2021).*

perform more challenging scenarios compared to wheeled ones. For instance, there is a need to cross the terrains for the robot's operation in industrial environments, such as climbing and stepping down the stairs Caron et al. (2019) and accessing narrow spaces that are impracticable for wheeled robots to accomplish. The Fig. 1.10 demonstrates an HRP-4 humanoid robot operating in the Airbus company Kheddar et al. (2019).

In order to improve the capabilities of the humanoid robot in diverse states and environments, additional contact modes (sliding, soft, etc.) need to be investigated and considered. Lately, few fascinating scenarios are designed in the aforementioned research direction in which the robot performs on soft contacts Henze et al. (2016) and skateboard Takasugi et al. (2016, 2019). Also, remarkable studies accomplish the shuffling motion Kojima et al. (2015); Koeda and Sugimoto (2018) and slip turn Koeda et al. (2011); Miura et al. (2013); Kojima et al. (2017) with the legged robot.

(a)

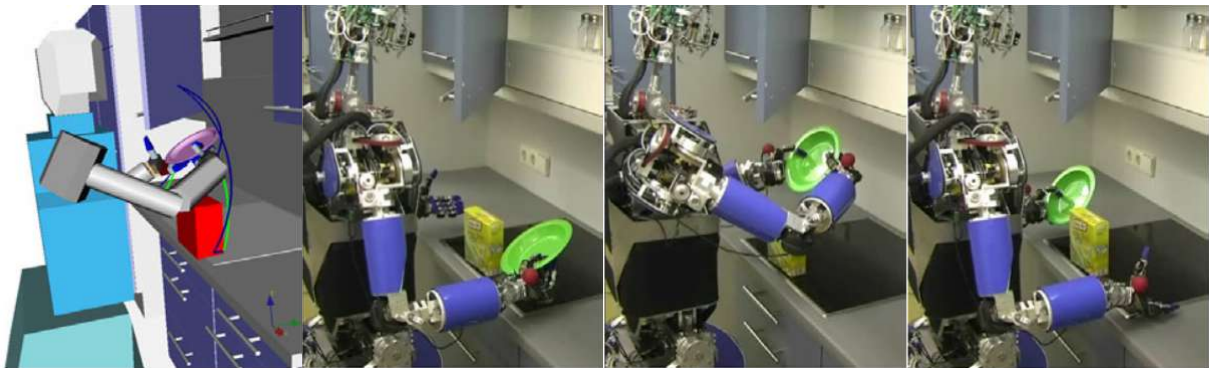

(b)

FIGURE 1.9 – *Humanoid robots performing (a) wiping motion on a surface Henze et al. (2016) and (b) grab and manipulation of dishes Vahrenkamp et al. (2009).*

FIGURE 1.10 – *TORO and HRP-4 humanoid robots operating multi-contact Kheddar et al. (2019) and stair climbing Caron et al. (2019) tasks in the industrial environments.*

The researches which contain sliding or soft contact modes are studied in uni- or bi-contact postures. However, for multi-contact scenarios, the balance criteria are very challenging. The online implementation of the balance with existing methods is not feasible and needs pre-computations. So, in the current study, we tackle the challenge of the real-time performance of multi-modal scenarios considering the dynamic balance.

The core objective for the humanoid robots is to perform the all human-like motions and activities which includes multi-modal contacts without any pre-computations. So

that they can perform any unplanned scenarios and react in presence of any perturbances.

1.6 Preliminaries

This section will introduce the preliminaries employed for the implementation of the controllers in the current study. The planning and controller schemes of this research constitute optimization-based structures. Therefore, we represent the formulation of the QP problem, which is utilized as the optimization method in this research. Moreover, the Finite State Machine (FSM) is used to determine the desired motions and accomplish the configuration transitions of the robot. The Controller and FSM features are implemented in a framework named `mc_rtc` [2]. In the following, we briefly present the specified preliminaries.

1.6.1 Quadratic Programming

Mathematical optimization (also known as mathematical programming) refers to a programming method that results in the selection of the *best* element among all possibilities and feasible solutions concerning the constraints and conditions. The optimization process is accomplished by minimizing a particular function, named the cost function. Considering a function $\mathcal{F}(\mathbf{x} \in \mathbb{E}) \in \mathbb{R}^n$, the objective of optimization problem is to find a viable argument of the function $\mathbf{x}^*$ in a way that:

$$\mathcal{F}(\mathbf{x}^*) = \min_{\mathbf{x} \in \mathbb{E}}. \mathcal{F}(\mathbf{x}). \tag{1.11}$$

Solving the optimization problem is equivalent to finding the argument $\mathbf{x}^*$. The Eq. (1.11) presents an unconstrained optimization problem. However, it can be solved under constrained formulation as

$$\mathcal{F}(\mathbf{x}^*) = \min_{\mathbf{x} \in \mathbb{E}}. \mathcal{F}(\mathbf{x}) \tag{1.12}$$

$$\text{s.t. } \mathbf{l} \leqslant \mathcal{G}(\mathbf{x}) \leqslant \mathbf{u} \tag{1.13}$$

where $\mathcal{G}(\mathbf{x}) \in \mathbb{E}$ is the governing function of the inequality constraints and $\mathbf{l}, \mathbf{u} \in \mathbb{R}^n$ vectors are representing the lower and upper bounds on the function $\mathcal{G}(\mathbf{x})$.

Different optimization methods can be integrated according to the expression of the $\mathcal{F}(\mathbf{x})$ and $\mathcal{G}(\mathbf{x})$ functions. The quadratic optimization function is the case that $\mathcal{F}(\mathbf{x})$ and $\mathcal{G}(\mathbf{x})$ can be represented as quadratic and linear forms, respectively. So, for all $\mathbf{x} \in \mathbb{R}^n$, the functions can be expressed as following:

$$\mathcal{F}(\mathbf{x}) = \frac{1}{2}\mathbf{x}^T\mathbf{P}\mathbf{x} + \mathbf{q}^T\mathbf{x} \tag{1.14}$$

$$\mathcal{G}(\mathbf{x}) = \mathbf{A}\mathbf{x} \tag{1.15}$$

2. https://github.com/jrl-umi3218/mc_rtc

where $\mathbf{P}$ is a positive semi-definite matrix accompanied by vector $\mathbf{q}$ for representing the function $\mathcal{F}(\mathbf{x})$. Also, $\mathbf{A}$ is a non-parametric matrix used for the linear interpretation of the constraint. So, the quadratic programming problem can be re-written in the following form:

$$\min_{\mathbf{x}\in\mathbb{E}} \quad \frac{1}{2}\mathbf{x}^T\mathbf{P}\mathbf{x} + \mathbf{q}^T\mathbf{x} \tag{1.16}$$

$$\text{s.t. } \mathbf{l} \leqslant \mathbf{A}\mathbf{x} \leqslant \mathbf{u} \tag{1.17}$$

There are several solvers designed for solving the QP problems in programming languages, mainly Python and C++, such as `CVXOPT` [3], `qpOASES` [4], `quadprog` [5], `CVXPY` [6], `Gurobi` [7], and `MOSEK` [8]. In our implementations, we use the C++ module of `quadprog` which is compatible with `Eigen3` [9] library.

1.6.2 Finite State Machine

The controller minimizes the cost functions as tasks by considering the constraints in QP formulation. This control structure is equipped with a finite-state machine (FSM). FSM is in charge of monitoring the accomplishment of the tasks and constraints. The planned states (derived from output of the planner) are sequence of statically stable configurations of the robot $\mathbf{q}$. The configuration of the robot is associated with the established contacts of the robot with environment, namely its stance.

The sequence of stances and configurations of the robot which is derived from the planner are named *sequentially adjacent* and *transition configurations* Bouyarmane and Kheddar (2011a), respectively. Within the sequence of stances, the next stance of the robot can be structured by adding or removing one contact. The transition of configurations also checks the static stability of motion and addition/deletion of contact forces from the corresponding added/removed contacts in the new configuration.

The tasks and constraints need to be defined within the FSM structure. The posture task is a default task that solves the redundancy issue of the robot while performing scenarios. The other default tasks mainly activated in the framework are dynamic (associated with control of dynamic balance and governing the Newton-Euler equations) and kinematic constraints, and (self-)collision avoidances.

1.6.3 mc_rtc Framework

`mc_rtc` is an interface for the robotic systems which provides both simulation and

3. http://cvxopt.org/
4. https://github.com/coin-or/qpOASES
5. https://pypi.org/project/quadprog/
6. https://www.cvxpy.org/
7. https://www.gurobi.com/
8. https://www.mosek.com/
9. https://gitlab.com/libeigen/eigen

implementation of the controllers and enables executing a wide range of industrial and academic simulations and experiments.

The robot's control system needs to supply the state of the robot, such as its configuration, sensor readings, etc., and `mc_rtc` will generate the relevant commands for performing the planned states (through FSM and controller specifications) practising assigned classes.

The `mc_rtc` framework contains relevant packages and libraries involved in the control of the robot, such as `SpaceVecAlg`[10], `RBDyn`[11] and `Tasks`[12] libraries and handles the FSM states and ROS communications. It enables the user to write the controller in both Python and C++ languages.

1.6.4 TVM Library

The Task with Variable Management (TVM)[13] is a library that enables users to write and solve linear control problems for robotic systems. It is an optimization framework with multiple serviceable features as variable management (that is needed in this research) and a convenient way of writing the constraints.

This library distinguished the problem writing with solving process. It allows the users to write the constraints close to their natural formulations and mathematical notations. As constructing the relevant matrices is the main challenge of re-formulating the constraints for users, this library handles matrix formulation automatically. This feature enhances the computational cost and duration of the problem.

The main features of this library can be counted as follows:

- decoupling of the writing of the problem (which is close to its mathematical formulation) with its solution process,
- a more handy way of declaring the task functions and constraints within the structure,
- the capability of extension in case of addition/removal of tasks,
- containing the classical robotic functions as dynamic/kinematic constraints, collision avoidances, etc.,
- compatible with consistently adding/removing decision variables,
- computation check for avoiding multiplication of process for deriving quantities.

10. https://github.com/jrl-umi3218/SpaceVecAlg
11. https://github.com/jrl-umi3218/RBDyn
12. https://github.com/jrl-umi3218/Tasks
13. https://github.com/jrl-umi3218/tvm

1.7 Conclusion

This chapter mainly focused on the principal applications of the multi-contact motions, the execution of relevant controllers on the robot, and their performance challenges within the environment. Several studies focus on generating and planning the multi-contact motions, performing challenging tasks like reaching, loco-manipulation, ladder climbing, accessing narrow spaces,... which are addressed throughout the chapter.

Contact modeling plays a significant role in the study of multi-contact motions. The application of the scenarios leads to the adoption of decent contact models such as rigid-body or compliant (interaction with stiff materials) models. Similarly, investigating the contact modes and conditions and considering the friction models and kinematic constraints are crucial for exploiting contact switching through the scenarios.

The planned states and motions regularly cover the contact conditions based on the contact models and constraints. However, the whole-body controller executes these states on the real robot by calculating the relevant joint commands to the robot. The controller also needs to ensure the balance of the robot. Evaluating the balance in multi-contact conditions can be achieved using CoM, ZMP, GIWC, or MPC-based methods. We reviewed the existing methods for assessing the balance criteria through the specified methods together with their strengths and shortages.

One of the prominent shortcomings of the multi-contact balance controllers refers to their computational cost. They are computationally expensive due to the need for the construction of balance regions. However, in the next chapter, we aim to tackle this challenge by introducing an analytical solution for the computation of these regions enabling the real-time implementation of the controller.

CHAPTER 2

FAST COMPUTATION OF THE STATIC EQUILIBRIUM REGION CONSIDERING SLIDING CONTACTS

The previous chapter covers the gross state of the art on many aspects of our work, altogether with the background in both software framework and the facilities available in our laboratory. We emphasized the knowledge and recent approaches dealing with all aspects of multi-contact behaviors for humanoids and the techniques for maintaining the robot's balance.

This chapter deals specifically with the balance of humanoids (or multi-legged robots) in a localized multi-contact setting (i.e., a localized floating base motion that does not result in high-dynamic transitions of the contacts). We consider that a subset of contacts is undergoing desired sliding-task motions while the remaining ones are enforced to not move, i.e., should be kept fixed. One method to sustain balance is to hold the CoM within an admissible convex set. This set is an area that is computed based on the contact positions of the robot limbs and subsequent applied forces by the environment or any equivalent motion constraint.

We introduce an analytical methodology to compute this CoM-support area (CSA) for intended multiple fixed and sliding contacts in real-time, enabling the controller's online implementation on the robot. To select the most appropriate CoM position within CSA, we account for:

1. constraints of multiple fixed and sliding contacts;
2. desired wrench distribution for contacts; and
3. desired CoM position (eventually dictated by other tasks).

We formulate the mentioned objectives as a quadratic programming (QP) optimization problem. We illustrate our approach by pushing against a wall and wiping scenarios. The experiments are conducted using the HRP-4 humanoid robot.

We structured this chapter as follows. First, in Section 2.1 we introduce the CoM support area for multiple fixed and sliding contacts. Holding the position of the CoM

inside this area guarantees the robot's balance while some chosen contacts slide and others do not. Section 2.2 presents our method for calculating the CoM position under constraints. Sections 2.3 and 2.4 shows experimental results and concludes this chapter, respectively.

2.1 CoM support area

The equation of the motion of the robot in the *static* mode (assuming zero CoM acceleration) can be described by Newton-Euler equations as follows:

$$\sum_{\text{contact } i} \mathbf{w}_i^c = -\mathbf{w}^g \tag{2.1}$$

where $\mathbf{w}_i^c \in \mathbb{R}^6$ and $\mathbf{w}^g \in \mathbb{R}^6$ are the i-th contact and the gravity wrenches respectively. We follow the common practice to write the resultant linear term (force) first in the wrench followed by the moment term; that is $\mathbf{w} = [\mathbf{f} \;\; \boldsymbol{\tau}]^T$. We can re-write Eq. (2.1) in the world frame by separating the forces and torques:

$$\sum_i \mathbf{f}_i^c = m\mathbf{g} \tag{2.2}$$

$$\sum_i \mathbf{p}_i \times \mathbf{f}_i^c = \mathbf{c} \times m\mathbf{g} \tag{2.3}$$

where m is the total mass of the robot, $\mathbf{p}_i, \mathbf{f}_i^c \in \mathbb{R}^3$ are the position and force of the i-th contact point respectively; $\mathbf{g} \in \mathbb{R}^3$ is the gravity vector and is equal to $\begin{bmatrix}0 & 0 & g\end{bmatrix}^{\mathrm{T}}$ for $g = -9.81\frac{\mathrm{m}}{\mathrm{s}^2}$, and $\mathbf{c} = [c^X \;\; c^Y \;\; c^Z]^T \in \mathbb{R}^3$ is the position of the CoM with respect to the lab (global) frame. By introducing the unit vector $\mathbf{e}_z$ as $\begin{bmatrix}0 & 0 & 1\end{bmatrix}^T$, we can separate the vertical component of the gravity vector:

$$\sum_i \mathbf{f}_i^c = mg\mathbf{e}_z \tag{2.4}$$

$$\sum_i \mathbf{p}_i \times \mathbf{f}_i^c = mg\mathbf{c} \times \mathbf{e}_z \tag{2.5}$$

Moreover, by applying a cross-product to both sides of Eq. (2.5) by $\mathbf{e}_z$, we get the following equation:

$$mg\mathbf{e}_z \times \mathbf{c} \times \mathbf{e}_z = \sum_i \mathbf{e}_z \times (\mathbf{p}_i \times \mathbf{f}_i) \tag{2.6}$$

Next, we use two well-known properties of the cross-product that are:

$$\mathbf{e}_z \times \mathbf{c} \times \mathbf{e}_z = \begin{pmatrix} c^X \\ c^Y \\ 0 \end{pmatrix} \tag{2.7}$$

$$\mathbf{a} \times (\mathbf{b} \times \mathbf{c}) = (\mathbf{a}.\mathbf{c})\mathbf{b} - (\mathbf{a}.\mathbf{b})\mathbf{c} \tag{2.8}$$

by applying equations 2.7 and 2.8 into Eq. (2.6) we have:

$$mg\mathbf{c}^s = \sum_i f_i^z \mathbf{p}_i - p_i^z \mathbf{f}_i \tag{2.9}$$

where $\mathbf{c}^s$ denotes the position of the CoM in the horizontal plane and is equal to $[c^x \; c^y \; 0]^T$. As a study case, let us consider a robot configuration that has three contacts ($i = 1, 2, 3$) with his surrounding. The position of the CoM from Eq. (2.9) will be formulated as follows:

$$\mathbf{c}^s = \frac{f_3^z}{mg}\mathbf{p}_3 + \frac{f_2^z}{mg}\mathbf{p}_2 + \frac{f_1^z}{mg}\mathbf{p}_1 - \frac{p_3^z}{mg}\mathbf{f}_3 - \frac{p_2^z}{mg}\mathbf{f}_2 - \frac{p_1^z}{mg}\mathbf{f}_1 \tag{2.10}$$

The Eq. (2.10) shows the general form of this formula by considering three contacts, regardless of their orientation and positions. As a particular case, we assume that both feet are on the ground so that $p_1^z = p_2^z = 0$. Consequently Eq. (2.10) becomes:

$$\mathbf{c}^s = \frac{f_1^z}{mg}\mathbf{p}_1 + \frac{f_2^z}{mg}\mathbf{p}_2 + \frac{f_3^z}{mg}\mathbf{p}_3 - \frac{p_3^z}{mg}\mathbf{f}_3 \tag{2.11}$$

In the following, we specify a region for the feasible position of CoM without losing the balance according to the multi-modal configurations. This region was introduced in Bretl and Lall (2008) as a static equilibrium CoM area and extended to 3D in Audren and Kheddar (2018). The computation of the oriented area in this chapter considers fixed and sliding contacts.

The purpose of our present work is to balance the robot in real-time for multi-contact configurations with fixed or sliding contacts. We introduce an analytical solution with inexpensive computational cost, which enables the online implementation of the controller. Furthermore, this method will guarantee the robot's balance for sliding contacts, such as wiping a board by hand or shuffling foot motions.

Let's consider a humanoid having its feet on the ground and one arm (e.g., right one) wiping a board (non-coplanar with the other contacts). Again, there is no limitation or constraint on wiping direction, and we can design and plan it at will. Hence, the position of the sliding contact is a pre-defined parameter according to the desired wiping trajectory. Therefore, the last two elements of Eq. (2.11) can be considered as constant variables at each iteration. We can define them as an independent constant value $\mathbf{\Gamma}$ – regarding $\mathbf{p}_1$ and $\mathbf{p}_2$ variables:

$$\mathbf{c}^s = \frac{f_1^z}{mg}\mathbf{p}_1 + \frac{f_2^z}{mg}\mathbf{p}_2 + \mathbf{\Gamma} \tag{2.12a}$$

$$\mathbf{\Gamma} = \frac{f_3^z}{mg}\mathbf{p}_3 - \frac{p_3^z}{mg}\mathbf{f}_3 \tag{2.12b}$$

then:

$$\mathbf{c}^s - \mathbf{\Gamma} = \frac{f_1^z}{mg}\mathbf{p}_1 + \frac{f_2^z}{mg}\mathbf{p}_2 \tag{2.13}$$

On the other hand, by considering Eq. (2.2) in vertical direction, we have the following *convex* combination:

$$\frac{f_1^z}{mg} + \frac{f_2^z}{mg} + \frac{f_3^z}{mg} = 1 \tag{2.14}$$

In order to formulate the right-hand side of Eq. (2.14) in the *convex* form, we re-write it as

$$\frac{f_1^z}{mg} + \frac{f_2^z}{mg} = \sigma_c \tag{2.15}$$

where

$$\sigma_c \overset{\text{def}}{=} 1 - \frac{f_3^z}{mg}. \tag{2.16}$$

So, Eq. (2.13) becomes:

$$\mathbf{c}^s - \mathbf{\Gamma} = \sum \alpha_i(\sigma_c \mathbf{p}_i) \tag{2.17a}$$

$$\alpha_i = \frac{f_i^z}{\sigma_c mg} \tag{2.17b}$$

where,

$$\sum_i \alpha_i = 1 \tag{2.18}$$

$$\alpha_i \geqslant 0. \tag{2.19}$$

The convex hull of a set of points or vectors is $conv(v_1, \ldots, v_n) = \sum_i \alpha_i v_i$. So, the Eq. (2.18) is a sufficient condition to show that the point $\mathbf{c}^s - \mathbf{\Gamma}$ is inside the convex polygon constructed by connecting $\mathbf{p}_i$ points.

There are two equivalent ways to represent the wrench applied by the environment on the robot under a surface contact:

1. Contact forces applied at the vertices of the contact area Caron et al. (2015b);
2. A single contact wrench applied at a given point Audren and Kheddar (2018).

Here, we continue with the first method. To be able to use the surface contact instead of single points, we replace each of these points ($\mathbf{p}_i$) with four edges of the related foot. Coordinates of new points are available by considering the 2-D dimension of each foot contact. According to the specified scenario, the CoM-support convex hull from Eq. (2.17) contains 8 contact points regarding the edges of the fixed contacts.

The convex hull of feasible CoM positions is executed on JVRC [1] humanoid model using Pymanoid [2]. Fig. 2.1 shows the evolution of the convex area during the wiping motion of the right-hand end-effector. The trajectory of wiping can be arbitrary, and here we keep it as straight segment lines, and the blue square inside the convex is the position of CoM.

CSA for the designed scenario is depicted in Fig. 2.2. The green area on the ground of Fig. 2.2(a) is CSA for close foot contacts, and Fig. 2.2(b) emphasizes this area for far feet contacts in wiping motion.

1. https://github.com/jvrc/model
2. https://github.com/stephane-caron/pymanoid/
3. http://choreonoid.org/en/

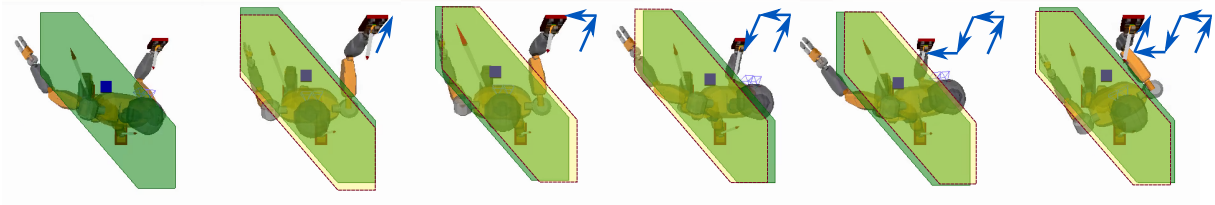

FIGURE 2.1 – *Evolution of the CSA while wiping the wall with the JVRC humanoid model. The order is from left to right, and blue arrows show the trajectory of wiping. The green and yellow CSAs are for the current and preceding screenshots, respectively.*

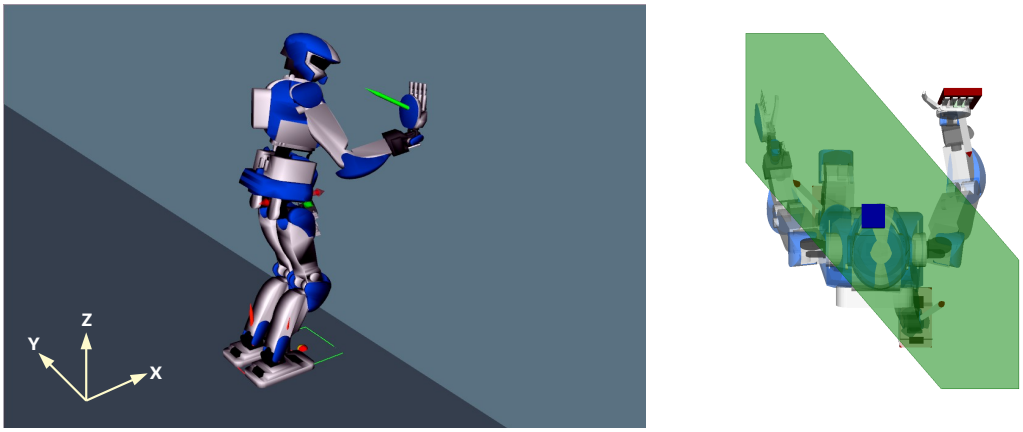

(a) (b)

FIGURE 2.2 – *Humanoid robot with sliding hand contact on the wall simulated dynamically by Choroenoid*[3] *(a) and prototyped in pymanoid (b).*

As a result, the CSA is constructed according to both sliding and multi-contact conditions. To maintain the balance of the robot, the CoM should remain inside the CSA during operating motions. Setting the exact position for the CoM inside the CSA is explained in the next section. By considering the desired tasks and motion constraints, a QP problem is formulated that outputs the CoM position and wrench distribution.

2.2 Centroidal Quadratic Program

A standard solution for keeping the robot's balance is to put a constraint on the position of the CoM and hold it inside the CSA. This constraint will ignore some parameters that affect the robot's performance, such as locating the CoM in the safest position and farest possible from the edges of the supporting region.

In this chapter, we specify a target for the CoM position rather than strictly constraining it (i.e., as equality on where to be). Furthermore, this target is provided in a way that has the maximum distance from the borders of the CSA. In this sense, the CoM position can be counted as the safest CoM target for the iteration.

2.2.1 Decision Variables

Collette *et al.* Collette et al. (2007) proposed a quadratic program that takes into account the position of CoM, linearized contact forces, and the gravity wrench in static equilibrium. Nevertheless, they consider all contacts to be fixed. On the other hand, they need to set a target for the CoM position, but their framework lacks any computation or application of the balance region.

To consider sliding contacts in the controller and apply sliding constraints to the selected contacts, we introduce the Centroidal QP. This QP is designed with the following decision variables:

$$\mathbf{Y} = \begin{bmatrix} \mathbf{c}^s & \mathbf{w}_{\text{rf}} & \mathbf{w}_{\text{lf}} & \mathbf{w}_{\text{rh}} \end{bmatrix}^T_{1\times 21} \tag{2.20}$$

where $\mathbf{w}$ denotes the contact wrench in the world frame and subscripts $\circ_{\text{rf}}$, $\circ_{\text{lf}}$ and $\circ_{\text{rh}}$ correspond to the right-foot, left-foot, and right-hand contacts, respectively. The centroidal QP computes the CoM position and the wrench distribution for all contacts. The next step is to realize the computed variables in the centroidal QP. This is done through the whole-body QP, which takes into account the respective tasks.

The static equilibrium of the system is given in Eq. (2.1). Accordingly, by considering three contacts (one hand contact and two feet contacts), the Newton-Euler equation writes:

$$\mathbf{w}^g + \mathbf{w}_{\text{rf}} + \mathbf{w}_{\text{lf}} + \mathbf{w}_{\text{rh}} = 0 \tag{2.21}$$

where wrenches can be formulated as follows:

$$\mathbf{w}^g = \begin{bmatrix} 0 & 0 & 0 \\ 0 & 0 & 0 \\ 0 & 0 & 0 \\ 0 & -mg & 0 \\ mg & 0 & 0 \\ 0 & 0 & 0 \end{bmatrix} \mathbf{c}^s + \begin{bmatrix} 0 \\ 0 \\ -mg \\ 0 \\ 0 \\ 0 \end{bmatrix} \tag{2.22}$$

$$\mathbf{w}_{\text{rf,lf}} = \begin{bmatrix} & I_{3\times 3} & & 0_{3\times 3} \\ 0 & -c^Z & c^Y & \\ c^Z & 0 & -c^X & I_{3\times 3} \\ -c^Y & 0 & c^X & \end{bmatrix} [\mathbf{R}]_{\text{rf,lf}}\, {}^l\mathbf{w}_{\text{rf,lf}} \tag{2.23}$$

where ${}^l\mathbf{w}$ shows the wrench in contact (local) frame and is equal to $[{}^l\mathbf{f} \in \mathbb{R}^3 \quad {}^l\boldsymbol{\tau} \in \mathbb{R}^3]^T$ and $[\mathbf{R}]_i$ represents the rotation matrix from local to the global frame. Also, $\mathbf{w}_{\text{rh}}$ is calculated in a same way with $\mathbf{w}_{\text{rf,lf}}$. In this way, we can shortly write the equations as:

$$\mathbf{w}_m = \mathbf{E}_{m1}\mathbf{c}^s + \mathbf{E}_{m2} \tag{2.24a}$$
$$\mathbf{w}_{\text{rf}} = \mathbf{E}_{\text{rf}}\, {}^l\mathbf{w}_{\text{rf}} \tag{2.24b}$$
$$\mathbf{w}_{\text{lf}} = \mathbf{E}_{\text{lf}}\, {}^l\mathbf{w}_{\text{lf}} \tag{2.24c}$$
$$\mathbf{w}_{\text{rh}} = \mathbf{E}_{\text{rh}}\, {}^l\mathbf{w}_{\text{rh}} \tag{2.24d}$$

2.2.2 Sliding Condition

The up-to-date studies in locomotion, multi-contact conditions, or motion generation for humanoids avoid slippage, whereas we aim for it when needed. In order to prevent slippage, it is common to use inequality constraints to hold each point-contact resultant force within its associated friction cone Bouyarmane et al. (2019a). Instead, we are implementing constraints to generate the sliding motion.

For generating controlled slipping motion, the force vector of the sliding contact ($\mathbf{f}_c$) should remain at the edge of the related contact's friction cone and hence express as equality constraints. However, contact torques are considered as inequality constraints to avoid tiltings during the slippage.

We continue the computations based on the designed scenario, which is the standing posture with the right hand on the vertical wall as shown in Fig. 2.2(a). To better understand the implementation of equations, we consider the global frame where the normal force to the hand is aligned to the Z direction of this frame. We introduce two matrices named $[\mathbf{S}^1]$ and $[\mathbf{S}^2]$ such that the normal and frictional sliding contact forces could be given to the QP as constraints:

$$[\mathbf{S}^1]_{6\times 6} = \begin{bmatrix} \mathbf{I}_{3\times 3} & \mathbf{0}_{3\times 3} \\ \mathbf{0}_{3\times 3} & \mathbf{0}_{3\times 3} \end{bmatrix} \tag{2.25}$$

so that

$$[\mathbf{S}^1]\mathbf{w}_{\text{rh}} = \begin{bmatrix} \mathbf{f}_{3\times 1} \\ \mathbf{0}_{3\times 1} \end{bmatrix}_{\text{rh}}. \tag{2.26}$$

In the global frame, f^{X}_{rh} shows the normal force applied to the sliding contact. Note that the direction X in the global frame of the scenario is perpendicular to the wiping trajectory and wall. According to the wiping trajectory, we can calculate the contact forces in Y and Z directions as frictional forces:

$$\begin{bmatrix} \mathbf{f}_{3\times 1} \\ \mathbf{0}_{3\times 1} \end{bmatrix}_{\text{rh}} = \begin{bmatrix} 0 & 0 & 0 & \dots & 0 \\ 0 & 0 & \frac{f^Y}{f^X} & \dots & 0 \\ \frac{f^Z}{f^X} & \vdots & & & \vdots \\ \vdots & & & & \\ 0 & 0 & \dots & & 0 \end{bmatrix}_{6\times 6} \mathbf{w}_{\text{rh}} + \begin{bmatrix} f^X \\ 0 \\ 0 \\ 0 \\ 0 \\ 0 \end{bmatrix} \tag{2.27}$$

where $\frac{f^Y}{f^X}$ and $\frac{f^Z}{f^X}$ are constant numbers, and they are independent of the forces. In fact, they correspond to the friction coefficient of the sliding contact by considering the wiping direction. So, based on the sliding movement, the respective elements can have positive or negative quantities. From Eq. (2.26) and Eq. (2.27), we have:

$$[\mathbf{S}^1]\mathbf{w}_{\text{rh}} = [\mathbf{S}^2]\mathbf{w}_{\text{rh}} + \mathbf{k} \tag{2.28}$$

thereby, we have the $[\mathbf{S}^2]$ as:

$$[\mathbf{S}^2] = \begin{bmatrix} 0 & 0 & 0 & \dots & 0 \\ 0 & 0 & \frac{f^Y}{f^X} & \dots & 0 \\ \frac{f^Z}{f^X} & \vdots & & & \vdots \\ \vdots & & & & \\ 0 & 0 & \dots & & 0 \end{bmatrix}. \tag{2.29}$$

So, Eq. (2.27) can be written as

$$[\mathbf{S}^1 - \mathbf{S}^2]\mathbf{w}_{\text{rh}} = \mathbf{k}. \tag{2.30}$$

The above equation contains the necessary condition for the sliding motion of the contact and will be applied to the Centroidal QP as an equality constraint.

2.2.3 Non-sliding Conditions

In the previous section, we showed that the sliding contacts are expressed with equality constraints. However, to keep the rest of the contacts fixed on the ground and surface, we must implement inequality constraints to maintain the related point-contact force within their respective friction cone. Also, we need to avoid tilting and detaching the contacts. So, the inequalities will apply to the whole contact wrench (forces and torques).

The general constraints that should be applied to contact wrenches in the local frame within the QP solver are expressed as in Caron (2015):

$$\begin{aligned} &\mid f^x \mid \leqslant \mu f^z \ , \ \mid f^y \mid \leqslant \mu f^z \ , \ f^z_{\min} \leqslant f^z \leqslant f^z_{\min} \\ &\mid \tau^x \mid \leqslant \mathbb{Y} f^z \ , \ \mid \tau^y \mid \leqslant \mathbb{X} f^z \ , \ \tau^z_{\min} \leqslant \tau^z \leqslant \tau^z_{\min} \end{aligned} \tag{2.31}$$

where $\mathbb{X}$ and $\mathbb{Y}$ are edge sizes of contact surfaces and can be measured by the shape of the contacts, so:

$$\tau^{\min}_z = -\mu(\mathbb{X}+\mathbb{Y})f_z + \mid \mathbb{Y} f_x - \mu\tau_x \mid + \mid \mathbb{X} f^y - \mu\tau^y \mid \tag{2.32}$$

and

$$\tau^z_{\max} = \mu(\mathbb{X}+\mathbb{Y})f^z - \mid \mathbb{Y} f^x + \mu\tau^x \mid - \mid \mathbb{X} f^y + \mu\tau^y \mid \tag{2.33}$$

The equations Eq. (2.31) are combined in the following form for fixed contacts:

$$\begin{bmatrix} f^x \\ f^y \\ f^z \\ \tau^x \\ \tau^y \end{bmatrix}_{\text{rf,lf}} \leqslant \begin{bmatrix} \mu f^z \\ \mu f^z \\ f^z_{\max} \\ \mathbb{Y} f^z \\ \mathbb{X} f^z \end{bmatrix}_{\text{rf,lf}} \tag{2.34}$$

$$-\begin{bmatrix} f^x \\ f^y \\ f^z \\ \tau^x \\ \tau^y \end{bmatrix}_{\text{rf,lf}} \leqslant \begin{bmatrix} \mu f^z \\ \mu f^z \\ f^z_{\max} \\ \mathbb{Y} f^z \\ \mathbb{X} f^z \end{bmatrix}_{\text{rf,lf}} \tag{2.35}$$

Furthermore, for sliding contacts, we consider torques similarly to Eq. (2.34) and Eq. (2.35) in all directions inside the inequality constraints. Because sliding contact forces have been considered as equality constraints to create the sliding motion. Note that there is no τ^z element inside the vectors, and it will be considered separately.

We need to generate vectors in a way that we can apply it as an inequality constraint to the system. For this reason, we re-write these equations using $\mathbf{G}_{\text{rf,lf,rh}} \in \mathbb{R}^{6\times 21}$ and $\mathbf{h}_{\text{rf,lf,rh}} \in \mathbb{R}^6$ matrices and vectors:

$$\mathbf{G}^1_{\text{rf,lf,rh}}\mathbf{Y} \leqslant \mathbf{h}^1_{\text{rf,lf,rh}} \tag{2.36}$$

$$\mathbf{G}^2_{\text{rf,lf,rh}}\mathbf{Y} \leqslant \mathbf{h}^2_{\text{rf,lf,rh}} \tag{2.37}$$

where:

$$\mathbf{G}^1_{\text{rf}} = \begin{bmatrix}\mathbf{0}_{6\times 3} & \boldsymbol{\Upsilon}^1_{\text{rf}} & \mathbf{0}_{6\times 12}\end{bmatrix} \tag{2.38a}$$

$$\mathbf{G}^2_{\text{rf}} = \begin{bmatrix}\mathbf{0}_{6\times 3} & \boldsymbol{\Upsilon}^2_{\text{rf}} & \mathbf{0}_{6\times 12}\end{bmatrix} \tag{2.38b}$$

$$\mathbf{G}^1_{\text{lf}} = \begin{bmatrix}\mathbf{0}_{6\times 9} & \boldsymbol{\Upsilon}^1_{\text{lf}} & \mathbf{0}_{6\times 6}\end{bmatrix} \tag{2.38c}$$

$$\mathbf{G}^2_{\text{lf}} = \begin{bmatrix}\mathbf{0}_{6\times 9} & \boldsymbol{\Upsilon}^2_{\text{lf}} & \mathbf{0}_{6\times 6}\end{bmatrix} \tag{2.38d}$$

$$\mathbf{G}^1_{\text{rh}} = \begin{bmatrix}\mathbf{0}_{6\times 15} & \boldsymbol{\Upsilon}^1_{\text{rh}}\end{bmatrix} \tag{2.38e}$$

$$\mathbf{G}^2_{\text{rh}} = \begin{bmatrix}\mathbf{0}_{6\times 15} & \boldsymbol{\Upsilon}^2_{\text{rh}}\end{bmatrix} \tag{2.38f}$$

where $\boldsymbol{\Upsilon}^1_{\text{rf,lf}} \in \mathbb{R}^{6\times 6}$ is defined as:

$$\boldsymbol{\Upsilon}^1_{\text{rf,lf}} = \begin{bmatrix} 1 & 0 & -\mu & 0 & \dots & \\ 0 & 1 & -\mu & \vdots & & \\ \vdots & 0 & 1 & & & \\ & & -\mathbb{Y}_{\text{rf,lf}} & 1 & & \\ & & -\mathbb{X}_{\text{rf,lf}} & & 1 & \vdots \\ 0 & & 0 & & \dots & 0 \end{bmatrix}$$

Note that $\boldsymbol{\Upsilon}^2_{\text{rf,lf}}$ is same as $\boldsymbol{\Upsilon}^1_{\text{rh,lf}}$ except the diagonal values of the matrix which should be multiplied by -1. Also, for the sliding contact, we have:

$$\boldsymbol{\Upsilon}^1_{\text{rh}} = \begin{bmatrix} 0 & 0 & \dots & & & 0 \\ 0 & & & & & \\ \vdots & & \ddots & & \vdots & \\ 0 & & & 0 & 0 & \vdots \\ \mathbb{X}_{\text{rh}} & 0 & \dots & 0 & 1 & 0 \\ \mathbb{Y}_{\text{rh}} & 0 & \dots & & 0 & 1 \end{bmatrix}$$

and for $\boldsymbol{\Upsilon}^2_{\text{rh}}$, replace two last elements on the diagonal of the matrix with -1. For the other side of the inequality, h is a zero vector for sliding contacts. For fixed contacts, we have:

$$\mathbf{h}^1_{\text{rf,lf}} = \begin{bmatrix}0 & 0 & f^z_{\max} & 0 & 0 & 0\end{bmatrix}^T \tag{2.39a}$$

$$\mathbf{h}^2_{\text{rf,lf}} = \begin{bmatrix}0 & 0 & f^z_{\min} & 0 & 0 & 0\end{bmatrix}^T \tag{2.39b}$$

$$\mathbf{h}^{1,2}_{\text{rh}} = \mathbf{0}_{6\times 1} \tag{2.39c}$$

Besides, we should consider inequality constraints on τ^z. According to Eq. (2.31), we divide it into two sets of boundaries which should be implemented for all contacts:

$$\tau^z - \tau^z_{\max} \leqslant 0 \tag{2.40}$$
$$-\tau^z + \tau^z_{\min} \leqslant 0 \tag{2.41}$$

Consider that there is two absolute values inside each of $\tau^z_{\max}$ and $\tau^z_{\min}$ based on Eq. (2.32) and Eq. (2.33) that each equation results in four more rows inside the inequality matrix that should be multiplied by $\mathbf{Y}$.

We introduce $\mathbf{Gz} \in \mathbb{R}^{4\times 21}$ matrices which covers the inequality constraints on τ^z element of wrenches:

$$\mathbf{Gz}^{1,2}_{\text{rf,lf,rh}}\mathbf{Y} \leqslant \mathbf{0}_{4\times 1} \tag{2.42}$$

where:

$$\mathbf{Gz}^1_{\text{rf}} = \begin{bmatrix}\mathbf{0}_{4\times 3} & \mathbf{\Psi}^1_{\text{rf}} & \mathbf{0}_{4\times 12}\end{bmatrix} \tag{2.43a}$$
$$\mathbf{Gz}^2_{\text{rf}} = \begin{bmatrix}\mathbf{0}_{4\times 3} & \mathbf{\Psi}^2_{\text{rf}} & \mathbf{0}_{4\times 12}\end{bmatrix} \tag{2.43b}$$
$$\mathbf{Gz}^1_{\text{lf}} = \begin{bmatrix}\mathbf{0}_{4\times 9} & \mathbf{\Psi}^1_{\text{lf}} & \mathbf{0}_{4\times 6}\end{bmatrix} \tag{2.43c}$$
$$\mathbf{Gz}^2_{\text{lf}} = \begin{bmatrix}\mathbf{0}_{4\times 9} & \mathbf{\Psi}^2_{\text{lf}} & \mathbf{0}_{4\times 6}\end{bmatrix} \tag{2.43d}$$
$$\mathbf{Gz}^1_{\text{rh}} = \begin{bmatrix}\mathbf{0}_{4\times 15} & \mathbf{\Psi}^1_{\text{rh}}\end{bmatrix} \tag{2.43e}$$
$$\mathbf{Gz}^2_{\text{rh}} = \begin{bmatrix}\mathbf{0}_{4\times 15} & \mathbf{\Psi}^2_{\text{rh}}\end{bmatrix} \tag{2.43f}$$

where the $\mathbf{\Psi} \in \mathbb{R}^{4\times 6}$ matrices are different for each contact and should be defined separately, and they are calculated as follows. Consider Eq. (2.40) for the right foot. By implementing the amount of $\tau^z_{\max}$ from Eq. (2.33) and considering positive sign for both of the absolute values, we get to the following equation:

$$\mathbb{Y}_{\text{rh}} f^x + \mathbb{X}_{\text{rh}} f^y + \mathcal{C}_{\text{rf}} f^z + \mu\tau^x + \mu\tau^y + \tau^z \leqslant 0$$

where $\mathcal{C}_{\text{rf}} = -\mu(\mathbb{X} + \mathbb{Y})$ and is computed in the same way for other contacts. By considering negative sign for absolute values, the other three equations are available, and $\mathbf{\Psi}$ matrix for the upper bound of the right foot is calculated:

$$\mathbf{\Psi}^1_{\text{rf}} = \begin{bmatrix} \mathbb{Y}_{\text{rf}} & \mathbb{X}_{\text{rf}} & \mathcal{C}_{\text{rf}} & \mu & \mu & 1 \\ -\mathbb{Y}_{\text{rf}} & \mathbb{X}_{\text{rf}} & \mathcal{C}_{\text{rf}} & -\mu & \mu & 1 \\ \mathbb{Y}_{\text{rf}} & -\mathbb{X}_{\text{rf}} & \mathcal{C}_{\text{rf}} & \mu & \mu & 1 \\ -\mathbb{Y}_{\text{rf}} & -\mathbb{X}_{\text{rf}} & \mathcal{C}_{\text{rf}} & -\mu & \mu & 1 \end{bmatrix}$$

Notice that the first row of this matrix corresponds to the above equation. We calculate the other matrices for the lower and upper bound of the contacts in the same way.

2.2.4 QP Formulation

In previous sections, we introduced the equality and inequality constraints to be taken into account in the control of the robot based on the equation of motion and

contact stability. To improve the performance, we define the desired tasks and objectives for the scenario. Finally, we write the problem in QP form with the CoM position and contact wrenches as decision variables.

The goal of Centroidal QP is to reach $\mathbf{Y}_{\text{des}}$ as the desired value of these decision variables while considering constraints. Therefore, the minimization problem is:

$$\min_{\mathbf{Y}} \|\mathbf{Y} - \mathbf{Y}_{\text{des}}\|^2 \tag{2.44}$$

The desired position for CoM is the barycenter of the CSA, and for the fixed contact, the desired wrench is set to be zero. According to the planned scenario, which has both feet as the only fixed contacts, the zero reference points to the equal wrench distribution between these contacts.

According to Eq. (2.44) as the objectives of the problem and also sliding and non-sliding conditions as equality and inequality constraints, the QP formulation is in the following form:

$$\min_{\mathbf{Y}} \frac{1}{2}\mathbf{Y}^T\mathbf{P}\mathbf{Y} + \boldsymbol{\upsilon}^T\mathbf{Y} \tag{2.45a}$$

$$\mathbf{G}\mathbf{Y} \leqslant \mathbf{h} \tag{2.45b}$$

$$\mathbf{A}\mathbf{Y} = \mathbf{b} \tag{2.45c}$$

where $\mathbf{P} = \mathbf{I}_{21\times 21}$ and $\boldsymbol{\upsilon} = -\mathbf{Y}_{\text{des}}$. By introducing $\mathbf{G}_{\text{rf}}^T$ as transpose matrix of $\mathbf{G}_{\text{rf}}$ and the same for the other contacts, matrices and vectors of the equality constraints in Eq. (2.45) are:

$$\mathbf{G} = \begin{bmatrix}\mathbf{G}_{\text{c}}^{i,T} & \mathbf{G}\mathbf{z}_{\text{c}}^{i,T}\end{bmatrix}^T_{21\times 60}; i = 1, 2; c = \text{rf, lf, rh} \tag{2.46a}$$

$$\mathbf{h} = \begin{bmatrix}\mathbf{h}_{\text{rf}}^{1,T} & \mathbf{h}_{\text{rf}}^{2,T} & \mathbf{h}_{\text{lf}}^{1,T} & \mathbf{h}_{\text{lf}}^{2,T} & \mathbf{h}_{\text{rh}}^{1,T} & \mathbf{h}_{\text{rh}}^{2,T}\end{bmatrix}^T_{1\times 21} \tag{2.46b}$$

On the other hand, the equality constraints are derived from Eq. (2.24) in section 2.2.1 and Eq. (2.30) in section 2.2.2. To combine these constraints in one equation and be able to use them in QP directly, matrix $\mathbf{A} \in \mathbb{R}^{12\times 21}$ and vector $\mathbf{b} \in \mathbb{R}^{12}$ are defined as follows:

$$\mathbf{A} = \begin{bmatrix}\mathbf{E}_{\text{m1}} & \mathbf{E}_{\text{rf}} & \mathbf{E}_{\text{lf}} & \mathbf{E}_{\text{rh}} \\ 0_{6\times 3} & 0_{6\times 6} & 0_{6\times 6} & \mathbf{S}^1 - \mathbf{S}^2\end{bmatrix} \tag{2.47a}$$

$$\mathbf{b} = \begin{bmatrix}-\mathbf{E}_{\text{m2}}^{\text{T}} \in \mathbb{R}^{6\times 1} & -\mathbf{f}_x & 0 & \dots & 0\end{bmatrix}^{\text{T}} \tag{2.47b}$$

The Eq. (2.45) is the Centroidal QP with the desired objectives of the motion written in the form of minimization tasks and contains the dynamic balance, contact stability, and sliding condition of selected contacts as equality and inequality constraints. Moreover, this QP outputs the safe position of CoM and respective wrench distribution of all contacts as a planner, which will be realized on the real robot.

In the next section, we describe the whole-body controller used to perform the planned tasks on the real robot. The role of this QP is to receive the planned states and values from Centroidal QP and execute them in the whole-body task-space control framework.

2.2.5 Controller Specification

The Centroidal QP calculates the position of the CoM and wrench distribution of contacts. These values should be applied to the real robot as commands and tasks to accomplish. For this purpose, we use a whole-body dynamic controller based on another weight-prioritized QP formulation introduced in Bouyarmane et al. (2019b). The main tasks to execute are stipulated as the following specifications.

Posture task

Posture task solves for the redundancy and the remaining joints' motion. In other words, the posture task is a regularization task based on degrees of freedom $\mathbf{q}$ that brings the robot to a reference joint-angle (e.g., to a half-sitting configuration $\mathbf{q}_{\text{half-sit}}$) its derivatives by considering task stiffness $\mathbf{K}_p$ via:

$$\ddot{\mathbf{q}} = \mathbf{K}_p(\mathbf{q}_{\text{half-sit}} - \mathbf{q}) - 2\sqrt{\mathbf{K}_p}\dot{\mathbf{q}} \tag{2.48}$$

End-effector admittance task

End-effector admittance task takes the desired position $\mathbf{p}^d \in \mathbb{R}^6$ as a target in world frame, desired wrench $\mathbf{w}^d \in \mathbb{R}^6$ in sensor frame and admittance gains $\mathcal{A} \in \mathbb{R}^6$. For a given degree of freedom i, the task is a position task if $\mathcal{A}_i = 0$ and a force task if $\mathcal{A}_i \neq 0$ and in this case, force feedback is applied by $\dot{\mathbf{p}}_i = \mathcal{A}_i(\mathbf{w}_i^d - \mathbf{w}_i)$. In experiments, we apply this task to the robot's right hand, which is in contact with the wall.

CoM task

CoM task takes a desired position $\mathbf{c}^d \in \mathbb{R}^3$, velocity $\dot{\mathbf{c}}^d \in \mathbb{R}^3$ and acceleration $\ddot{\mathbf{c}}^d \in \mathbb{R}^3$ of the CoM in world frame as target. This is a standard second-order task. Internally, it will realize:

$$\ddot{\mathbf{c}} = \mathbf{K}_c(\mathbf{c}^d - \mathbf{c}) + \mathbf{B}(\dot{\mathbf{c}}^d - \dot{\mathbf{c}}) + \ddot{\mathbf{c}}^d \tag{2.49}$$

where B is the task damping (usually $2\sqrt{\mathbf{K}_c}$) and $\dot{\mathbf{c}} = \mathbf{J}_{\text{com}}\dot{\mathbf{q}}$ is the CoM velocity where $\mathbf{J}$ shows CoM Jacobian matrix.

Finally, we regulate the weight distribution between the two feet on the ground while the robot's end-effector acts on the contact surface. For this purpose, we use foot force difference control (FFDC).

Foot force difference control Kajita et al. (2010), Kajita et al. (2013)

This control scheme applies to two co-planar end-effectors, which are the balancing contacts of the robot. As a standing posture in our case, the contacts are the left and

right feet. FFDC servos both CoP and normal force targets of each foot. The force difference of target value $(f_{\text{lf}}^{z,tar} - f_{\text{rf}}^{z,tar})$ provided by the centroidal QP is regulated to the measured value $(f_{\text{lf}}^{z,mes} - f_{\text{rf}}^{z,mes})$ by applying damping control to a virtual offset z. FFDC can be implemented as:

$$\dot{z}_{\text{lf}} = \dot{z}_{\text{lf}}^{d} - 0.5v_f + 0.5v_p \tag{2.50}$$

$$\dot{z}_{\text{rf}} = \dot{z}_{\text{rf}}^{d} + 0.5v_f + 0.5v_p \tag{2.51}$$

$$v_f \equiv A_f((f_{\text{lf}}^{z,tar} - f_{\text{rf}}^{z,tar}) - (f_{\text{lf}}^{z,mes} - f_{\text{rf}}^{z,mes})) \tag{2.52}$$

$$v_p \equiv A_p((p_{\text{lf}}^{z,tar} + p_{\text{rf}}^{z,tar}) - (p_{\text{lf}}^{z,sur} + p_{\text{rf}}^{z,sur})) \tag{2.53}$$

where the superscripts $\circ^{tar}$ and $\circ^{mes}$ point to the target and measured values of the respective variable. p is the center of pressure (CoP) of the sole, and $\circ^{sur}$ refers to the surface pose of the sole center. The velocity term v_f performs a damping control that raises the foot with high normal force and drops the other. This velocity is tuned by the admittance gain A_f. The other velocity term v_p is supplemented for vertical drift coverage. The frequency gain A_p set to 1 Hz in practice.

2.2.6 Controller Schematic

According to the provided content, we present an overall scheme of the controller in this section. First, as shown in the Fig. 2.3, the FSM determines the planned states. Then, according to these states, CSA is computed in real-time for each iteration of the designed scenario. Ultimately, we send the CoM reference to the Centroidal QP as a safe position in the sense of the robot's balance.

This QP calculates the CoM target and contact wrenches, considering the robot's dynamic balance and desired tasks. The outputs of the Centroidal QP are then sent to the whole-body QP for the online execution of the controller. Next, the whole-body QP realizes the CoM and force targets within a task-space formulation. Finally, the joint commands are sent to the real robot, and the measured and estimated states of the robot are directed to the planner.

2.3 Experiments and Results

We implemented the proposed methodology based on Centroidal QP and kept the balance through several experiments with the HRP-4 humanoid robot. In this section, we present three of these experiments and show the performance of our controller in pushing and wiping scenarios. So, all the scenarios are in multi-contact condition and consist of fixed (co-planar) and sliding contacts.

The baseline for our study is considering a fixed position for the robot's CoM while executing the scenario. Because, as mentioned before, the existing methods use pre-computation to assess the balance region. Without pre-computations, we can set a constant position for the robot's CoM, which is in the middle of the supporting foot contacts.

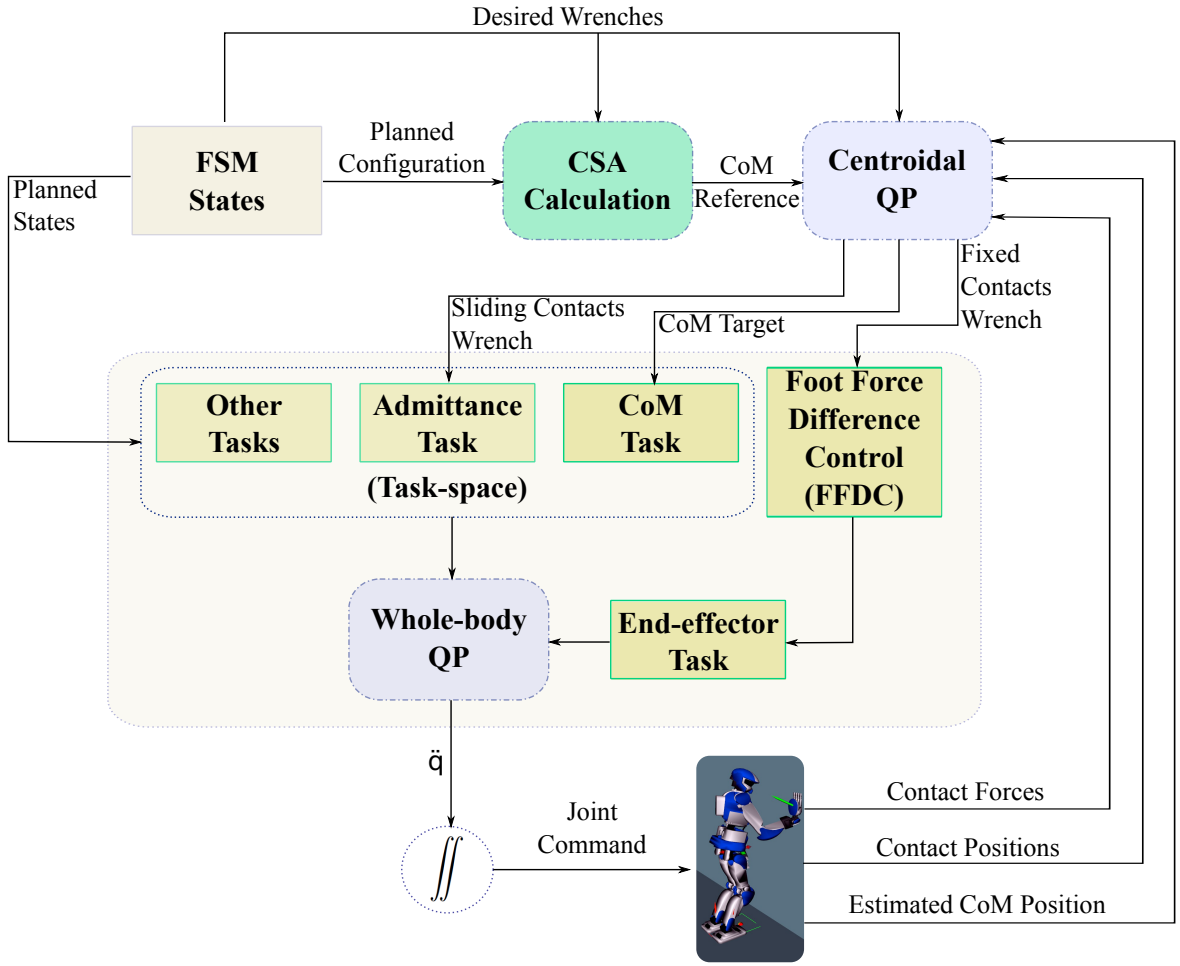

FIGURE 2.3 – *Schematic of the overall task-space control framework with Centroidal QP.*

For example, Figure 2.5 shows the robot scrabbling to increase the normal force on the hand contact and achieve the target force of 60 N but fails. This failure is because of the kinematic chain, which tries to keep CoM in the middle, and the controller is not taking the third contact into account in the balance criteria. Force tracking of admittance control shows that the failure occurs in less than 20 N normal force, and the robot cannot achieve the target force with this posture anymore.

On the other hand, we did the same experiment with the proposed controller. The scenario aims to push against the wall with the maximum force of 50 N. The Fig. 2.7 shows successful tracking of the normal force with the generated posture of the robot due to the position of CoM and kinematics of the robot. The black mat under the robot's feet is to have the desired friction of the fixed contacts, which helps to apply high normal forces like this 50 N.

Also, the trajectory of CoM while increasing and decreasing the right-hand force is shown in Fig. 2.8. As you can see, the position of the CoM moves forward by increasing the normal target force and lays back by decreasing the force without losing the balance. It is a more human-like performance enabled by taking all contacts into account while evaluating the balance criteria in real-time.

The last experiment deals with sliding contact and shows the controller's perfor-

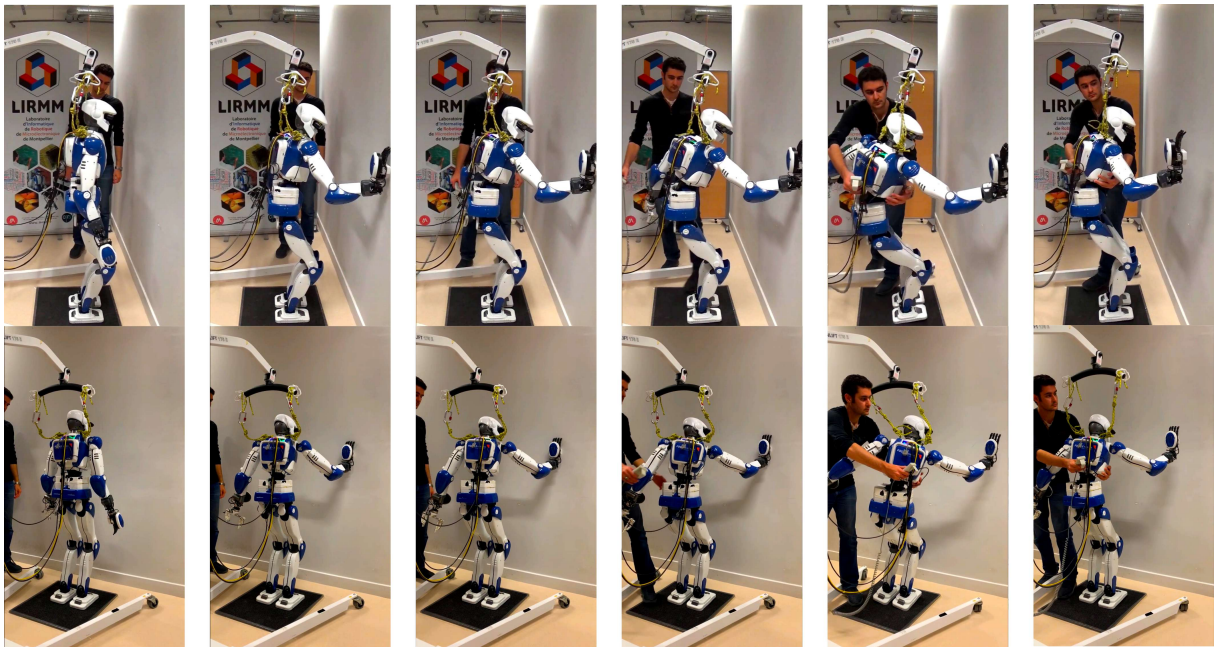

FIGURE 2.4 – *Pushing the wall using fixed CoM.*

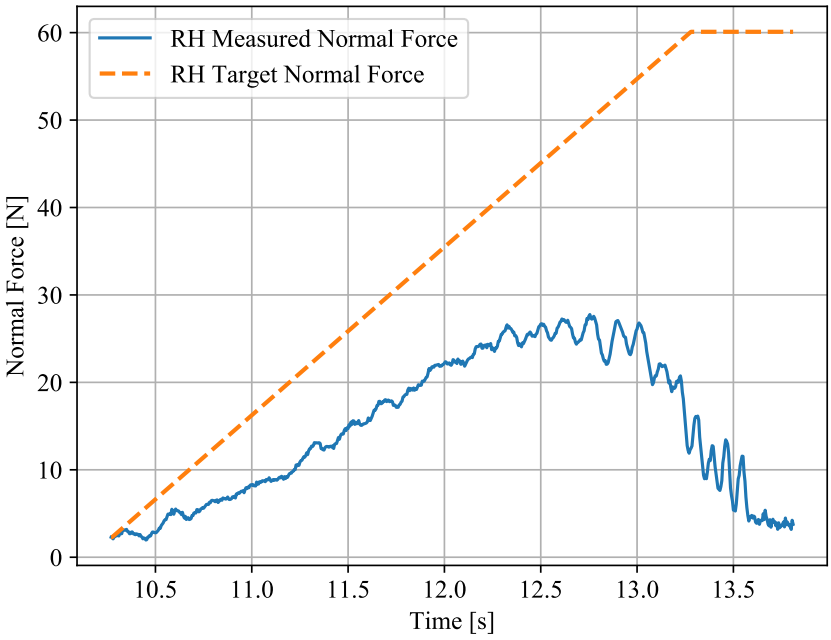

FIGURE 2.5 – *Normal force tracking while pushing the wall using fixed CoM.*

mance while wiping a vertical surface with a normal force of 30 N on sliding contact. It starts with establishing contact with the wall by zero force and increasing it to the desired quantity. This step is the same as the previous pushing experiment. Afterward, the robot starts to wipe along with keeping the CoM inside the CSA. Fig. 2.10 shows the normal force tracking of sliding contact from the beginning of the scenario until removing the contact as the final FSM state.

In this experiment, the normal force is set to 30 N. We use the admittance task of the

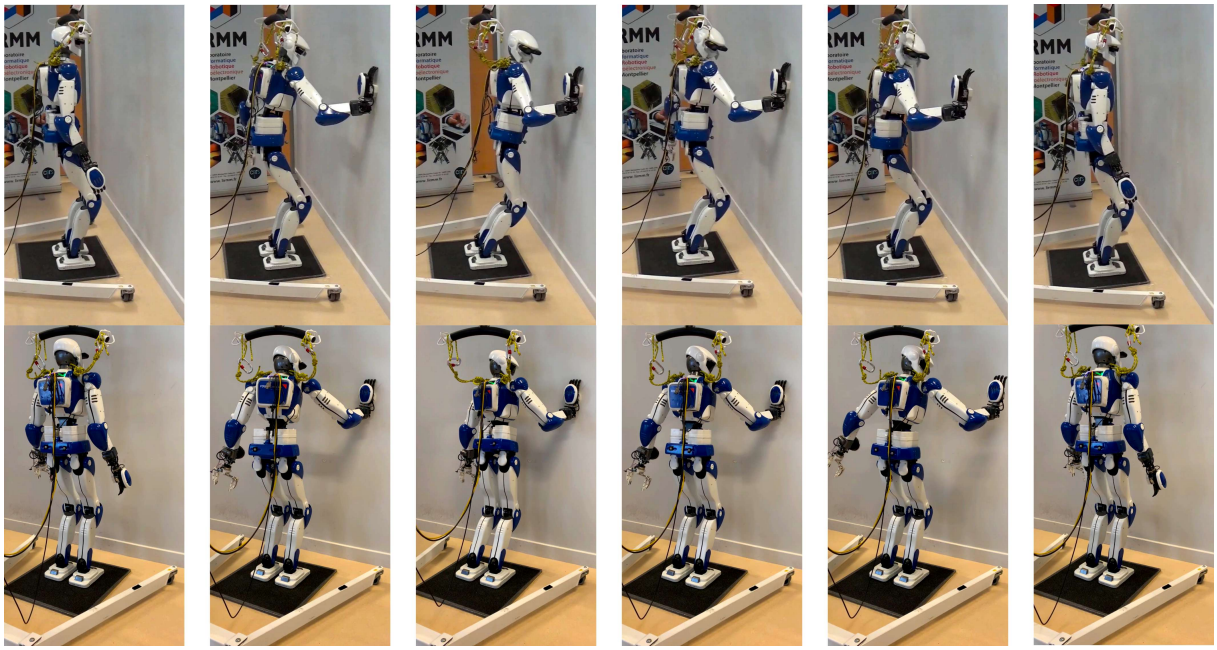

FIGURE 2.6 – *Pushing the wall using the proposed method.*

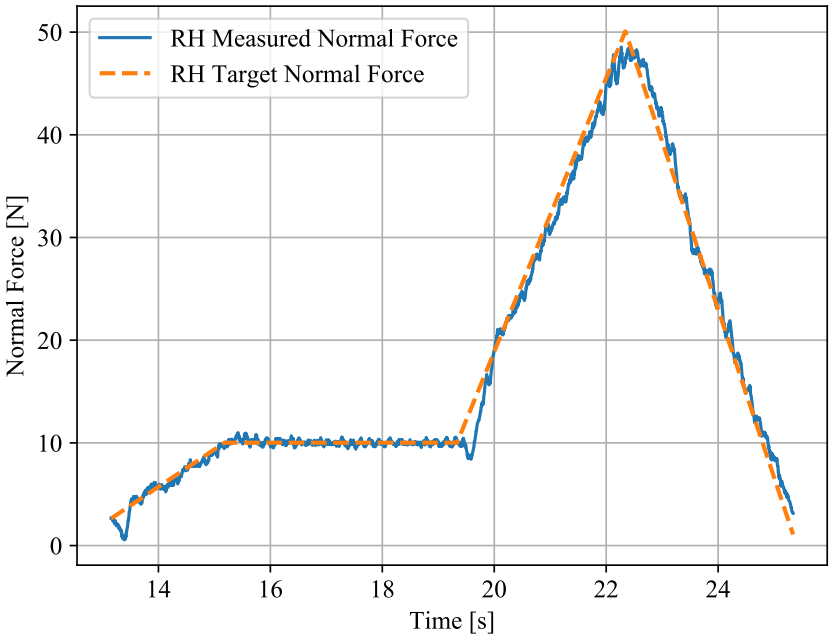

FIGURE 2.7 – *Normal force tracking while pushing the wall using our strategy.*

controller as a force control strategy. The wiping motion starts wiping from 16^{th} second after reaching the desired normal force. There is a jerky force tracking when starting the wiping motion because of the sudden switch between the fixed and contact mode. The error happens at the beginning of the plot, which is the moment of establishing contact. After these jumps in force tracking, the normal force converges perfectly to the target value. Videos of the experiments [4] and the open-source code of the controller [5]

4. https://www.youtube.com/watch?v=Wai-Lp4e5FE
5. https://github.com/SaeidSamadi/SlidingContact_CentroidalQP

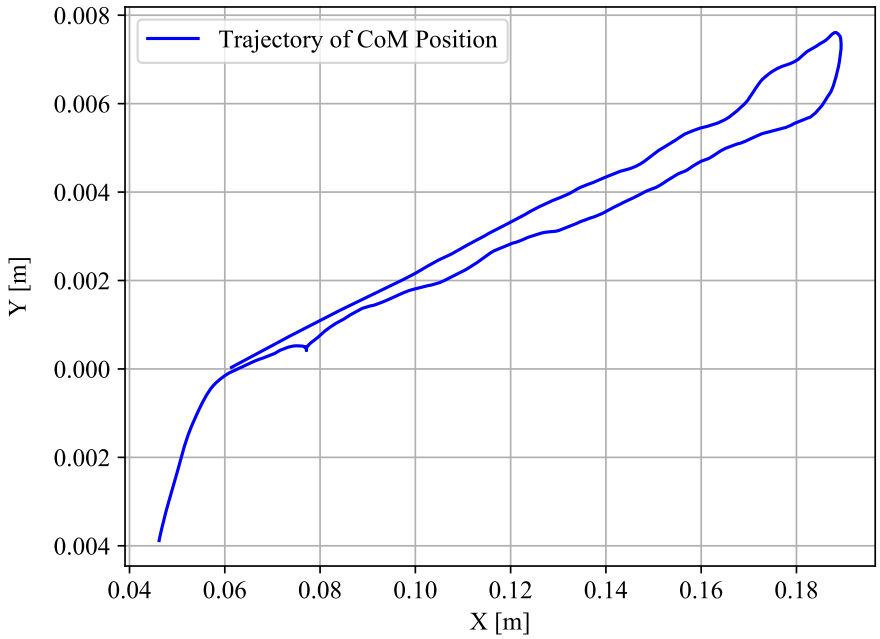

FIGURE 2.8 – *Position of CoM while pushing the wall*

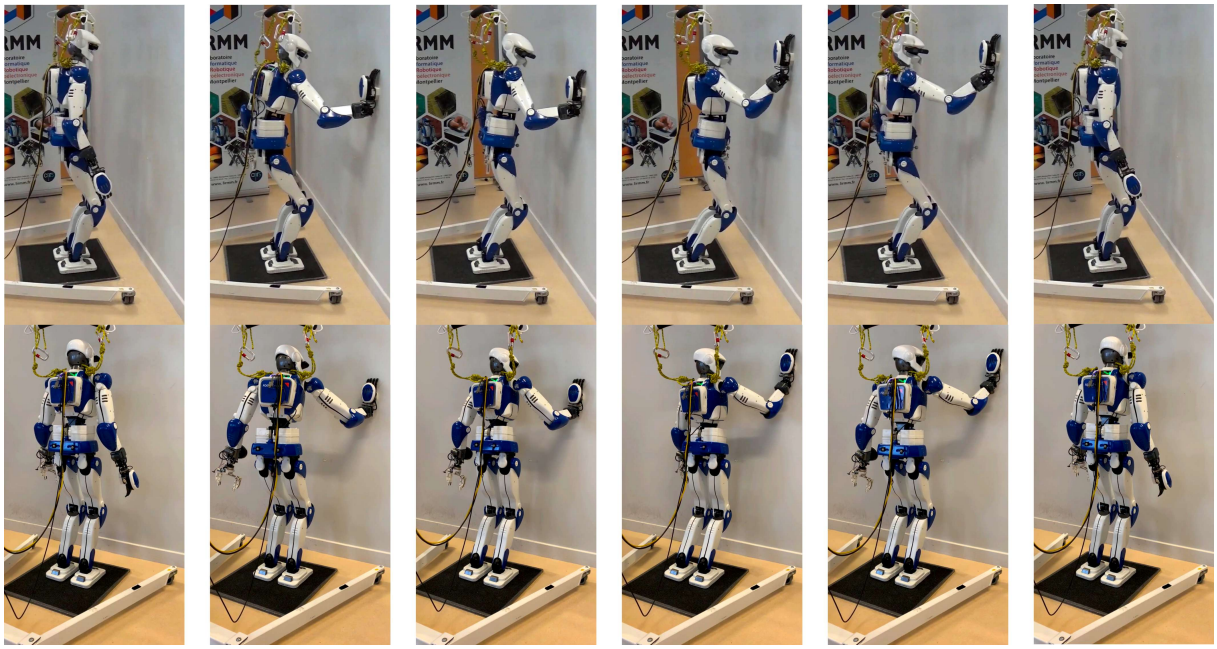

FIGURE 2.9 – *Wiping the wall using proposed strategy.*

are available online.

The experiments show that the proposed methodology keeps the balance of the robot in multi-contact settings. Also, the experiments include sliding contacts. All the implementations on the robot were online, and there was no pre-computation of the balance region. However, the limitation of the method is the co-planarity of the fixed contacts. As you noticed from the experiments, feet were the fixed contacts, and they were on the same plane (ground). For the pushing scenario, we kept the sliding as-

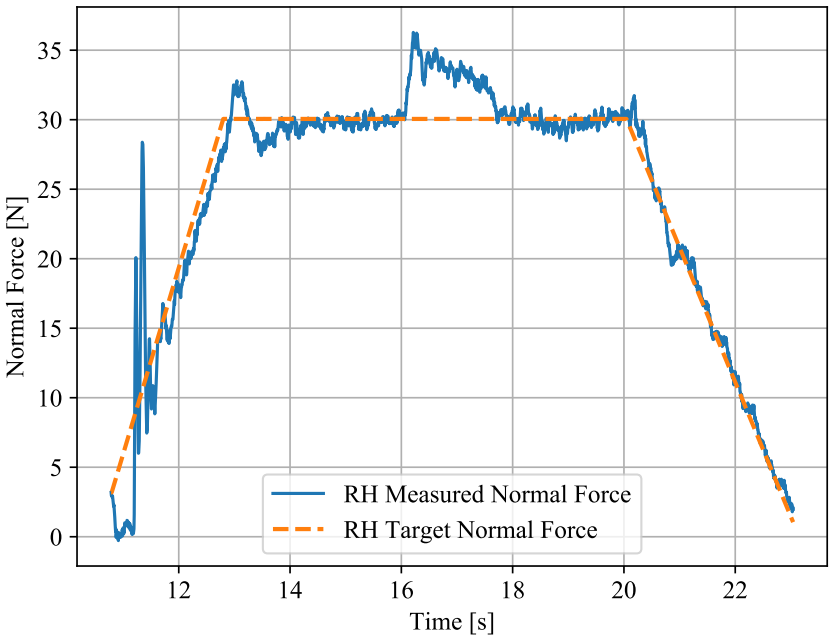

FIGURE 2.10 – *Normal force tracking while wiping the wall using proposed strategy*

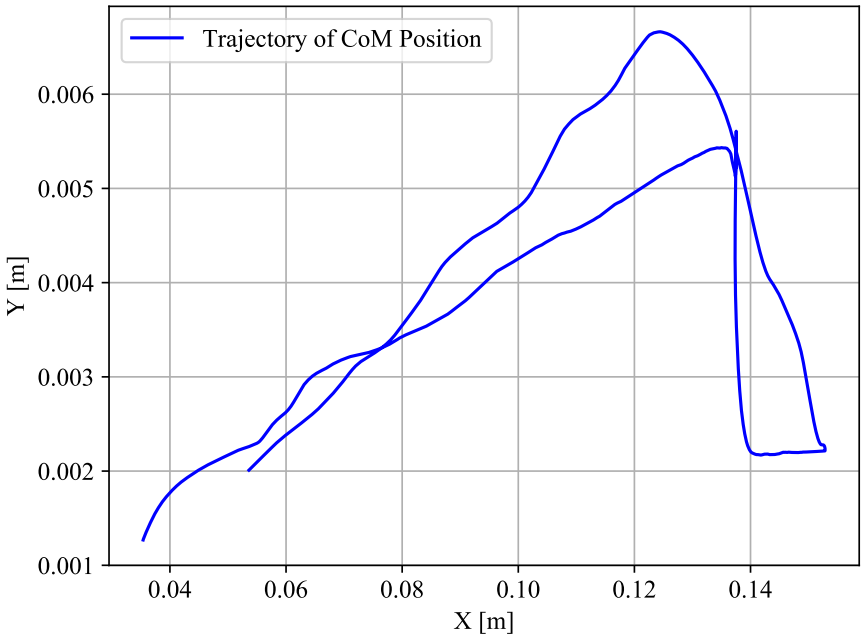

FIGURE 2.11 – *Position of CoM while wiping the wall*

sumption of the right hand with zero tangential velocity.

2.4 Conclusion

In this chapter, we studied humanoids' equilibrium criteria based on the position of the CoM in a multi-contact localized motion setting. Furthermore, a methodology for constructing balance region (CSA) in multi-contact conditions is introduced. Our method computes the area under limiting assumptions in a closed-form analytical solution. This solution can be implemented online thanks to its low computational cost.

Our method applies in a multi-contact setting where a subset of contacts is fixed whereas some of the remaining subset is allowed to slide to achieve a sliding task. For setting the CoM inside the CSA, we use Centroidal QP with contact and dynamic balance constraints. In this QP, the sliding and fixed conditions of the selected contacts are considered. The outputs of the QP are the CoM position and wrench distribution of the contacts.

We assessed our developments through real experiments on the HRP-4 humanoid robot. The latter achieves the desired configuration and tasks by implementing our whole-body task-space controller. This is done through the whole-body QP and implemented the desired CoM position and contact wrenches in task space.

Simulations and experiments show that our balance control is valid for both fixed and sliding contacts in practice. Also, by using our method, the robot can achieve a proper body configuration to reach target forces in contact without losing balance. However, the transition between fixed and sliding contact modes is still challenging to solve, as it causes errors in target force tracking.

In the next chapter, we tackle the main limitation of the proposed method: coplanarity of the fixed contacts, among other light technical shortcomings. Accordingly, we introduce a technique that can be applied in real-time and has no limitation of the chosen multi-contact configuration. Furthermore, this method also allows switching between any contact to be sliding or fixed at will. Also, we implement a simple friction estimation for the sliding contacts in order to improve the sliding performance during the control.

CHAPTER 3

REGION-FREE MULTI-CONTACT BALANCE CONTROL

In the previous chapter, we developed an analytical closed-form solution for humanoid balance in multi-contact settings including fixed and sliding contacts. Nevertheless, this was possible because the fixed contacts are assumed to be co-planar. This is very limiting in many situations; for example Kheddar et al. (2019) reported a tasks (bracket gluing on an airplane fuselage) where fixed contacts (feet and robot gripper's palm) are not coplanar when the other arm is achieving a light sliding due to positioning a glueing the bracket.

In this chapter we get rid of the previous limitation (co-planarity of fixed contacts) and propose a whole-body control strategy for humanoid robots in multi-contact settings, enabling switching between fixed and sliding contacts at will, under active dynamic balance. We compute, in real-time, a safe CoM position and wrench distribution of the contact points based on the so-called Chebyshev center method.

Our solution is formulated as a quadratic programming problem without the need for *a priori* computation of balance regions. We assess our approach with experiments highlighting switches between fixed and sliding contact modes in non-coplanar multi-contact configurations. A humanoid robot demonstrates such contact interchanges from fully-fixed to multi-sliding and also shuffling of the foot.

Our proposed experimental scenario, with the HRP-4 humanoid robot, illustrates the performance of our control scheme in achieving the desired forces, CoM position attractor, and planned trajectories while actively maintaining multi-contact balancing. Beside, the computational cost performance enables online planning and whole-body control in a closed-loop fashion.

3.1 Background

Two main ingredients shall be considered for a stable dynamic balance of humanoid robots Featherstone (2014): (i) a good control of the robot/environment interaction forces, and (ii) a good control of the dynamic motion, governed by Newton-Euler

equations, contact constraints and balancing of the external wrench. To maintain the robot's dynamic balance, we need to incorporate all contacts in the computations and avoid excluding the interacting contacts.

Standing or walking with a stable balance on flat terrains Wieber (2006); Brasseur et al. (2015) can be achieved by maintaining the ZMP inside its contacts support area Senoo and Ishikawa (2017); the latter being the convex hull of all the contact points. Whereas for non-coplanar multi-contact postures and motions, sustaining stable balance is less trivial to achieve.

3.1.1 Related Works and Contribution

Enforcing dynamic balance of humanoid robots in multi-contact non-coplanar configurations can be addressed with one of the following inclusions:

- constraining the gravito-inertial wrench within the GIWC, e.g. Caron et al. (2015a);
- building a safe region (convex polyhedron) for the CoM concerning a given CoM acceleration convex set and contact friction cones, e.g. Audren and Kheddar (2018);
- building a safe region (convex polyhedral cone) within which the CoM acceleration shall safely lie for a given CoM convex set and contact friction cones, e.g. Caron and Kheddar (2016).

The fast computation and efficiency of these balance equilibrium regions have been thoroughly investigated. For this purpose, numerous computational procedures have been introduced, which have their benefits and limitations.

The proposed method in Caron et al. (2015a) fulfilled the multi-contact balance criterion by computing the GIWC for each stance. In this approach, there is no need to update the GIWC for fixed contact stances. However, GIWC needs to be re-computed at each iteration in the case of moving or sliding contacts. Unfortunately, since calculating the GIWC is computationally expensive, it is impossible to use this method in closed-loop control.

In a recent work, Abi-Farraj et al. (2019) challenged shortcoming related to the calculation cost. They are specifying two different sets of contacts in multi-contact motion settings: *interacting* (hence moving) contacts, and *balancing* contacts that are chosen and constrained to be fixed (i.e. static contacts). Subsequently, only balancing contacts are used to compute the GIWC. Other contacts are considered as external forces induced by tasks to be balanced altogether with the robot dynamics. This approach is appropriate when the external contacts are concerned with holding a free-floating object.

However, Abi-Farraj et al. (2019) is limiting in all the other cases that can exploit task-induced contacts (including the moving ones) for balance (e.g. pushing an object, sliding, etc.). This is because with Abi-Farraj et al. (2019), task contacts won't be allowed to contribute to balance, and this is clearly not the way we as humans perform. By

this categorization of contacts (even if switches are possible), the multi-contact GIWC pre-calculation is made on a subset of contact (those fixed) for balance, hence relatively tractable; yet it excludes all other contacts that could eventually contribute to balance.

Computation efficiency also exists for the CoM-support regions Audren and Kheddar (2018). It was leveraged using 3D morphing techniques between two regions Audren et al. (2016) but without guarantee on the balance validity all along the morphing shape pathway between the two regions. To control a humanoid in multi-contact, Sentis (2010) used the virtual-linkage model. Their method consists of constructing a multi-contact CoM area as the envelope of valid points.

In our recent previous work Samadi et al. (2020) as explicitely described in the last chapter, we introduced an analytical solution to compute the CoM-support area in real-time. However, these developments apply only when the fixed contacts are coplanar. This coplanarity can not be the case for general and more complex scenarios.

We propose an alternative formulation that allows balance criteria to be used in closed-loop control. This formulation applies to moving/sliding and fixed contacts. It also permits on-the-fly switching between these contact modes. Our approach do not separate balancing and interacting contacts with different contact modes, when the latter can contribute to balance (and *vice versa*, i.e. balance contribute to achieving the task). Our approach distinguishes from existing work as follows:

- No need for constructing or pre-computing explicitly the multi-contact balance region (GIWC);
- Fast computation performances enabling real-time closed-loop control;
- Calculating CoM position and wrench distribution of contacts using the Chebyshev center;
- Covering all types of contact modes (e.g. multi-sliding contacts) without any of the limitations pointed in Samadi et al. (2020);
- contrary to Abi-Farraj et al. (2019), we do not exclude interacting contacts to contribute to dynamic balance stability.

3.1.2 Centroidal Model

Same as the previous chapter, we consider semi-dynamic motion scenarios without locomotion as stated by Eq. (2.1). The two main approaches for deriving the equation of motion of the robotic systems are through Euler-Lagrange or Newton-Euler formulations. We leverage the latter for deriving the static equilibrium of the robot for l limbs in contact with the environment:

$$\mathbf{w}^g + \sum_{i=1}^{l} \mathbf{w}_i^c = 0 \tag{3.1}$$

where $\mathbf{w}^g \in \mathbb{R}^6$ and $\mathbf{w}_i^c \in \mathbb{R}^6$ are gravity wrench and the i^{th} contact wrench in the world frame respectively, and $\mathbf{w} = [\mathbf{f} \;\; \boldsymbol{\tau}]^T$. Note that in Eq. (3.1), the CoM acceleration is not

appeared due to the static assumption of the motion. Gravity and contact wrenches are specified in the following form:

$$\mathbf{w}^g = \begin{bmatrix} \mathbf{f}^g \\ \mathbf{c} \times \mathbf{f}^g \end{bmatrix} \tag{3.2a}$$

$$\mathbf{w}_i^c = \begin{bmatrix} \mathbf{f}_i^c \\ \mathbf{p}_i \times \mathbf{f}_i^c + \boldsymbol{\tau}_i^c \end{bmatrix} \tag{3.2b}$$

In the above equations $\mathbf{f}^g = [0 \;\; 0 \;\; mg]^T$ is the gravity force, $\mathbf{c} = [c^X \;\; c^Y \;\; c^Z]^T$ the position of the CoM, and contact points $\mathbf{p}_i$ are given with respect to a global frame. Note that the contact wrenches are mapped from the local to the global frame by rotation matrix $[\mathbf{R}]_i \in \mathbb{R}^{6\times6}$:

$$\mathbf{w}_i^c = [\mathbf{R}]_i \, {}^l\mathbf{w}_i^c \tag{3.3}$$

where ${}^l\circ$ denotes the contact point in the local frame, the wrenches without this notation refer to the global frame.

We consider the following state variables to be computed at each iteration:

$$\mathbf{Y} = [\mathbf{c} \;\; \mathbf{w}_1^c \;\; \mathbf{w}_2^c \;\; \ldots \;\; \mathbf{w}_l^c] \tag{3.4}$$

which is comparable with the decision variables represented by Eq. (2.20) containing the desired number of contacting limbs and no restriction on the normal direction of CoM position.

Sliding and equality bounds on contact forces

For every contact of the robot, we determine the wrench. Equation Eq. (3.2) can be re-written as:

$$\mathbf{w}^g = \mathbf{A}^g\mathbf{c} - \mathbf{b}^g \tag{3.5}$$

$$\mathbf{w}_i^c = \mathbf{A}_i^c \, {}^l\mathbf{w}_i^c \quad \text{where } i = 1, \ldots, l \tag{3.6}$$

On the other hand, the sliding condition of the desired contact comes with additional equality constraints as stated in Samadi et al. (2020). In this chapter, we are aiming to cover the generic configurations of the robot. Therefore, contrary to the previous chapter, we need to write all equations based on local frames and rotation matrices. So, the normal contact force (f_i^z) in local frame for sliding is aligned to the normal of the local surface frame by convention. The dynamic friction coefficient (μ_i) of each sliding contact is estimated online during the motion and updated at each iteration.

The force along other axes (f_i^x and f_i^y) of the tangent space is derived from the pre-defined velocity and trajectory of the sliding motion. Let,

$${}^l\mathbf{f}_i = \begin{bmatrix} f_i^x & f_i^y & f_i^z \end{bmatrix}^T \quad i = 1, \ldots, s, \tag{3.7}$$

be the sliding contact forces in the local frame, and s being the number of sliding contacts. We can write in a matrix form

$${}^l\mathbf{f}_k = \begin{bmatrix} 0 & 0 & \mu_k^x \\ 0 & 0 & \mu_k^y \\ 0 & 0 & 0 \end{bmatrix} {}^l\mathbf{f}_k + \begin{bmatrix} 0 \\ 0 \\ f_k^z \end{bmatrix} \tag{3.8}$$

or,

$$\begin{bmatrix} 1 & 0 & -\mu_k^x \\ 0 & 1 & -\mu_k^y \\ 0 & 0 & 1 \end{bmatrix} {}^l\mathbf{f}_k = \begin{bmatrix} 0 \\ 0 \\ f_k^z \end{bmatrix} \tag{3.9}$$

giving the k^{th} sliding contact velocity as

$$\mathbf{v}_k = v_k^x i + v_k^y j,$$

and

$$\mu_k^x = \mu_k \alpha_k^x,$$
$$\mu_k^y = \mu_k \alpha_k^y,$$

from which

$$\alpha_k^x = \frac{v_k^x}{\|\mathbf{v}_k\|},$$
$$\alpha_k^y = \frac{v_k^y}{\|\mathbf{v}_k\|},$$

and μ_k is the k^{th} dynamic friction coefficient. We can write Eq. (3.9) in a compact form:

$$\mathbf{C}\ {}^l\mathbf{f}_k = \mathcal{K} \tag{3.10}$$

$\det(\mathbf{C}) = 1$, $\mathbf{C}$ is an invertible matrix, hence:

$${}^l\mathbf{f}_k = \mathbf{C}^{-1}\mathcal{K} \tag{3.11}$$

Also, by using matrix transforms, we change the coordinate to the global frame:

$$\mathbf{f}_k^c = [\mathbf{R}_k]_{3\times3}\mathbf{C}^{-1}\mathcal{K} \tag{3.12}$$

which can be written using the selection matrix $[\mathbf{S}]_{3\times6} = [I_{3\times3}\ \ 0_{3\times3}]$ as:

$$[\mathbf{S}]\mathbf{w}_k^c = [\mathbf{R}_k]_{3\times3}\mathbf{C}^{-1}\mathcal{K} \tag{3.13}$$

Eq. (3.13) is embedded to the controller along with eqs. Eq. (3.5) and Eq. (3.6), and can be written as:

$$\mathbf{A}_i^{sl}\ {}^l\mathbf{w}_i - \mathbf{b}_i^{sl} = 0; \quad i = 1, \ldots, s. \tag{3.14}$$

This equation is applied to the s sliding contacts with respect to their desired sliding forces. Hence, in this equation ${}^l\mathbf{w}_i$ refers to sliding contacts only.

Fixed contacts

The non-sliding condition of contacts is fulfilled when the contact force lies strictly within the friction cone. Linearized equations for non-sliding conditions were thoroughly discussed in Caron (2015). The equations introduced in previous chapter Eq. (2.31)

are sufficient conditions to avoid slippage and tilting of the contacts in all $\mathbb{R}^6$ coordinate of the local frame. By considering n non-sliding contacts, the inequality constraints are in the following form:

$$\boldsymbol{\Upsilon}_i^{ub}\ {}^l\mathbf{w}_i \leqslant \mathbf{h}_i^{ub} \quad i = 1, \ldots, n \tag{3.15a}$$

$$\boldsymbol{\Upsilon}_i^{lb}\ {}^l\mathbf{w}_i \leqslant \mathbf{h}_i^{lb} \quad i = 1, \ldots, n \tag{3.15b}$$

where superscripts $\circ^{ub}$ and $\circ^{lb}$ show the upper and lower bounds. $\boldsymbol{\Upsilon}_i$ matrices and $\mathbf{h}_i$ vectors are introduced in Eq. (2.38) and Eq. (2.39) in the previous section for both sliding and fixed contacts. Also, $\boldsymbol{\Psi}_i$ enforces inequality constraints on τ_z element of wrenches:

$$\boldsymbol{\Psi}_i^{ub}\ {}^l\mathbf{w}_i \leqslant 0_{4\times 1} \quad i = 1, \ldots, n \tag{3.16a}$$

$$\boldsymbol{\Psi}_i^{lb}\ {}^l\mathbf{w}_i \leqslant 0_{4\times 1} \quad i = 1, \ldots, n \tag{3.16b}$$

For the sliding contacts, the same inequalities as Eq. (3.16) constraints need to be implemented (on the torque of the contact wrenches) to avoid the tilting of the rotational slippages. However, for the contact forces, the equality constraints introduced in Eq. (3.14) need to be considered.

3.2 Optimal Control Framework

As stated in the last section, for the purpose of implementing the controller in multi-contact settings, it is required to inquire about the dynamic balance criteria of the robot during the entire scenario. We need to introduce and practice an optimal control framework for controlling the balance in real-time without any computational and configuration limitations.

In this section, we propose the implementation of the Chebyshev center theorem Beck and Eldar (2007) in a two-level control framework. Inspired from Collette et al. (2007); Samadi et al. (2020) such an implementation can be formulated as a first-level quadratic program (QP) that outputs the CoM position and contact wrenches distribution together with the Chebyshev center and its radius.

The low computation cost of this calculation enables the real-time implementation of the controller. The outputs of the first-level QP are then integrated as task objectives or constraints in a running whole-body task-space controller formulated as a second-level QP Bouyarmane et al. (2019b) (see later Section 3.4). In the following, we present the concept of the Chebyshev center method and implement this method in our problem.

3.2.1 Chebyshev Center

Let $\mathbf{U} \in \mathbb{R}^n$ be a set of inequality constraints describing a bounded polygon, and $\mathbf{x} \in \mathbf{U}$. We introduce $depth$ and $dist$ operators indicating the depth and distance of a

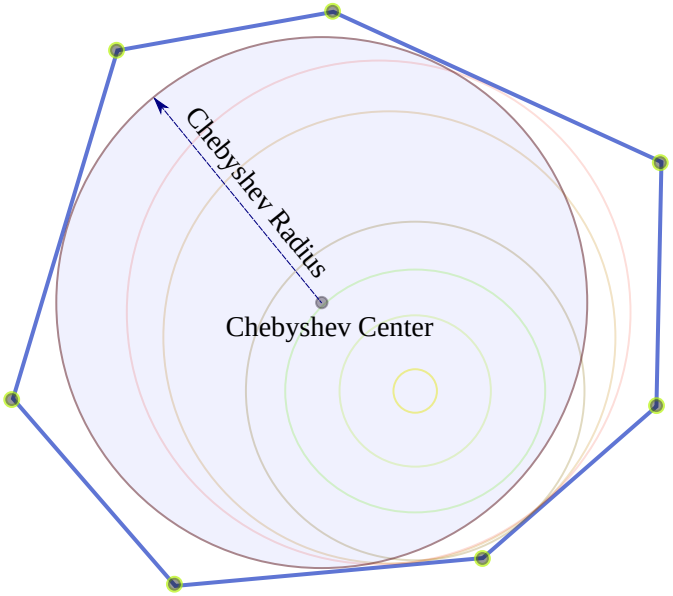

FIGURE 3.1 – *Chebyshev circle enclosed in a polygon.*

point within the bounded set. The depth of the point $\mathbf{x}$ is defined as

$$depth(\mathbf{x}, \mathbf{U}) = dist(\mathbf{x}, \mathbb{R}^n \backslash \mathbf{U}) \tag{3.17}$$

The $dist$ operator shows the distance of $\mathbf{x}$ from exterior of $\mathbf{U}$ and $depth$ operator calculates the radius of the largest ball inside $\mathbf{U}$ and centered on $\mathbf{x}$. So, the *Chebyshev center* is calculated as the argument which results in the maximum radius:

$$\mathbf{x}_{cheb}(\mathbf{U}) = \arg\max \ depth(\mathbf{x}, \mathbf{U}) \tag{3.18}$$

So, as stated, the Chebyshev center of U is the *center of the largest enclosure circle* Amir (1984). Fig. 3.1 illustrates the Chebyshev center and radius of a given polygon. Based on the computations of the Chebyshev center, we do not need to build the vertices of the polygon (i.e., no need for the v-representation of U). Consequently, in concise form, for a point, x in the interior of U, the Chebyshev center $\hat{x}$ is a point among all possible x such that Knitter (1988):

$$\arg\min_{x} \max_{\hat{x} \in U} ||x - \hat{x}||^2 \tag{3.19}$$

In the following, we are introducing the definition of the Chebyshev center for convex sets and Polyhedra.

Chebyshev Center of a Convex Set

For the convex set of $\mathbf{U}$, the depth of this set is a concave function for $\mathbf{x} \in \mathbf{U}$. Accordingly, the computation of the Chebyshev center becomes a convex optimization problem. Suppose a set of convex inequalities defines $\mathbf{U} \in \mathbb{R}^n$ which applies to any bounded non-empty *convex set*:

$$\mathbf{U} = \{\mathbf{x} \mid f_i(\mathbf{x}) \leqslant 0; i = 1, \ldots, n\}, \tag{3.20}$$

where $\mathbf{x}$ is a vector of a given dimension, and n the number of inequalities. These inequalities are valid for all points inside the convex set. Hence, constituent points of

the Chebyshev ball enclosed in the convex set, with center $\hat{x}$ and radius r fulfill the inequalities too. The idea is to compute the largest Chebyshev ball, which satisfies the convex condition Eq. (3.20):

$$\max\ r \tag{3.21a}$$

$$\text{s.t. } h_{i=1,\dots,n}(\mathbf{x}, r) \leqslant 0 \tag{3.21b}$$

where the function h_i is defined as:

$$h_{i=1,\dots,n} = \sup_{\|\mathbf{a}\| \leqslant 1} f_{i=1,\dots,n}(\mathbf{x} + r\mathbf{a}) \leqslant 0 \tag{3.22}$$

The Eq. (3.21b) is an optimization problem. Each function of h_i is convex and elected as the pointwise maximum of a class of convex functions of $\mathbf{x}$ and r. The supremum form of Eq. (3.22) allows accessing all points within the ball according to the variable $\mathbf{a}$.

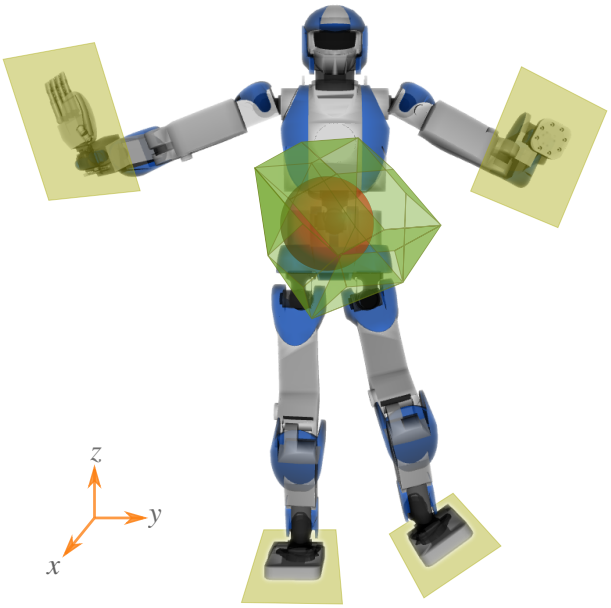

FIGURE 3.2 – *Illustration of the Chebyshev center of an enclosed Euclidean ball within a multi-contact balance GIWC.*

Chebyshev Center of a Polyhedron

For a polytope, the inequalities are in the form of $\{\boldsymbol{\alpha}_i^T \mathbf{x} - \boldsymbol{\beta}_i \leqslant \mathbf{0},\ i = 1, \dots, n\}$. So the condition Eq. (3.22) is modified as following:

$$h_{i=1,\dots,n} = \sup_{\|\mathbf{a}\| \leqslant 1} \boldsymbol{\alpha}_i^T (\mathbf{x} + r\mathbf{a}) - \boldsymbol{\beta}_i = \boldsymbol{\alpha}_i^T \mathbf{x} + r \|\mathbf{a}\|_* - \boldsymbol{\beta}_i \tag{3.23}$$

Note that by substituting the inequality of the *polytope* into Eq. (3.21b), the term $\boldsymbol{\alpha}_i^T r\mathbf{a}$ appears. Supremum of this term will provide $r \|\boldsymbol{\alpha}_i\|_*$. The trace norm, $\|\|_*$, is introduced for computing the norm of the matrices. In case of vectors, one can use the simple

l_1 or l_2 vector norms. Consequently, the optimization problem is:

$$\max r \tag{3.24a}$$
$$\text{s.t. } \boldsymbol{\alpha}_i^T \mathbf{x} + r \left\| \boldsymbol{\alpha}_i \right\| - \boldsymbol{\beta}_i \leqslant \mathbf{0} \quad i = 1, \ldots, n \tag{3.24b}$$
$$r \geqslant \mathbf{0} \tag{3.24c}$$

Fig. 3.2 illustrates the link between the above generalities concerning the Chebyshev center and humanoid balance. The polyhedron represents the GIWC that can be obtained as in e.g. Abi-Farraj et al. (2019). The advantage of computing the Chebyshev center instead of the GIWC is undeniably the speed. The price to pay for the speed is the conservativeness of the balance region, as can clearly be seen in Fig. 3.2.

3.2.2 Chebyshev Quadratic Programming

Recall from Eq. (3.4) that the decision variables are noted as $\mathbf{Y} = [\mathbf{c} \ \mathbf{w}_{i=1,\ldots,l}]^T$ where $\mathbf{Y} \in \mathbb{R}^{3+6k}$. The QP formulation is structured based on the equality and inequality constraints introduced in section 3.1.2 expressed as:

$$\mathbf{A}\mathbf{Y} = \mathbf{b} \tag{3.25a}$$
$$\mathbf{G}\mathbf{Y} \leqslant \mathbf{h} \tag{3.25b}$$

whereas:

$$\mathbf{A} = \begin{bmatrix} \mathbf{A}^g & \mathbf{A}^c \\ \mathbf{0}_{6n\times 3} & \mathbf{A}^{sl} \end{bmatrix}_{(6+6n)\times(3+6k)} \tag{3.26}$$

and the matrices $\mathbf{A}^c$ and $\mathbf{A}^{sl}$ are defined as:

$$\mathbf{A}^c = \begin{bmatrix} \mathbf{A}_1^c & \ldots & \mathbf{A}_k^c \end{bmatrix}_{6\times 6k} \tag{3.27}$$
$$\mathbf{A}^{sl} = [\mathrm{diag}(\mathbf{A}_i^{sl})]\boldsymbol{\rho}^{sl};\ i = 1, \ldots, n \tag{3.28}$$

The equation above contains a selection matrix $\boldsymbol{\rho}^{sl}_{6n\times 6k}$ for the elements related to the sliding contacts in the $\mathbf{A}^{sl}$ matrix and $\mathrm{diag}()$ refers to the diagonal matrix structure. The rest of the parameters of Eq. (3.25) are defined as:

$$\mathbf{b} = \begin{bmatrix} -\mathbf{b}^g & \mathbf{b}_1^{sl} & \ldots & \mathbf{b}_n^{sl} \end{bmatrix}^T_{1\times 7n} \tag{3.29}$$
$$\mathbf{G} = [\mathrm{diag}(\boldsymbol{\Upsilon}_i, \boldsymbol{\Psi}_i)]_{20k\times 10k}\boldsymbol{\rho}^G;\ i = 1, \ldots, k \tag{3.30}$$
$$\mathbf{h} = \begin{bmatrix} \mathbf{h}_i^{ub} & \mathbf{h}_i^{lb} & \mathbf{0}_{1\times 8k} \end{bmatrix}^T_{1\times 20k};\ i = 1, \ldots, k \tag{3.31}$$

and $\boldsymbol{\rho}^G_{20k\times 3+6k}$ is the selection matrix for the $\mathbf{G}$ matrix.

For maximizing the radius and selecting the optimal Chebyshev center, inequality constraint Eq. (3.25b) is modified in the following form, based on Eq. (3.24b), in presence of Chebyshev radius r:

$$\mathbf{G}\mathbf{Y} + r\boldsymbol{\xi} \leqslant \mathbf{h} \tag{3.32}$$

where $\boldsymbol{\xi} \in \mathbb{R}^{20k}$ is a vector which consists of the norm of the rows of $\mathbf{G}$ matrix separately:

$$\boldsymbol{\xi} = [\xi_1,\ \xi_2,\ \ldots,\ \xi_{20k}] \tag{3.33}$$
$$\xi_j = \|\mathbf{G}(j,:)\|\ ;\ j = 1, \ldots, 20k \tag{3.34}$$

and the operator $(j,:)$ shows the j^{th} row of the matrix. The vector $\boldsymbol{\xi}$ in Eq. (3.32) is equivalent to the vector $\|\boldsymbol{\alpha}\|$ where the i-th element of the vector

$$\boldsymbol{\alpha}(i) = \boldsymbol{\alpha}_i\ \forall i \in \{1, \ldots, n\}$$

in Eq. (3.24b). This way, we aim at maximizing the Chebyshev radius by taking into account all inequalities without the need to compute the GIWC or any balance region. The decision variables of this first-level QP are the position of CoM, wrench distribution, and r. Next, we modify the vectors and matrices in order to include the Chebyshev radius within the decision variables as follows:

$$\mathbf{X} = [\mathbf{Y}\ \ r]^T \tag{3.35}$$
$$\mathbf{A}^* = [\mathbf{A}\ \ 0] \tag{3.36}$$
$$\mathbf{G}^* = \begin{bmatrix} \mathbf{G} & \boldsymbol{\xi} \\ \mathbf{0} & -1 \end{bmatrix} \tag{3.37}$$
$$\mathbf{h}^* = [\mathbf{h}\ \ 0]^T \tag{3.38}$$

Maximizing the Chebyshev radius is equivalent to minimizing $(-r)$. Other objectives of the QP can be:

- Setting the current position of the CoM as a target for the next iteration (smoothing CoM trajectory)
- Minimizing the wrench distribution: sharing the load on non-constrained (contact) force.

These objectives can be defined through $\mathbf{X}_{\text{des}} = [\mathbf{Y}_{\text{des}}\ \ r_{\text{des}}]$, and the optimization framework writes:

$$\min_{\mathbf{X}}\ \ \|\mathbf{X} - \mathbf{X}_{\text{des}}\|^2 - r\ \equiv\ \frac{1}{2}\mathbf{X}^T\mathbf{P}\mathbf{X} + \mathbf{q}^T\mathbf{X} \tag{3.39a}$$
$$\mathbf{G}^*\mathbf{X} \leqslant \mathbf{h}^* \tag{3.39b}$$
$$\mathbf{A}^*\mathbf{X} = \mathbf{b} \tag{3.39c}$$

where

$$\mathbf{P} = 2\mathcal{Q} \tag{3.40}$$
$$\mathbf{q} = [\mathbf{Y}_{\text{des}}\ \ -1] \tag{3.41}$$

We prioritize the solution of the QP by using a weight matrix $\mathcal{Q}_{(4+6k)\times(4+6k)}$ with chosen weights on the corresponding decision variables. The weights are implemented

through the diagonal elements of the $\mathcal{Q}$ matrix. However, we do not set any target for the Chebyshev radius.

We need to adopt a low computation weight for r_{des}. Because, there is no target given for the Chebyshev radius. On the other hand, we keep this decision variable in the formulation to maximize it. That is to say:

$$\min_{\mathbf{X}} \quad \|\mathbf{X} - \mathbf{X}_{\text{des}}\|^2 - \mathbf{r} \tag{3.42}$$

with the computations, we have:

$$\begin{aligned}\|\mathbf{X} - \mathbf{X}_{\text{des}}\|^2 - \mathbf{r} &= (\mathbf{X} - \mathbf{X}_{\text{des}})^T \mathcal{Q} (\mathbf{X} - \mathbf{X}_{\text{des}}) - \mathbf{r} \\ &= \mathbf{X}^T \mathcal{Q} \mathbf{X} - \mathbf{X}^{\mathcal{T}} \mathcal{Q} \mathbf{X}_{\text{des}} - \mathbf{X}_{\text{des}}{}^{\mathcal{T}} \mathcal{Q} \mathbf{X} + \mathbf{X}_{\text{des}}{}^{\mathcal{T}} \mathcal{Q} \mathbf{X}_{\text{des}} - \mathbf{r} \\ &= \mathbf{X}^T \mathcal{Q} \mathbf{X} - 2\mathbf{X}_{\text{des}}{}^{\mathcal{T}} \mathcal{Q} \mathbf{X} - \mathbf{r}\end{aligned}$$

We give a very small weight ϵ for the Chebyshev radius (ignoring $\mathbf{r}_{\text{des}}$) in the corresponding element of the weight matrix $\mathcal{Q}$. So, the precise form of Eq. (3.41) for the quadratic form Eq. (3.39) is in the following format:

$$\mathbf{P} = 2\mathbf{Q} \tag{3.43}$$

$$\mathbf{q} = [\mathbf{Y}_{\text{des}} \quad -1 + \epsilon] \tag{3.44}$$

We avoid supplying zero value as weight because the QP solver requires $\mathbf{P}$ to be positive definite. Yet, we still have the quadratic form with almost no emphasis on the $\mathbf{r}_{\text{des}}$. This QP problem, named Chebyshev QP for the rest of the paper, provides the optimal position of CoM and wrench distribution by maximizing the Chebyshev radius.

3.2.3 Online Estimation of the Friction Coefficient

In this work, we are dealing with multi-sliding contacts. Implementing the sliding motion of contact needs a good estimation of the friction coefficient. This implementation is considered in Eq. (3.8) and has a major role in matrix $\mathbf{A}^{sl}$ of Eq. (3.26). Dynamic and static friction coefficients are defined as a property of a pair of surfaces in contact and can not be known intrinsically. So, we need to estimate the friction coefficient of the sliding contacts to advance the movement.

Let ${}^l f_i^{\text{tan}}$ and ${}^l f_i^{\text{nor}}$ be the tangential and normal forces respectively in the local frame of the i-th contact surface, the norm of the Coulomb friction equation Greenwood and Williamson (1966) leads us to the following formulation:

$$\left\| {}^l f_i^{\text{tan}} \right\|_2 = \mu^{\text{mes}} \mid {}^l f_i^{\text{nor}} \mid \tag{3.45}$$

where ${}^l f_i^{\text{tan}} = [{}^l f_i^x \; {}^l f_i^y]^T$ and μ^{mes} is the calculated friction coefficient from the measured local forces of the force sensors:

$$\mu^{\text{mes}} = \frac{\sqrt{{}^l f_i^{x\,2} + {}^l f_i^{y\,2}}}{\mid {}^l f_i^z \mid} \tag{3.46}$$

To minimize the effect of the force measurements noise, we also apply a simple filter with $0 \leqslant \gamma \leqslant 1$ and calculate the filtered friction coefficient at each time iteration t:

$$\mu_t^{\text{filt}} = \gamma \mu_{t-1}^{\text{mes}} + (1-\gamma)\mu_t^{\text{mes}} \tag{3.47}$$

The plots of the experimental results include the measured and estimated friction coefficient of the sliding contacts, which you will notice in section 3.5.

3.3 Radius Denotation in Balance Regions

As mentioned in the previous section, employing the region-free approach allows us to bypass the construction of balance regions. This exclusion results in high computational speed, which facilitates the real-time implementation besides paying for conservativeness. Nevertheless, to investigate the relation of the computed properties such as Chebyshev radius with the balance region, we will analyze the problem more specifically.

3.3.1 Dynamic and Contact Stabilities

We can write the equation of motion of a robot that has point or surface contacts with the environment, as

$$\mathbf{M}(\mathbf{q})\ddot{\mathbf{q}} + \mathbf{h}(\mathbf{q}, \dot{\mathbf{q}}) = \mathbf{S}^T \boldsymbol{\tau}_a + \sum_{contact\ i} \mathbf{J}_i^T \boldsymbol{\omega}_i \tag{3.48}$$

where

- $\mathbf{q},\ \dot{\mathbf{q}},\ \ddot{\mathbf{q}}$ are the n-dimensional vectors of degrees of freedom (DOF),
- $\mathbf{h}(\mathbf{q}, \dot{\mathbf{q}})$ is the n-dimensional vector of *gravity* and *Coriolis* forces,
- $\boldsymbol{\tau}_a$ is n_a-dimensional vector of torques at the actuated joints and $\mathbf{S}$ is selection matrix,
- $\boldsymbol{\omega}_i$ denotes the contact wrench taken with respect to a single contact point C_i on link i,
- $\mathbf{J}_i = [\mathbf{J}_{C_i}^T \quad \mathbf{J}_i^{rot,\,T}]^T$ denotes the $6 \times n$ matrix obtained by stacking vertically the translation and rotation jacobians.

Dynamic Equilibrium

This robotic system is considered as a set of connected links as its kinematic chain. The linear momentum $\mathbf{P}$ and angular momentum $\mathbf{L}_{CoM}$ of the system are defined by

$$\mathbf{P} \coloneqq \frac{1}{m} \sum_{link\ k} m_i \dot{\mathbf{c}}_i \tag{3.49}$$

$$\mathbf{L}_{CoM} \coloneqq \sum_{link\ k} m_i (\mathbf{p}_i - \mathbf{c}) \times \dot{\mathbf{c}}_i + \mathbf{I}_i \boldsymbol{\omega}_i. \tag{3.50}$$

In the above equations, $\mathbf{I}_i$ and $\boldsymbol{\omega}_i$ are inertial matrix and angular velocity of the link in the absolute frame and $\mathbf{c}$ and $\mathbf{p}_i$ account for position of the CoM of the robot and links, respectively. The *dynamic wrench* of the robot at CoM is noted as the wrench $(\dot{\mathbf{P}},\ \dot{\mathbf{L}}_{CoM})$ which can be derived by forward kinematics from joint-angle positions, velocities and accelerations. The *dynamic wrench* of the robot is equal to the total wrench of forces acting on the system:

$$\begin{bmatrix} \dot{\mathbf{P}} \\ \dot{\mathbf{L}}_{CoM} \end{bmatrix} = \begin{bmatrix} \mathbf{f}^g \\ 0 \end{bmatrix} + \sum_{contact\ i} \begin{bmatrix} \mathbf{f}_i \\ (\mathbf{p}_i - \mathbf{c}) \times \mathbf{f}_i \end{bmatrix} \tag{3.51}$$

where $\mathbf{f}^g$ is the gravity force acting on the CoM. This equation is also called *dynamic balance* or the *dynamic equilibrium* of the system. The Gravito-Inertial Wrench (GIW) $\mathbf{w}^{gi}$, is defined concerning a fixed point O as following:

$$\mathbf{w}_O^{gi} \coloneqq \begin{bmatrix} \mathbf{f}^{gi} \\ \boldsymbol{\tau}_O^{gi} \end{bmatrix} \coloneqq \begin{bmatrix} \mathbf{f}^g - \dot{\mathbf{P}} \\ (\mathbf{c} - \mathbf{p}_O) \times (\mathbf{f}^g - \dot{\mathbf{P}}) - \dot{\mathbf{L}}_{CoM} \end{bmatrix} \tag{3.52}$$

Meanwhile, the contact wrench $\mathbf{w}^c$ is represented as:

$$\mathbf{w}_O^c \coloneqq \begin{bmatrix} \mathbf{f}^c \\ \boldsymbol{\tau}_O^c \end{bmatrix} \coloneqq \sum_{contact\ i} \begin{bmatrix} \mathbf{f} \\ \mathbf{p}_i \times \mathbf{f}_i \end{bmatrix} \tag{3.53}$$

So, the *dynamic equilibrium* or *balance* of the system can then be written as

$$\mathbf{w}^{gi} + \mathbf{w}^c = 0. \tag{3.54}$$

The dynamic equilibrium in form of Eq. (3.54) is known as *wrench-space* formulation. The underlying reason behind this formulation is that

- the *gravito-inertial wrench* describes the motion of the overall system,
- while the *contact wrench* describes its interactions with the environment.

Contact Stability

According to the contact stability criterion from Caron (2015) and Pang and Trinkle (2000), there exists a solution $(\ddot{\mathbf{q}},\ \boldsymbol{\tau},\ \mathbf{w}_1,\ ...,\ \mathbf{w}_n)$ of the equations of motion satisfying the contact mode for all contacting links. For instance for a fixed contact we have

- no relative motion of the contacting link: $\mathbf{J}_i\dot{\mathbf{q}} = 0$,
- torque limits are satisfied,
- contact wrenches are in their respective CWCs.

On the other hand, as all local contact wrenches lie in wrench cones, the whole-body wrench cone must lie in the (whole-body) contact wrench cone C (sum of local contact wrench cones). Note that a polyhedral convex cone image by a linear mapping is itself a polyhedral convex cone. Since the gravito-inertial and contact wrenches are simply opposites, the gravito-inertial wrench also lies in a cone $-C$. So, the proposition states that the motion of the robot is (weak-contact) stable if and only if the contact wrench (resp. gravito-inertial wrench) it generates belongs to the CWC (resp. GIWC).

The GIWC is called as a general multi-contact stability criterion. According to Hirukawa et al. (2006), If $(\mathbf{f}^{gi},\ \boldsymbol{\tau}_O^{gi})$ is an internal element of the CWC, then the contact is strongly stable to $(\mathbf{f}^{gi},\ \boldsymbol{\tau}_O^{gi})$. However, Caron et al. (2015a) noticed that their proof of stability was wrong. This is because of the assumption they made in their computations. They assumed the humanoid robot to act like a rigid body in which the fixed contacting links result in the fixed position of CoM. But, according to the redundancy in the actuation of the robot, this hypothesis can be voided.

3.3.2 Calculation of the Range of Contact Wrench and GIW

Chebyshev radius is the output of the minimization problem Eq. (3.39). However, this radius indicates a range that applies to all contact wrenches. We can additionally calculate the range of the gravito-inertial wrench within the GIWC based on the computed radius. This can be done by considering this radius within the computation process of the GIWC.

Note that the contact wrench cone is simply the opposite of the GIWC. So, the calculation for range accounts for both whole-body contact and gravito-inertial wrenches. Assuming a set of contact wrenches, expressed at CoM, within their respective contact wrench cones $\mathbf{w}_i \in \mathcal{C}_i$ for $i = 1, \ldots, l$, and representation of region-free method Eq. (3.21b), we have

$$\mathbf{w}_i + r\mathbf{a} \in \mathcal{C}_i \tag{3.55}$$

Regarding the sum of contact wrenches and their ranges ($r\mathbf{a}$), we can write

$$\sum_{i=1}^{l} \mathbf{w}_i + l \times r\mathbf{a} \in \mathcal{C}_1 \oplus \ldots \oplus \mathcal{C}_l \tag{3.56}$$

where $\oplus$ denotes the Minkowski sum of the contact wrenches cones which is the explicit definition of the CWC. So, the range for the valid whole body contact and gravito-inertial wrenches is the sphere with the radius of

$$r_{cwc} = l \times r \tag{3.57}$$

Next, we show the reason why we need to implement the Minkowski sum with a numerical example.

Minkowski Sum

Assume that $\mathcal{A}$ and $\mathcal{B}$ are convex sets in *wrench space* and $\mathbf{a}$ and $\mathbf{b}$ are wrenches in which $\mathbf{a} \in \mathcal{A}$ and $\mathbf{b} \in \mathcal{B}$. Then we can write

$$\mathbf{a} = \sum_i \alpha_i \mathbf{v}_i; \quad \alpha_i \geqslant 0, \sum_i \alpha_i = 1 \tag{3.58}$$

$$\mathbf{b} = \sum_j \beta_j \mathbf{w}_j; \quad \beta_j \geqslant 0, \sum_j \beta_j = 1 \tag{3.59}$$

where $\mathbf{v}_i$ and $\mathbf{w}_i$ are vertices of $\mathcal{A}$ and $\mathcal{B}$ accordingly, and i and j are the number of vertices of $\mathcal{A}$ and $\mathcal{B}$. We aim for finding the convex hull containing all possible $\mathbf{a} + \mathbf{b}$:

$$\begin{aligned}
\mathbf{a} + \mathbf{b} &= \sum_i \alpha_i \mathbf{v}_i + \sum_j \beta_j \mathbf{w}_j \\
&= \sum_i \alpha_i (\mathbf{v}_i + \sum_j \beta_j \mathbf{w}_j) \\
&= \sum_i \alpha_i (\sum_j \beta_j (\mathbf{v}_i + \mathbf{w}_j)) \\
&= \sum_i \sum_j \alpha_i \beta_j (\mathbf{v}_i + \mathbf{w}_j) \\
\Rightarrow \mathbf{a} + \mathbf{b} &= \sum_{i,j} \alpha_i \beta_j (\mathbf{v}_i + \mathbf{w}_j)
\end{aligned}$$

According to the properties of coefficients, we have

$$\left.\begin{matrix} \sum_i \alpha_i = 1 \\ \sum_j \beta_j = 1 \end{matrix}\right\} \Rightarrow \sum_i \alpha_i \sum_j \beta_j = 1 \Rightarrow \sum_{i,j} \alpha_i \beta_j = 1 \tag{3.60a}$$

$$\left.\begin{matrix} \alpha_i \geqslant 0 \\ \beta_j \geqslant 0 \end{matrix}\right\} \Rightarrow \alpha_i \beta_j \geqslant 0 \tag{3.60b}$$

According to Eq. (3.60), $\mathbf{a} + \mathbf{b}$ is in the convex hull of $\mathbf{v}_i + \mathbf{w}_j$ vertices, named $\mathcal{C}$ where the mathematical notation for this operation is $\mathcal{C} = \mathcal{A} \oplus \mathcal{B}$.

Numerical Example

Here we consider a simple numerical example to clarify the concept of Minkowski sum and range of GIW. As shown in Fig. 3.3, the contact forces and their convex polyhedra are considered in 3D. For two contact points in Euclidean space

- positions are $\mathbf{p}_{c1} = [0.25 \;\; 0 \;\; 0]^T$ and $\mathbf{p}_{c2} = [-0.25 \;\; 0 \;\; 0]^T$ with respect to O,
- orientations are $\boldsymbol{\theta}_{c1} = [20 \;\; 20 \;\; 0]^T$ and $\boldsymbol{\theta}_{c2} = [10 \;\; -10 \;\; 0]^T$ in degrees with respect to O,

- friction coefficients are $\mu_1 = 0.5$ and $\mu_1 = 0.35$

According to the friction coefficients of the contacts, Fig. 3.3(b) illustrates the corresponding friction cones. Note that the friction cones are in vector space, which is not shown to avoid the figure's complexity.

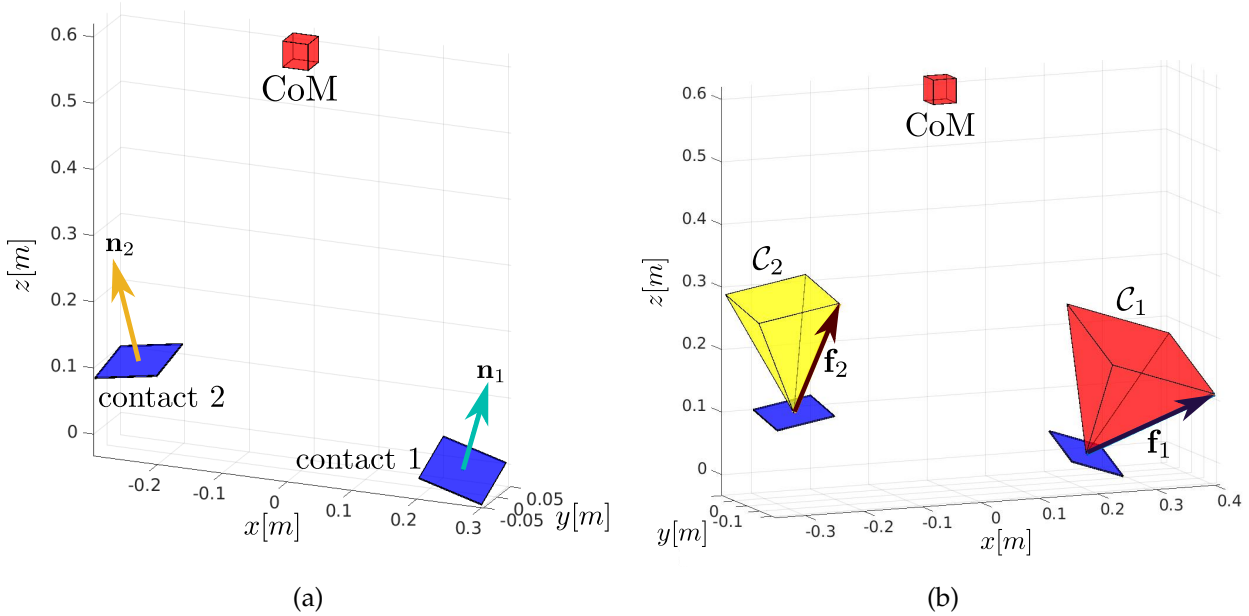

(a) (b)

FIGURE 3.3 – *A numerical example of the standing robot with two feet contacts. (a) demonstrates the position of contacts, their normal vectors, and CoM in the proposed coordinate system, and (b) is a scaled illustration of the corresponding friction cones of the contacts.*

We choose the position of CoM to be $\mathbf{p}_G = [0 \;\; 0 \;\; 0.6]^T$. Fig. 3.4(a), Represents the translation of the polyhedra and forces in the location where CoM exists. The polyhedron in the CoM position is the Minkowski sum of contact polyhedra.

In order to have a clear vision of the CWC, we illustrate arbitrary forces which lie on the edge of their corresponding friction cone in Fig. 3.3(a). The translated sum of these forces to the position of CoM is shown in the Fig. 3.4(a). As pointed in the picture, The resultant force is inside the Minkowski sum of the friction cones, namely CWC.

In the calculation of the friction cones, we considered the upper limit for the normal force. So, the cones have ceilings. The computed wrench and Chebyshev radius results in spheres for all contacts within their cones as shown in the Fig. 3.4(b). Consequently, the larger sphere inside the GIWC has a radius equal to twice the Chebyshev radius (the sum of small spheres). This sphere is always located inside the GIWC or CWC and the conservativeness of the approach is demonstrated geometrically.

Finally, in this section, we determined the radius r_{cwc} from Eq. (3.57) which indicates the minimum distance which the GIW or contact wrench will keep from the borders of the GIWC or CWC accordingly. This distance will support the balance of the robot with a safe margin. Moreover, over retaining this distance, we can constantly generate CoM accelerations in every direction before losing the balance.

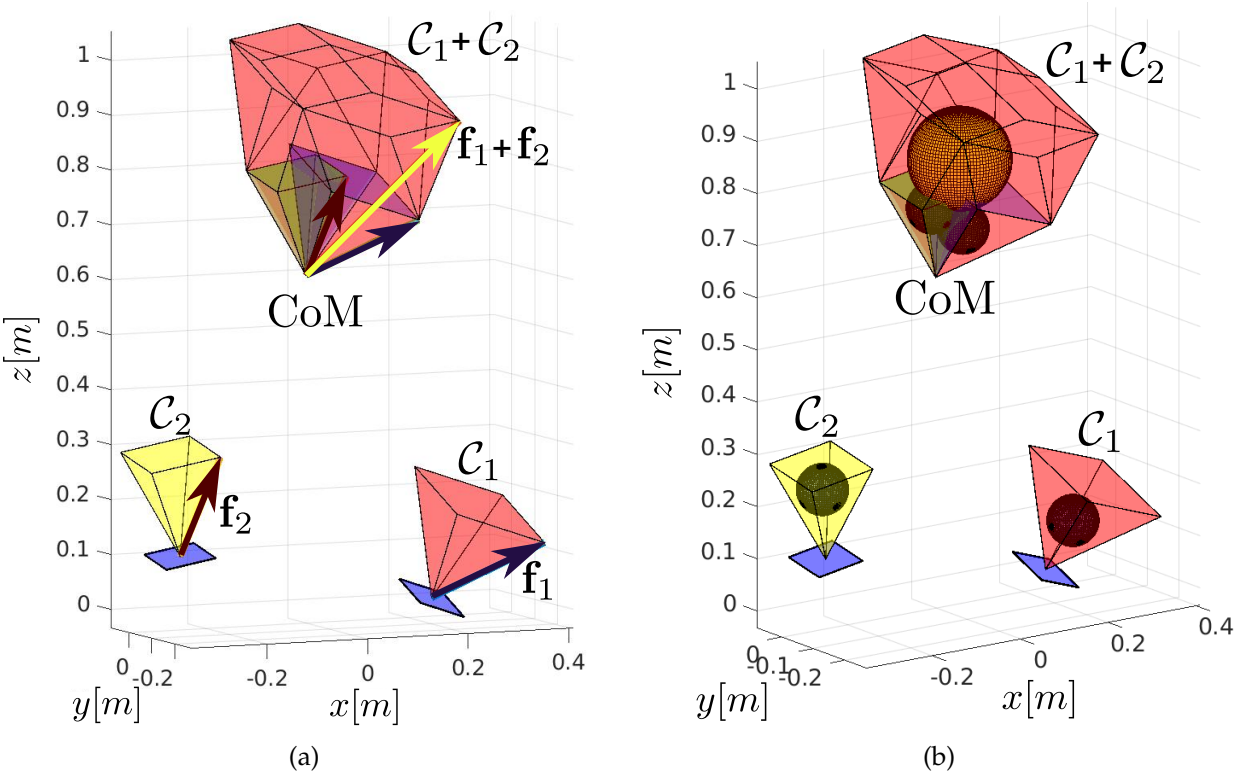

FIGURE 3.4 – *Illustration of the Minkowski sum of the friction cones in the position of CoM. (a) includes the arbitrary forces which lie on the edge of their corresponding friction cone (for illustration purposes) and the translated sum of these forces to the position of CoM. (b) shows the spheres as a result of the computed wrenches and Chebyshev radius in contact points. The radius of the larger sphere is equal to the sum of small ones.*

3.3.3 Calculation of the Range of CoM Position

Now, we are aiming for translating the Chebyshev radius into the static equilibrium region and calculate the range for CoM position. First we represent the CWC, $\mathbf{W}$, at a fixed point O:

$$\mathbf{A}_O\mathbf{W}_O \leqslant \mathbf{0} \tag{3.61}$$

According to the section 3.3.2, we apply the Chebyshev range for contact wrench as $r_{cwc}$to the $i-th$ row of A_O. The inequality becomes:

$$\mathbf{A}_{O,i}\mathbf{W}_O + r_{cwc}\,\|\mathbf{A}_{O,i}\| \leqslant \mathbf{b}_i \tag{3.62}$$

According to $\mathbf{W}_O = [\mathbf{f} \quad \boldsymbol{\tau}_O]^T$ and using the *dual twist* representation of the inequality from Caron and Kheddar (2016) as $[\mathbf{a}_O \quad \mathbf{a}]^T$, we can re-write the above equation as

$$\mathbf{a}_O.\mathbf{f} + \mathbf{a}.\boldsymbol{\tau}_O + r_{cwc}\,\|\mathbf{A}_{O,i}\| \leqslant \mathbf{b}_i \tag{3.63}$$

where $\mathbf{a}_O = [a_{Ox} \quad a_{Oy} \quad a_{Oz}]^T$ and $\mathbf{a} = [a_x \quad a_y \quad a_z]^T$. By considering static equilibrium ($\boldsymbol{\tau}_G = \mathbf{0}$ and $\mathbf{f} = m\mathbf{g}$) and representing the inequality at point G, we continue the

calculation as following:

$$\begin{aligned} m(\mathbf{a}_O + \mathbf{a} \times \mathbf{p}_G).\mathbf{g} + r_{cwc} \left\| \mathbf{A}_{O,i} \right\| &\leqslant \mathbf{b}_i \\ -mg(\mathbf{a}_{Oz} - \mathbf{a}_y x_G + \mathbf{a}_x y_G) + r_{cwc} \left\| \mathbf{A}_{O,i} \right\| &\leqslant \mathbf{b}_i \\ \frac{-1}{\left\| \mathbf{A}_{O,i} \right\|}(\mathbf{a}_{Oz} - \mathbf{a}_y x_G + \mathbf{a}_x y_G) + \frac{r_{cwc}}{mg} &\leqslant \frac{\mathbf{b}_i}{mg \left\| \mathbf{A}_{O,i} \right\|} \\ \frac{-1}{\left\| \mathbf{A}_{O,i} \right\|}(\mathbf{a}_{Oz} - \mathbf{a}_y x_G + \mathbf{a}_x y_G) - \frac{\mathbf{b}_i}{mg \left\| \mathbf{A}_{O,i} \right\|} &\leqslant -\frac{r_{cwc}}{mg} \end{aligned}$$

Without loss of generality, we can assume $\left\| \mathbf{A}_{O,i} \right\| = 1$. So, the inequality Eq. (3.61) becomes:

$$-(\mathbf{a}_{Oz} - \mathbf{a}_y x_G + \mathbf{a}_x y_G - \frac{\mathbf{b}_i}{mg}) \leqslant -\frac{r_{cwc}}{mg} \tag{3.64}$$

We denote the signed distance between $(x_G,\ y_G)$ and the supporting line $-\mathbf{a}_{Oz} + \mathbf{a}_y x_G - \mathbf{a}_x y_G + \frac{\mathbf{b}_i}{mg} = 0$ of the corresponding equilibrium polygon's edge as

$$\sigma_{A,i}(x_G,\ y_G) = \mathbf{a}_{Oz} - \mathbf{a}_y x_G + \mathbf{a}_x y_G - \frac{\mathbf{b}_i}{mg} \tag{3.65}$$

The above inequality indicates that the minimum distance of the CoM from the borders of static equilibrium region (from Bretl) is $r_{com} = \frac{r_{cwc}}{mg}$

3.4 Whole-body Admittance Controller

In this section, we present the overall task-space whole-body admittance controller as shown in Fig. 3.5. For each scenario, a Finite State Machine (FSM) is designed/planned. Each state of the FSM, defines a set of tasks and constraints for the controller as well as desired positions, forces, and sliding conditions for each contact, if any.

The Chebyshev QP computes optimal and safe contact wrenches and CoM position depending on the current state of the robot and planned FSM targets. These optimal wrenches and CoM position are then used as objectives for tasks driven by the whole-body QP (WBQP) framework.

Each task is formulated as a cost function and/or eventually associated constraints on joint acceleration (or torque for torque-based humanoids) and contact forces. The resulting joint acceleration is integrated twice (or torques) and sent as a target for the robot actuators' low-level controllers, see Bouyarmane et al. (2019b).

Ordinarily, the measured and estimated state of the robot is used to close the loop at the task level. In order to maintain the balance of the robot at the control level, we use the Chebyshev formulation for closing this loop, as you can see in Fig. 3.5. We compute the optimal CoM position and wrench distribution from the desired contact force and the measured and estimated states of the robot. This method guarantees the dynamic balance of the robot in real-time. For sliding contacts, we implement an online friction estimation accompanying by a first-order filter.

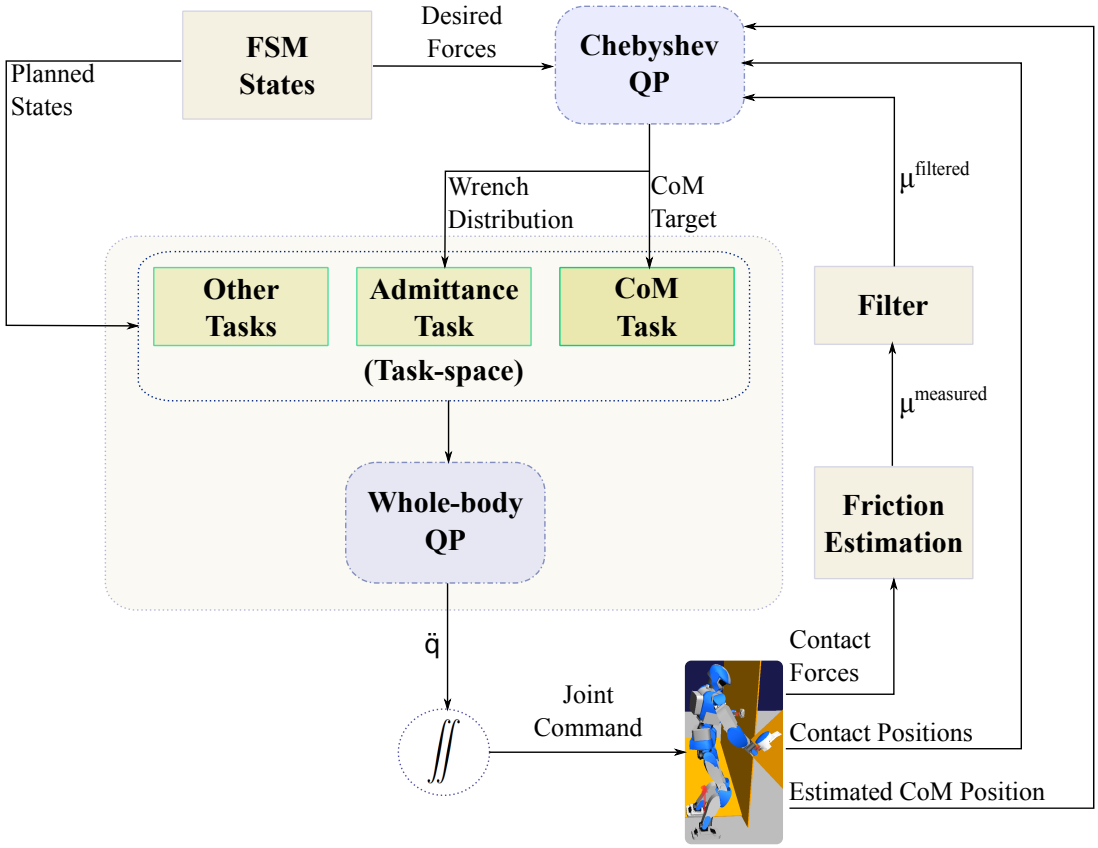

FIGURE 3.5 – *Schematic of the overall task-space control framework with Chebyshev QP.*

The main tasks we used in our experiments are the following: (i) CoM task, to eventually track the optimal CoM position, (ii) Admittance tasks for the desired wrench which map wrench error to contact surface velocity which in turn is used as a target for an end effector trajectory task.

3.5 Experimental Results

In order to assess our approach, we performed experiments with the HRP-4 humanoid robot. We investigate the capabilities of our proposed optimal control framework through a multi-contact scenario under active dynamic balance that exhibits:

- combination and switching of fixed and sliding modes;
- multi-fixed-and-sliding contacts on non-coplanar surfaces;
- shuffling of the foot on a tilted surface.

We prepared a non-coplanar multi-contact set-up consisting of a tilted fake wooden slope for the left foot, a tilted wooden board for the right hand, and a wall for the left hand. The right foot is on the experimental room ground. The three materials have different friction coefficients, which are not measured beforehand. The scenario starts by setting the HRP-4 in a half-sitting pose, both feet on the grounds.

The motion begins with stepping the left foot up the slope and establishing a planar contact with the wall by the left hand. Then contact is established by the right hand on the tilted board (slope of $\simeq 50°$). Each contact is established while sustaining the existing ones and moving the whole body while keeping the CoM close to the suggested one by the Chebychev QP.

Alike in Kheddar et al. (2019) and since we use guarded motion and a calibrated environment, embedded robot vision was not used this time. At this stage, we have four contacts. Then HRP-4 gets prepared for the co-wiping motion under user-specified surface normal forces: 10 N for the right hand and 15 N for the left hand. Setting contacts and preparation for the co-wiping state are shown in Fig. 3.6.

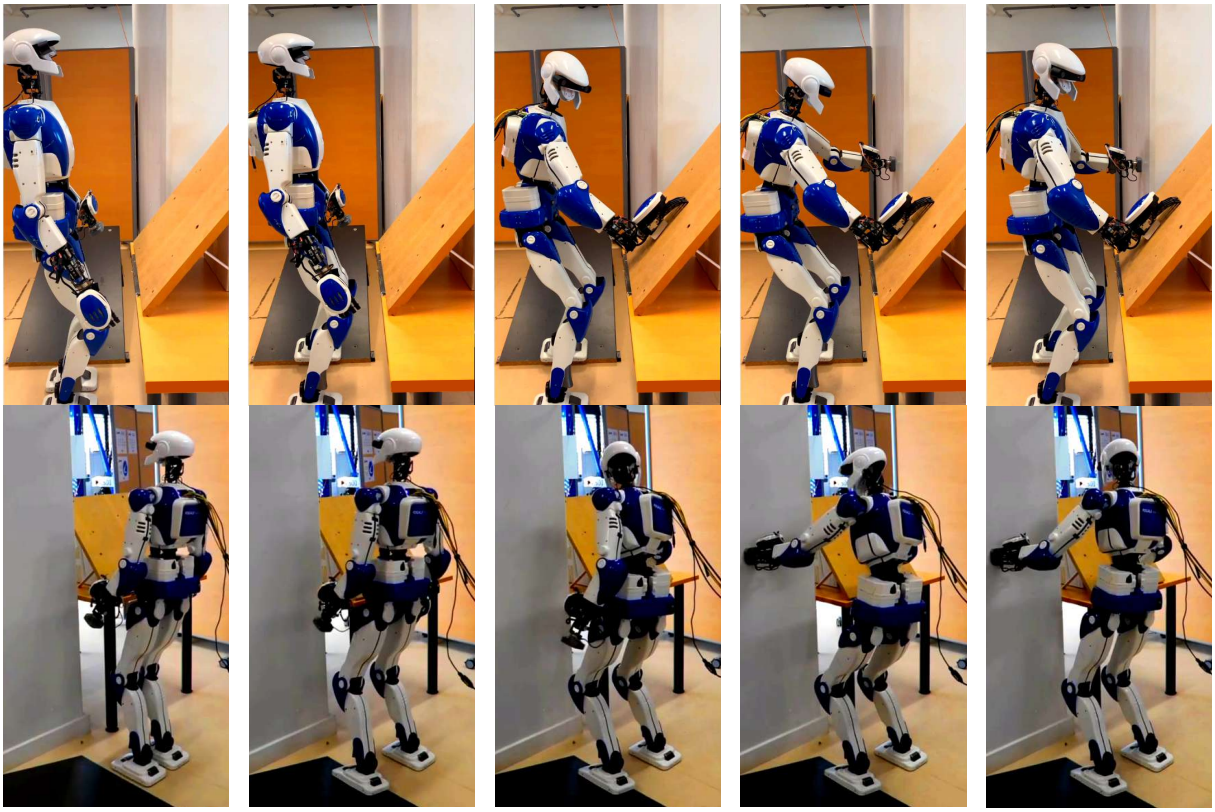

FIGURE 3.6 – *Establishing fixed contacts and preparing for sliding motions.*

The next stage is the wiping motion of both hands simultaneously. During co-wiping, the end effectors track the desired normal force and planned trajectories of circles with a radius of 10 and 8 cm for right and left hands, respectively. Notice that in a multi-contact non-coplanar setting, the range of motion of HRP-4 is limited due to intrinsic kinematics closed-chain constraints. Figures Fig. 3.7 and Fig. 3.8 illustrate the co-wiping experiment and force tracking of the end-effectors contacts using admittance force control discussed in Bouyarmane et al. (2019b).

The alignment of the end effectors with surfaces while establishing the contacts is guaranteed by zeroing the torques reference in x and y directions with respect to the local contact frame. The trajectory tracking of end-effectors is shown in Fig. 3.9.

Once the co-wiping tasks are achieved, both contacts switch from sliding to fixed modes, and the left foot contact switches from fixed to sliding mode. Now we have

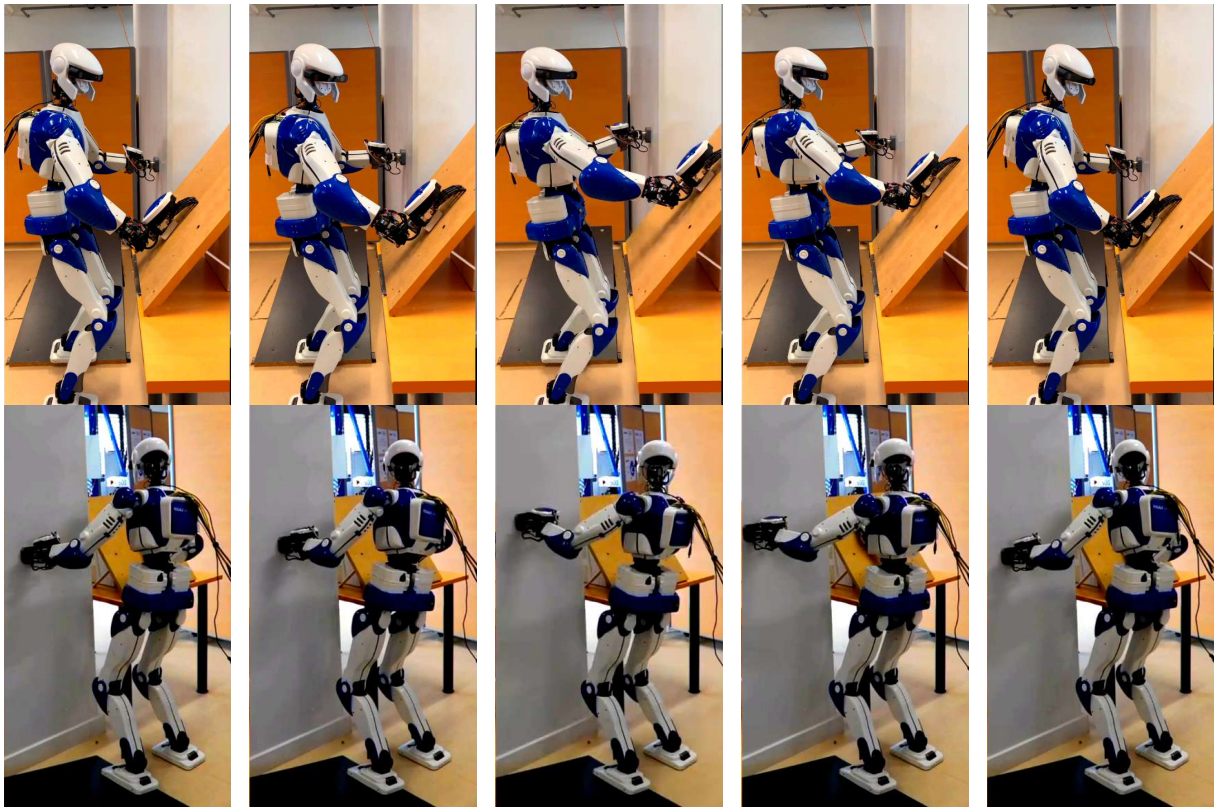

FIGURE 3.7 – *Simultaneous sliding of both hands on non-coplanar wooden board and wall surfaces.*

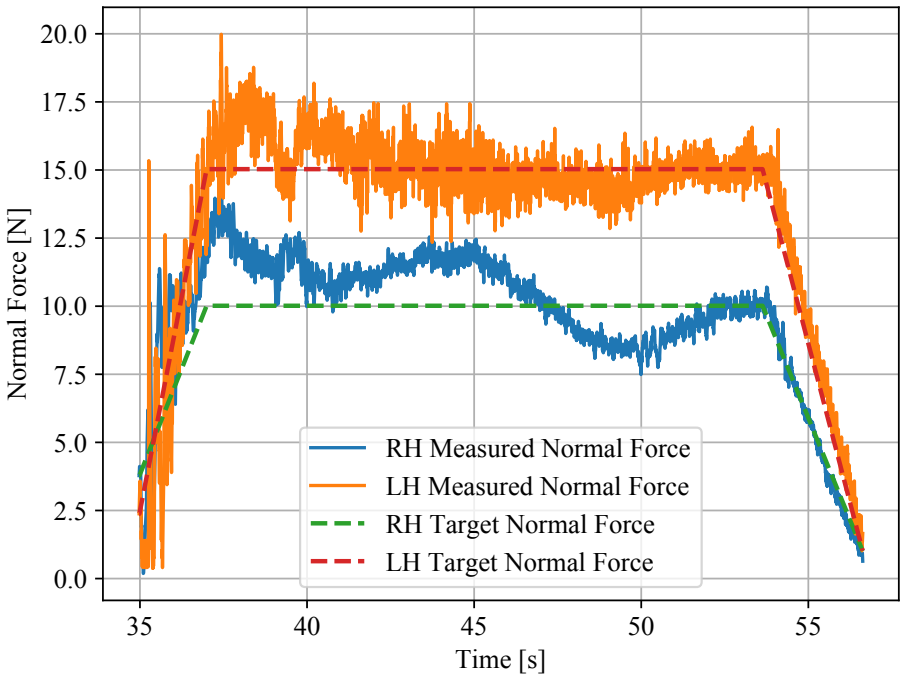

FIGURE 3.8 – *Force tracking of the end-effectors during co-wiping tasks.*

three fixed contacts and one sliding. The left foot on the slope shuffles back and forward. Fig. 3.10 shows the shuffling experiment and the normal force tracking for the end effectors, respectively.

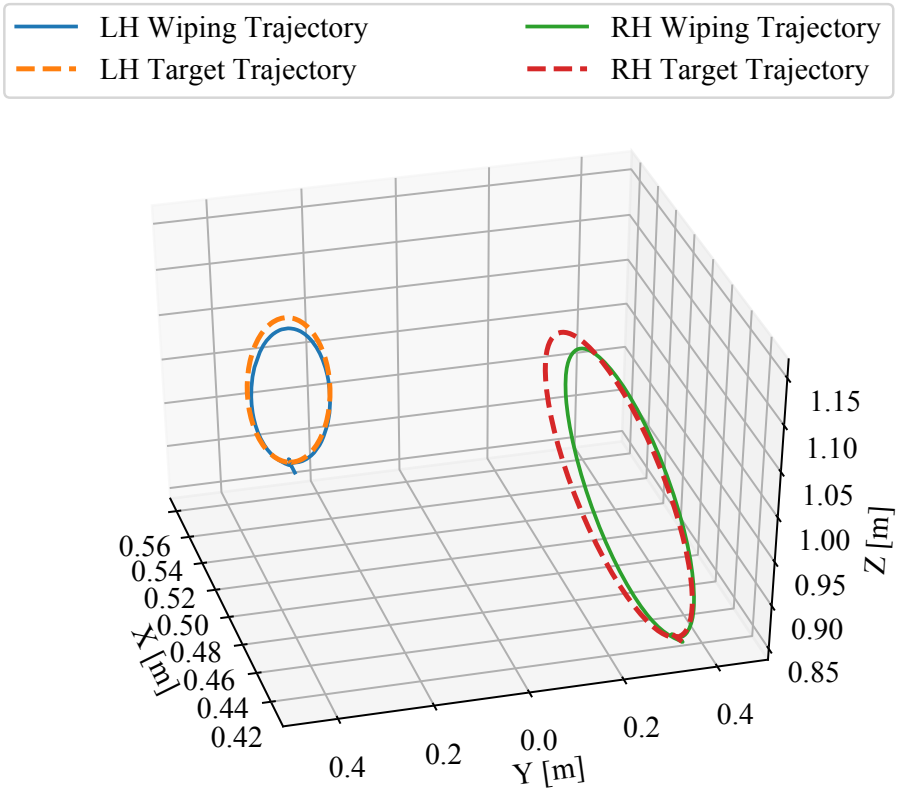

FIGURE 3.9 – *Target trajectory tracking of the sliding hands. The light discrepancies are due to uncertainties of planed board and wall position with respect to HRP-4.*

In the last part of the scenario, HRP-4 releases both hands at a time and steps back to the floor (initial pose). During all sliding motions, online friction estimation Eq. (3.47) is executed. The estimation process begins with initial guesses, as shown in Fig. 3.12, and computes friction only when the normal forces are above a given threshold. Moreover, the CoM position tracking of both co-wiping and shuffling scenarios during the entire experiment is displayed in Fig. 3.13.

The experiments computations were made by a laptop computer having Intel(R) Xeon(R) E-2276M CPU at 2.80 GHz$\times 12$. With this setup, we noted the average computation times for the Chebyshev QP and the whole framework as 0.2 and 1 ms, respectively. These values are largely within the implemented real-time control loop with `mc_rtc` framework that is 5 ms.

3.6 Conclusion

This chapter devised a whole-body humanoid non-coplanar multi-contact motion planning and control for mixed sliding and fixed contacts that can be switched at will. Our method does not require the construction of GIWC or CoM-support polytopes, thanks to a single and fast optimization problem based on the Chebyshev center. This formulation makes it suitable for closed-loop control because there is no need for any time-consuming pre-computation of balance regions.

The previous works on multi-contact applications classified the supporting and interacting contacts to exclude the interaction ones from dynamic balance. The Chebyshev QP formulation also allows exploiting all the contacts, including moving/sliding ones, for dynamic balance when possible and permits balance contacts also to contribute to force tasks.

We assess our approach through complex scenarios with the HRP-4 humanoid robot: four contacts are controlled in force under dynamic balance with switches between fixed and sliding contact modes at the user's will. A simple online friction estimator is implemented to update the friction coefficient of the sliding contacts. A video of the experiments [1] and the open-source code of the controller [2] are available online.

In future work, we aim at improving the force tracking based on the extension of Pham and Pham (2020) that is currently limited to translation forces (i.e. non-moments). We are also considering the extension of multi-contact modalities to include soft supports. That is to say, contact that combines fixed, sliding, pushing, and rolling eventually on soft supports. We then need to develop more sophisticated friction identification models and associated filters. These modalities would then cover almost all spectrum of possible contacts encountered in the targeted applications. Robustness consideration concerning uncertain dynamic parameters shall also be accounted (e.g., considering relative forces instead of absolute ones).

Finally, we shall cover multi-contact planning that considers such multi-modal contacts to achieve tasks requiring accessing narrow or cumbersome passages. These skills will be deployed in real use-case scenarios defined by two large-scale manufacturing industrial partners, one of which is the continuation of Kheddar et al. (2019) and in physical human-robot assistive robotics Bolotnikova et al. (2020).

In the next chapter, we are aiming to merge the region-free method with the whole-body QP. This way, a single QP will compute the demanded targets for execution on the robot. However, all involved tasks will associate in calculating the QP together with the Chebyshev implementation. Also, to reflect the dynamic motion, the decision variable will contain the CoM acceleration rather than the position.

1. https://youtu.be/cFYd9oQueRE
2. https://github.com/SaeidSamadi/Multi-sliding-Contacts

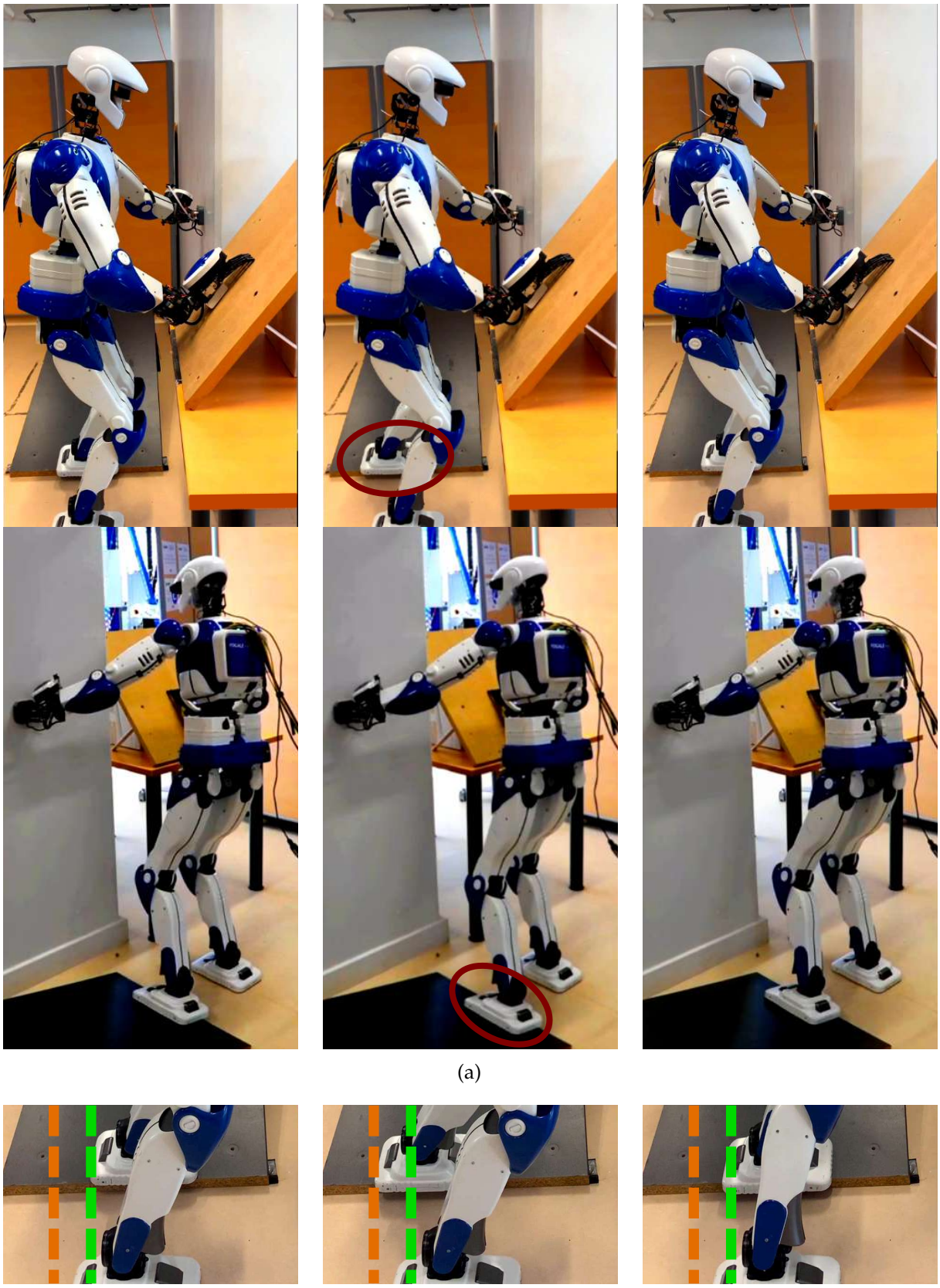

(a)

(b)

FIGURE 3.10 – *Preparing posture for shuffling scenario (a) while keeping the hands as fixed contacts and (b) shuffling of the left foot on a slope tilted by* $20°$*. w.r.t. the ground in a multi-contact setting.*

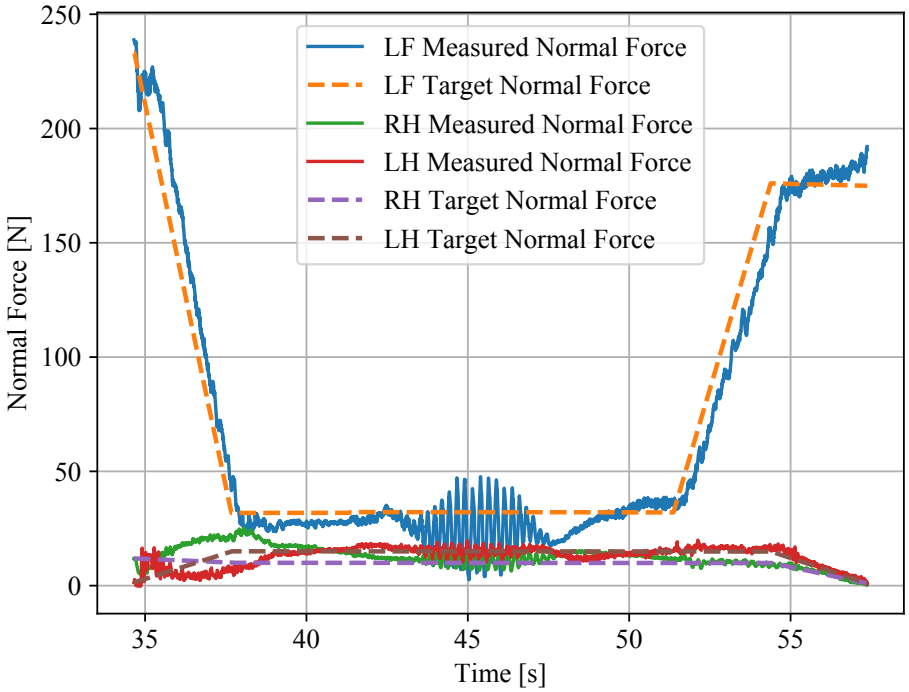

FIGURE 3.11 – *Normal Force tracking of hands and left foot contact during the shuffling motion. The oscillations are due to the change into the reverse direction in the shuffling motion.*

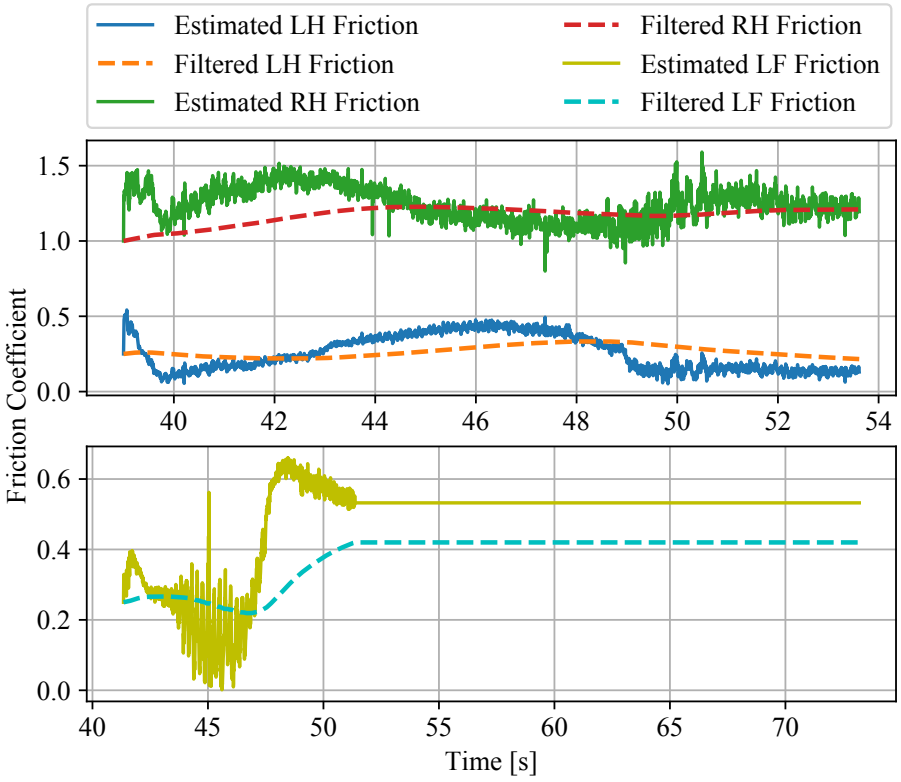

FIGURE 3.12 – *Estimated and filtered dynamic friction coefficient for co-wiping (up) and shuffling scenarios (bottom).*

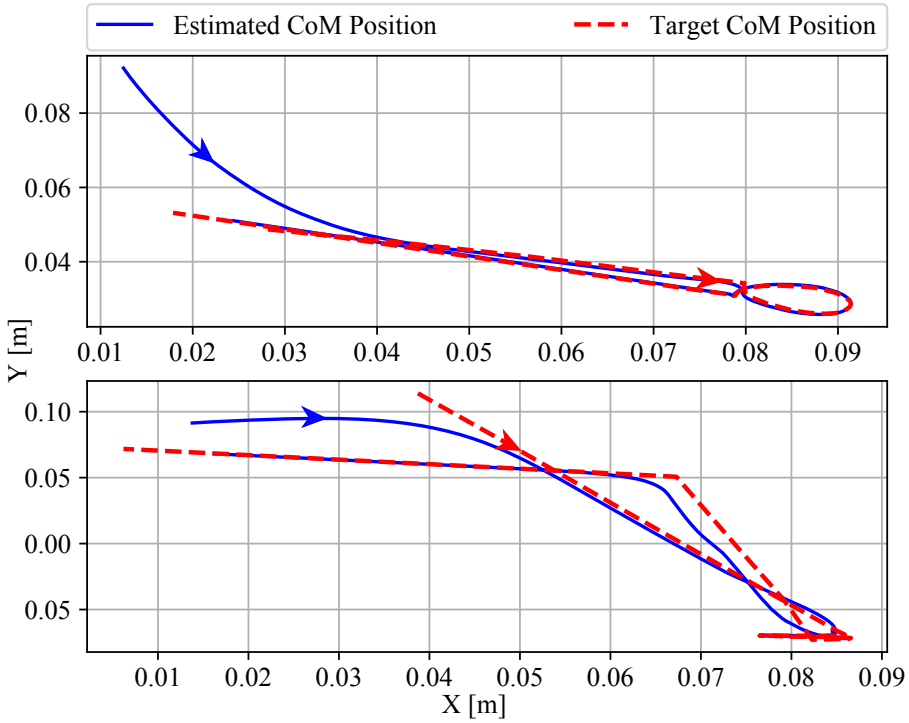

FIGURE 3.13 – *CoM trajectory tracking in x and y directions for co-wiping (up) and shuffling scenarios (bottom)*

CHAPTER 4

INTEGRATED WHOLE-BODY BALANCE CONTROL OF HUMANOIDS IN MULTI-CONTACT MODES

The previous chapter investigated the robot's balance within the multi-contact scenarios employing a region-free approach. This method enables the real-time implementation of the whole control framework without pre-computation of the balance regions. This framework consists of a planner, which holds the centroidal dynamics of the robot together with the implemented balance criteria, and the whole-body controller for realizing the desired motion parameters from the planner on the robot.

An online-executable planner needs to generate the balancing parameters with the minimum motion feedback such as contact points, force measurement, and CoM position estimation. However, the full range of the motion features, essentially real-time motion tasks and configurations, are kept beyond the scope of the planner. In simple words, if for instance, an end-effector trajectory task is carried out during a control state, the planner is not aware of this movement until the robot contacts the environment.

The current chapter aims to integrate a balancing strategy within the controller rather than the planner. We consider the balance criteria–based on the region-free approach–and all active motion tasks in an online framework through this integration. So, the whole-body controller of the robot also accounts for the balance of the robot. Moreover, we consider the robot's centroidal and actuated dynamics, which results in the whole-body motion of the robot.

Consequently, By considering the whole-body motion of the humanoid, inverse kinematics provides the joint commands required for accomplishing the desired trajectory of the CoM and the respective body configuration within the controller. In the following, we reformulate the actuated and under-actuated dynamics of the robot to be compatible with the framework accompanied by region-free balance control. The framework also covers the sliding contact mode as investigated in previous chapters.

4.1 Whole-body and Centroidal Dynamics

The humanoid robot is considered a floating-based system. Assuming j as the number of joints, the system has $6+j$ DoF. The whole-body dynamics govern $6+j$ equations connecting the joint configurations $\mathbf{q} = [\mathbf{q}^u \;\; \mathbf{q}^a]^T$ and its derivations (containing unactuated $\mathbf{q}^u \in \mathbb{R}^6$ and actuated $\mathbf{q}^a \in \mathbb{R}^j$ terms) with the actuator torques $\boldsymbol{\tau}^a$ and contact wrenches $\mathbf{w}_i \in \mathbb{R}^6$ as

$$\mathbf{M}(\mathbf{q})\ddot{\mathbf{q}} + \mathbf{N}(\mathbf{q}, \dot{\mathbf{q}}) = \begin{bmatrix} \mathbf{0}_6 \\ \boldsymbol{\tau}^a \end{bmatrix} + \sum_{\text{contact } i} \mathbf{J}_i^T \mathbf{w}_i. \tag{4.1}$$

Note that the first six rows of Eq. (4.1) reflect the under-actuated dynamics of the robot, namely the centroidal dynamics Orin et al. (2013). Also, $\mathbf{M}$ is the generalized mass matrix, $\mathbf{N}$ contains the centrifugal and Coriolis effects, and $\mathbf{J}_i$ refers to the i-th contact Jacobian.

The Newton-Euler equation is associated with centroidal dynamics. Assuming that the robot has u links, the linear ($\mathcal{P}$) and angular ($\mathcal{L}$) momentum terms are defined as following in the global frame:

$$\mathcal{P} \overset{\text{def}}{=} m\dot{\mathbf{c}} \tag{4.2a}$$

$$\mathcal{L} \overset{\text{def}}{=} \mathbb{I}_u \boldsymbol{\omega}_u + \sum_{\text{link } u} (\mathbf{p}_u - \mathbf{c}) \times m\dot{\mathbf{c}} \tag{4.2b}$$

where $\mathbb{I}_u$, $\boldsymbol{\omega}_u$, and $\mathbf{p}_u$ refer to the inertia matrix, angular velocity and position of CoM of the link u, respectively. Also, $\mathbf{c} = [c^x \;\; c^y \;\; c^z]^T$ is the position of the CoM in global frame. The centroidal dynamics of Eq. (4.1) can be expressed by derivative of momenta Caron et al. (2015a):

$$\dot{\mathcal{P}} = \sum_{\text{contact } i} \mathbf{f}_i + m\mathbf{g} \tag{4.3a}$$

$$\dot{\mathcal{L}} = \sum_{\text{contact } i} (\mathbf{p}_i - \mathbf{c}) \times \mathbf{f}_i + \boldsymbol{\tau}_i \tag{4.3b}$$

whereas $\mathbf{g} = [0 \;\; 0 \;\; -9.81]$. In the following, we aim for re-writing Eq. (4.3) in terms of gravito-inertial wrench $\mathbf{w}^g = [\mathbf{f}^g \;\; \boldsymbol{\tau}^g]$ which are defined as follows:

$$\mathbf{f}^g \overset{\text{def}}{=} m(\mathbf{g} - \ddot{\mathbf{c}}) \tag{4.4a}$$

$$\boldsymbol{\tau}^g \overset{\text{def}}{=} \mathbf{c} \times m(\mathbf{g} - \ddot{\mathbf{c}}) - \dot{\mathcal{L}}. \tag{4.4b}$$

By substituting Eq. (4.4) into Eq. (4.3) and considering $\dot{\mathcal{P}} = m\ddot{\mathbf{c}}$, we have:

$$\mathbf{f}^g = -\sum_{\text{contact } i} \mathbf{f}_i \tag{4.5a}$$

$$\boldsymbol{\tau}^g = -\sum_{\text{contact } i} \mathbf{p}_i \times \mathbf{f}_i + \boldsymbol{\tau}_i. \tag{4.5b}$$

We recall the dynamic equilibrium of the robot by Newton-Euler equation for l limbs in contact with the environment is represented in Eq. (3.1),

$$\mathbf{w}^g + \sum_{i=1}^{l} \mathbf{w}_i = 0,$$

for the gravity and contact wrenches specified in Eq. (3.2) as the following form:

$$\mathbf{w}^g = \begin{bmatrix} \mathbf{f}^g \\ \mathbf{c} \times \mathbf{f}^g \end{bmatrix}$$
$$\mathbf{w}_i = \begin{bmatrix} \mathbf{f}_i \\ \mathbf{p}_i \times \mathbf{f}_i + \boldsymbol{\tau}_i \end{bmatrix}.$$

Contrary to Samadi et al. (2021) which accounts for the static equation of motion, we consider the dynamic motion of the robot. The Newton-Euler equation Eq. (3.1) for decoupled force and torques becomes:

$$\sum_i \mathbf{f}_i = m(\ddot{\mathbf{c}} - \mathbf{g}) \tag{4.6a}$$
$$\sum_i (\mathbf{p}_i \times \mathbf{f}_i + \boldsymbol{\tau}_i) = m\mathbf{c} \times (\ddot{\mathbf{c}} - \mathbf{g}) \tag{4.6b}$$

where all vectors are represented with respect to the inertial frame, m is the total mass of the robot.

4.2 Constraints of the Motion

The whole-body controller framework is formulated in task space and solved as a QP problem. This section introduces the constraints of the motion that we need to fulfill in the QP formulation. These constraints consist of both equality and inequality forms. Also, we need to specify the decision variables of this formulation. We write the framework in task-space as a quadratic problem that solves for

- configuration accelerations, $\ddot{\mathbf{q}}$,
- contact wrenches, $\mathbf{w}_i$,
- actuator torques, $\boldsymbol{\tau}^a$, and
- Chebyshev radius, $\mathbf{r}$, which will be thoroughly addressed in the next section.

In the following, we define motion constraints to be formulated and implemented as a function of decision variables.

4.2.1 Equation of Motion

Previous chapters [1] were containing two separate QPs for the planner and whole-body controller which CoM position was considered as one of the decision variables of the planner. However, in the present study, we implement the computations within the

1. Researchs are also published in Samadi et al. (2021) and Samadi et al. (2020).

whole-body framework. Therefore, we need to formulate the equations based on CoM acceleration rather than its position as it is straightforward to derive CoM acceleration from $\ddot{\mathbf{q}}$ thanks to the CoM Jacobian $\mathbf{J}_{CoM}$:

$$\ddot{\mathbf{c}} = \mathbf{J}_{CoM}\ddot{\mathbf{q}} + \dot{\mathbf{J}}_{CoM}\dot{\mathbf{q}}. \tag{4.7}$$

Note that we can directly calculate the term $\dot{\mathbf{J}}_{CoM}\dot{\mathbf{q}}$ using the outputs of the last iterations. Besides, Eq. (4.7) is considered as the initial equality constrain of the QP formulation. Therefore, we do not need to add the CoM acceleration among the decision variables of the whole-body QP, and it can be explicitly derived and replaced by this equation.

The cross product in Eq. (4.6b) results in a nonlinear equation with respect to $\mathbf{c}$ and $\ddot{\mathbf{c}}$ variables. However, to keep the CoM acceleration as a decision variable in the QP calculation, we consider $\mathbf{c} = [c^X \; c^Y \; c^Z]^T$ as a constant value (by reference of lab frame) at each iteration. So, we can re-write Eq. (4.6) as:

$$\sum_i \mathbf{f}_i - m\ddot{\mathbf{c}} = -m\mathbf{g} \tag{4.8a}$$

$$\sum_i (\mathbf{p}_i \times \mathbf{f}_i + \boldsymbol{\tau}_i) - m[\mathbf{c}]_\times \ddot{\mathbf{c}} = -m[\mathbf{c}]_\times \mathbf{g} \tag{4.8b}$$

where $[\mathbf{c}]_\times$ is the skew-symmetric matrix of $\mathbf{c}$:

$$[\mathbf{c}]_\times = \begin{bmatrix} 0 & -c^Z & c^Y \\ c^Z & 0 & -c^X \\ -c^Y & c^X & 0 \end{bmatrix}.$$

The dynamic equation of motion is specified in Eq. (4.8). In this equation, the current position of the CoM is considered as the constant value of each iteration for computing $[\mathbf{c}]_\times$. So, this skew-symmetric matrix becomes constant at each calculation stage. Then the equation of motion Eq. (4.8) can be written as:

$$\sum_i \mathbf{w}_i - m \begin{bmatrix} \mathbf{I}_{3\times 3} \\ [\mathbf{c}]_\times \end{bmatrix} \ddot{\mathbf{c}} = -m \begin{bmatrix} \mathbf{g} \\ [\mathbf{c}]_\times \mathbf{g} \end{bmatrix} \tag{4.9}$$

So, by considering a constant $[\mathbf{c}]_\times$ matrix, the right-hand term of the above equation is noted as a consistent value at each iteration, and the equation Eq. (4.9) can be written as a function of $[\ddot{\mathbf{c}} \;\; \mathbf{w}_1 \;\; \dots \;\; \mathbf{w}_i]^T$:

$$\mathbf{A}^{EoM} \begin{bmatrix} \ddot{\mathbf{c}} \\ \mathbf{w}_1 \\ \vdots \\ \mathbf{w}_i \end{bmatrix} = \mathbf{b}^{EoM} \tag{4.10}$$

where:

$$\mathbf{A}^{EoM} = \begin{bmatrix} -m \begin{bmatrix} \mathbf{I}_{3\times 3} \\ [\mathbf{c}]_\times \end{bmatrix} & \mathbf{I}^1_{6\times 6} & \dots & \mathbf{I}^l_{6\times 6} \end{bmatrix} \tag{4.11}$$

$$\mathbf{b}^{EoM} = -m \begin{bmatrix} \mathbf{g} \\ [\mathbf{c}]_\times \mathbf{g} \end{bmatrix} \tag{4.12}$$

The superscript $\circ^{EoM}$ indicates the *Equation of Motion*. Note that the elements $\mathbf{I}^{i}_{6\times 6}$ are all identity matrices, and $\circ^{i}$ shows the number of components that are equal to the number of contacts l.

4.2.2 Contact Modes

The robot can contact the surrounding with multiple modes as fixed, sliding, soft, etc. We need to consider the proper model of the contact modes within the framework. Here we consider the fixed and sliding contacts which are also discussed in previous chapters (Section 2.2 and Section 3.1.2). Here we recall the contact constraints for fixed and sliding modes. As stated in Eq. (2.31), by considering μ_s as static coefficient of friction, we can realize the inner approximation of friction cone by $\mu = \mu_s/\sqrt{2}$. Regarding the x and y as tangential unit vectors, the linearized Coulomb condition in the complementary form becomes

$$|f^x| \leqslant \mu f^z, \tag{4.13}$$
$$|f^y| \leqslant \mu f^z, \tag{4.14}$$
$$f^z > 0. \tag{4.15}$$

Also, assuming that $\boldsymbol{\tau}^c = [\tau^x\ \tau^y\ \tau^z]^T$ is the contact torque exerted by its force around the point o (where the contact wrench is defined in local frame), the following conditions are also determined to avoid tilting and rotational slippages:

$$|\tau^x_o| \leqslant D^x f^z, \tag{4.16}$$
$$|\tau^y_o| \leqslant D^y f^z, \tag{4.17}$$
$$\tau^z_{min} \leqslant \tau^z_o \leqslant \tau^z_{max} \tag{4.18}$$

where

$$\tau^z_{max} \coloneqq +\mu(D^x + D^y)f^z - |D^y f^x + \mu\tau^x_o| - |D^x f^y + \mu\tau^y_o|$$
$$\tau^z_{min} \coloneqq -\mu(D^x + D^y)f^z + |D^y f^x - \mu\tau^x_o| + |D^x f^y - \mu\tau^y_o|$$

and $D^{x,y}$ are scalars and calculated based on the distance of the point o with the edges of the rectangular contact surface Caron (2015).

On the other hand, the constraints are different for sliding contacts. According to the Fig. 1.6, when the contact force lies on the edge of friction cone, the box starts the sliding motion. Based on Coulomb's friction model, the sliding contact mode occurs with a governing formula as $f^t = \mu^d f^n$ for f^t, f^n, and μ^d as tangential and normal contact forces, and dynamic (kinetic) friction coefficient, respectively.

The value of frictional forces of i-th sliding contact in the tangential directions are associated their velocity $\mathbf{v}_i = [v^x_i\ \ v^y_i]^T$, assuming no detachment of contact ($v^z_i = 0$). So, the the equality constraints governing the sliding conditions are

$$f^{\{x,y\}}_i = \mu^d_i f^z_i \frac{v^{\{x,y\}}_i}{\|\mathbf{v}_i\|} \tag{4.19}$$

Furthermore, the normal force control is of interest during the sliding motion and is mainly controlled to converge the desired value $f^z_{i,des}$. So, this condition ($f^z_i = f^z_{i,des}$) will be added to the equality constraints together with Eq. (4.19) in the following matrix form:

$$\begin{bmatrix} 1 & 0 & -\mu^d_i \frac{v^x_i}{\|\mathbf{v}_i\|} \\ 0 & 1 & -\mu^d_i \frac{v^y_i}{\|\mathbf{v}_i\|} \\ 0 & 0 & 1 \end{bmatrix} \mathbf{f}^c_i = \begin{bmatrix} 0 \\ 0 \\ f^z_{i,des} \end{bmatrix} \tag{4.20}$$

For the sliding contacts, the inequalities on contact torques need to be applied as Eq. (4.18) to avoid tilting and rotational slippages. Also, the contact forces in Eq. (4.20) are expressed in the local frame.

4.2.3 Joint Constraints

One of the decision variables of the whole-body controller is the joint accelerations as mentioned in Section 4.2. This controller needs to accomplish the motion tasks within the feasible actuator limits. Therefore, the robot's motion needs to fulfill certain joint-related limits, characterized in the following items.

Joint position limits

The robot consists of multiple actuators, each of which has its operational range due to mechanical design and hardware limits. Throughout each robot scenario, regardless of the planner and controllers, these constraints need to be fulfilled. Therefore, the workspace of the actuators need to be constrained based on the design of the robot as

$$\mathbf{q}^a_{min} \leqslant \mathbf{q}^a \leqslant \mathbf{q}^a_{max}. \tag{4.21}$$

The Eq. (4.22) needs to be written in terms of the decision variables of the robot Bouyarmane et al. (2019b). We can re-write this equation with respect to the configuration acceleration of the robot ($\ddot{\mathbf{q}}$) and consideration of the time iteration Δt in the following form:

$$\frac{\mathbf{q}^a_{min} - \mathbf{q}^a - \dot{\mathbf{q}}^a \Delta t}{\frac{1}{2}\Delta t^2} \leqslant \ddot{\mathbf{q}} \leqslant \frac{\mathbf{q}^a_{max} - \mathbf{q}^a - \dot{\mathbf{q}}^a \Delta t}{\frac{1}{2}\Delta t^2}. \tag{4.22}$$

This equation needs to be an active inequality constraint during the whole motion of the robot.

Joint velocity limits

The current of the actuators can generate an explicit range of actuator velocities. These velocities need to be in the feasible capacity to operate. So, in addition to the joint positions' constraints, we need to take care of the joint velocity. The restriction on

the joint velocity can be directly imposed by derivation of the actuator configuration vector as

$$\dot{\mathbf{q}}^a_{min} \leqslant \dot{\mathbf{q}}^a \leqslant \dot{\mathbf{q}}^a_{max}. \tag{4.23}$$

Same as Eq. (4.22), we need to translate this inequality in terms of the joint accelerations:

$$\frac{\dot{\mathbf{q}}^a_{min} - \dot{\mathbf{q}}^a}{\Delta t} \leqslant \ddot{\mathbf{q}} \leqslant \frac{\dot{\mathbf{q}}^a_{max} - \dot{\mathbf{q}}^a}{\Delta t}. \tag{4.24}$$

Utilizing Eq. (4.24) within the inequality constraints of the whole-body QP fulfills the velocity limitation of joints during the robot's motion.

Joint torque limits

A common challenge in using the robotic setups, especially while performing the challenging scenarios, is the over-torquing issue which burns the actuator. Due to the expense of the motors, it is of high importance to restrict the actuator torques within a safe range by applying a safety margin. According to the decision variables of the whole-body QP, which contains the joint torques, we can explicitly apply the torque limits by

$$\boldsymbol{\tau}^a_{min} \leqslant \boldsymbol{\tau}^a \leqslant \boldsymbol{\tau}^a_{max}. \tag{4.25}$$

Typically, if a scenario rides one of the actuator torques to its maximum/minimum limit, the safest option for the robot would be to stop the controller and servo off the robot immediately.

Collision-avoidance

Throughout the execution of a scenario, the robot needs to avoid the collision of its links. This constraint needs to be formulated regarding the distance between the two specified links a and b, vis. $d(a, b)$:

$$\dot{d}(a, b) \geqslant k^{dmp} \frac{d(a, b) - \delta_{min}}{\delta_{max} - \delta_{min}} \tag{4.26}$$

where k^{dmp} represents the damping coefficient of the joint velocities. Also, δ_{max} and δ_{min} refer to the distance between links which the constraint needs to be activated, and the minimum distance threshold, respectively. This equation can be re-written in terms of a constraint on $\ddot{\mathbf{q}}$ as

$$\ddot{d}(a, b) \leqslant \frac{1}{\Delta t}(-k^{dmp} \frac{d(a, b) - \delta_{min}}{\delta_{max} - \delta_{min}} - \dot{d}(a, b)) \tag{4.27}$$

4.3 Region-free Whole-body Control Structure

According to the studies, for keeping the robot's balance, the contact stability criterion is a necessary condition but not sufficient. The balance of the robot needs to be evaluated through the balance regions. However, the computation of these regions is a time-consuming process, and therefore, there is a need for offline pre-computations. So, the online implementation of the complete balance criterion is still a challenge.

We recently tackled the real-time implementation of the balance controller on the robot by introducing an analytical solution limited to specific configurations in Chapter 2 (see also Samadi et al. (2020)). Later, we resolved these limitations and extended the method for more generic scenarios by introducing the QP formulation based on the Chebyshev center method in Chapter 3 (see also Samadi et al. (2021)). However, in the mentioned study, we implemented the region-free approach on the planner QP. Therefore, the QP was not considering the real-time motion tasks (such as position and orientation tasks, etc.) in the balance control.

The current chapter aims to implement the region-free (Chebyshev) method within the Whole-body controller framework that accounts for all existing tasks and constraints in the balance control. In the following, we concisely summon back to Section 3.2.1 to recall the Chebyshev center method and its employment in the balance control problem.

4.3.1 Integration of Region-Free Method

We will use the proposed region-free method introduced in Chapter 3 within the whole-body controller. Therefore, we briefly recall the technique and discuss its integration with the controller.

Recall of Chebyshev Center Method

The Chebyshev center method was first introduced by Garkavi (1964) and is an optimization process for computing the largest enclosure ball and its center inside a specified bounded set with non-empty interior Amir (1984). This set is defined by inequalities, which need to be modified by the Chebyshev radius, r_c, as an additional term. Assume the set $\mathbf{U} \in \mathbb{R}^n$ in the following form:

$$\mathbf{U} = \{\mathbf{x} \,|\boldsymbol{\alpha}_i^T \mathbf{x} - \boldsymbol{\beta}_i \leqslant \mathbf{0},\ i = 1, \dots, n\} \tag{4.28}$$

which is defined as a bounded polytope for $\mathbf{x} \in \mathbf{U}$. The following optimization problem (equivalent to Eq. (3.24b)) results in the optimal center $\mathbf{x}_c$, namely Chebyshev center, by maximizing the radius of enclosure sphere Boyd and Vandenberghe (2004):

$$\max_{\mathbf{x}, r_c} \ r_c \tag{4.29a}$$

$$\text{s.t. } \boldsymbol{\alpha}_i^T \mathbf{x} + r_c \left\|\boldsymbol{\alpha}_i\right\| - \boldsymbol{\beta}_i \leqslant \mathbf{0} \quad i = 1, \dots, n \tag{4.29b}$$

$$r_c \geqslant \mathbf{0} \tag{4.29c}$$

Note that the implementation of the region-free method rests in the alteration of the respective inequality constraints and maximizing the radius. As you can see, Eq. (4.28) is modified to Eq. (4.29b) by considering the r_c. We refer the readers to Chapter 3 and Boyd and Vandenberghe (2004) for more detail on the Chebyshev center method and its applications.

Chebyshev Implementation for Balance Control

For the balance control of the robot, instead of computing the balance regions geometrically, we leverage the corresponding inequalities which define the polytopes and implement the region-free approach by modifying them as mentioned in Section 4.3.1.

The inequalities on the contact forces for non-sliding contacts, Eq. (1.10) and Eq. (4.18), represent the contact friction cones as shown in Fig. 1.6. The *Minkowski sum* Fukuda et al. (2004) of these cones results in the CWC Hirukawa et al. (2006) or GIWC Caron et al. (2015a) which are used for evaluating the contact stability criterion Pang and Trinkle (2000). The balance regions, such as CoM Bretl and Lall (2008) or CoM acceleration Audren and Kheddar (2018) regions, can be relatively derived based on the equation of motion.

The inequalities of the non-sliding contacts in Eq. (1.10) can be represented in the global frame and re-written in the matrix form:

$$\mathbf{G}_i \mathbf{R}_i \mathbf{f}_i^c \leqslant \mathbf{0}_{3\times 1} \tag{4.30}$$

where

$$\mathbf{G}_i = \begin{bmatrix} 1 & 0 & -\mu \\ -1 & 0 & -\mu \\ 0 & 1 & -\mu \\ 0 & -1 & -\mu \\ 0 & 0 & -1 \end{bmatrix}, \quad \mathbf{f}_i^c = \begin{bmatrix} f_i^x \\ f_i^y \\ f_i^z \end{bmatrix}.$$

Note that the rotation matrix is orthogonal with $\|\mathbf{R}_i\| = 1$, and preserves the norm of three-dimensional vectors (rows of $\mathbf{G}_i$ matrix). So, the multiplication of $\mathbf{R}_i$ in Eq. (4.30) does not affect the norm of these vectors.

In order to implement the region-free method, we need to modify the constraints on the contact friction forces and also consider the positive values for the Chebyshev radius as in Eq. (4.29c). So, the inequality constraint Eq. (4.30) for i-th non-sliding contact becomes:

$$\begin{bmatrix} \mathbf{G}_i & \boldsymbol{\zeta}_i \\ \mathbf{0}_{1\times 3} & -1 \end{bmatrix} \begin{bmatrix} \mathbf{R}_i & 0 \\ 0 & 1 \end{bmatrix} \begin{bmatrix} \mathbf{f}_i^c \\ r_c \end{bmatrix} \leqslant \mathbf{0}_{4\times 1}. \tag{4.31}$$

Denoting that $\mathbf{G}_i(j,:)$ and $\boldsymbol{\zeta}_i(j)$ represent the j-th row and element of $\mathbf{G}_i$ matrix and $\boldsymbol{\zeta}_i$ vector, respectively, we have:

$$\boldsymbol{\zeta}_i(j) = \|\mathbf{G}_i(j,:)\| \tag{4.32}$$

Also, in the Eq. (4.31), the first matrix on the left-hand side of the equation contains the -1 value, which is for considering the $r_c \geqslant 0$ condition.

4.3.2 Reducing Conservativeness of the Region-Free Method

In the previous chapter, we considered a single Chebyshev radius within variables for all contact forces and torques, as stated in Eq. (3.35). The computed Chebyshev radius must be valid for all contacts through the QP problem. In other words, the computed wrench distribution of contacts and a specific range around them (a sphere with Chebyshev radius) should be within the corresponding cones.

As a numerical example, we can consider a humanoid robot in contact with the environment by two points, as shown in Fig. 4.1. In this figure, we displayed the linearized friction cones of forces with different coefficients of frictions. Considering a single Chebyshev radius in the problem reveals that the respective spheres within cones are not always the most extensive ones. In other words, in Fig. 4.1(a) the radii of spheres inside $\mathcal{C}_1$ and $\mathcal{C}_2$ need to have the same values, and therefore, the sphere within $\mathcal{C}_2$ is not the largest possible sphere within this cone.

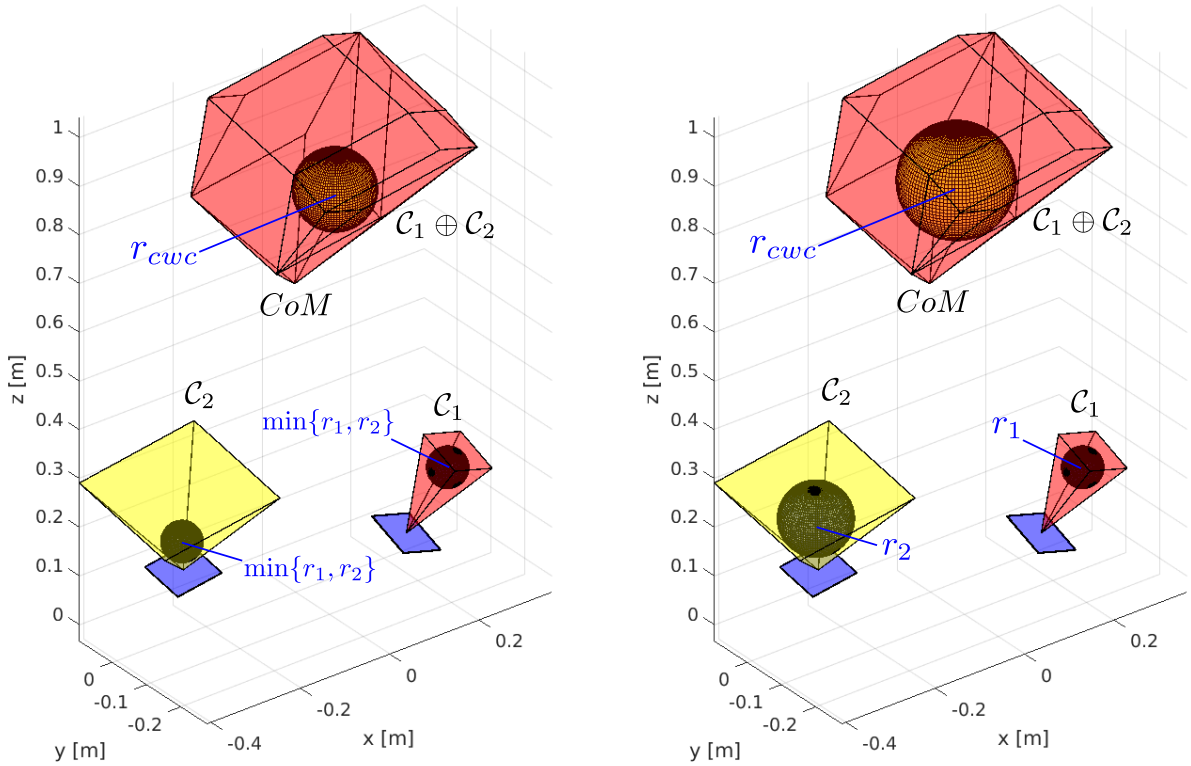

(a) (b)

FIGURE 4.1 – *Comparison of the resultant sphere within the CWC.*

In the current study, we define independent Chebyshev radii for each contact. This way, each frictional cone will contain the most extensive corresponding sphere of feasible wrenches. As an illustration of the numerical example, Fig. 4.1(b) represents r_1 and r_2 as related radii for $\mathcal{C}_1$ and $\mathcal{C}_2$, respectively. Therefore, the resultant sphere within the CWC has a larger r_{cwc} than the sphere defined in Fig. 4.1(a). So, the resultant sphere covers more space of the exact CWC. Consequently, the conservativeness of the approach reduces.

According to Samadi et al. (2021), the radius of the feasible sphere within the GIWC or CWC, r_{cwc}, is equal to the number of contacts (n_c) multiplied by the Chebyshev radius, $r_{cwc} = n_c \times r_c$, in case of considering only one Chebyshev radius for all contacts (Fig. 4.1(a)). However, by considering multiple radii, the resulting sphere will be sum of them as

$$r_{cwc} = \sum_{i=1}^{n_c} r_{c,i}.$$

By considering the unique radius as in previous chapter, we select the minimum value among possible contact wrench ranges. However, regarding multiple radii helps enlarge the sphere in CWC and reduces the *conservativeness* of the approach because the contact wrench can have a more comprehensive feasibility range. We can evaluate this conservativeness by calculating the sphere induced by the Chebyshev implementation within the CoM regions. Therefore, in the following, we translate the computed Chebyshev radius into the CoM position and acceleration regions as static and dynamic solutions.

4.3.3 Evaluation of Balance Criterion

According to Eq. (3.57), the radius of the feasible sphere within the GIWC or CWC, r_{cwc}, is equal to the number of contacts (n_c) multiplied by the Chebyshev radius,

$$r_{cwc} = n_c \times r_c.$$

As indicated in Section 3.3.3, the contact stability of the motion is qualified by the implementation of the Chebyshev center method. However, for evaluating the balance of the robot, contact stability is required but not sufficient. The geometrical balance regions for CoM position or acceleration have been investigated as sufficient balance criteria in the literature. However, as mentioned before, the computation of these regions is time-consuming and prohibits the online implementation of balance criterion.

Leveraging the Chebyshev center method, we can guarantee the balance of the robot sufficiently without the need for geometric calculation of the balance regions. In Section 3.3.3, we investigated the translation of the Chebyshev radius into the static equilibrium region. In the following, we derive the half-space representation of the regions mentioned above for dynamic motions with their respective safety margins.

Note that the region-free approach significantly decreases the computational cost and enables the balance control's real-time implementation. There is no need for any computation of the balance region. Accordingly, the following analysis is carried out interdependently to examine the balancing appearances of the method.

A mathematical proof is provided for the evaluation of the static equilibrium while integrating the region-free method through Eq. (3.65). To continue, we assess the dynamic balance control within the CoM acceleration region.

The contact wrench with respect to the fixed point O (which is the origin of the lab

frame as shown in Fig. 1.6) is defined according to Eq. (4.6) as

$$\mathbf{w}_O \overset{\text{def}}{=} \begin{bmatrix} \mathbf{f} \\ \boldsymbol{\tau}_O \end{bmatrix} = \sum_i \begin{bmatrix} \mathbf{f}_i \\ \mathbf{p}_i \times \mathbf{f}_i \end{bmatrix}. \tag{4.33}$$

We can represent the CWC at this point by

$$\mathbf{A}_O \boldsymbol{\omega}_O \leqslant \mathbf{0}. \tag{4.34}$$

According to the calculated r_{cwc} radius within the CWC, we can re-formulate Eq. (4.34) for the $i-th$ row of this inequality based on the Chebyshev implementation Eq. (3.24b) in the following form:

$$\mathbf{A}_{O,i} \boldsymbol{\omega}_O + r_{cwc} \left\| \mathbf{A}_{O,i} \right\| \leqslant \mathbf{0} \tag{4.35}$$

Next, we present the $\mathbf{A}_{O,i}$ by the dual twist $[\mathbf{a}_O \ \mathbf{a}] \in \mathbb{R}^6$ Featherstone (2014). So, Eq. (4.35) becomes

$$\mathbf{a}_O.\mathbf{f} + \mathbf{a}.\boldsymbol{\tau}_O + r_{cwc} \left\| \mathbf{A}_{O,i} \right\| \leqslant \mathbf{0}. \tag{4.36}$$

We can represent the above equation in another point as CoM. For this purpose, we need to replace $\mathbf{a}_O$ with $\mathbf{a}_c = \mathbf{a}_O + \mathbf{a} \times \mathbf{c}$ Caron and Kheddar (2016) based on the Varignon formula Moore (2021):

$$\mathbf{a}_c.\mathbf{f} + \mathbf{a}.\boldsymbol{\tau}_c + r_{cwc} \left\| \mathbf{A}_{O,i} \right\| \leqslant \mathbf{0}. \tag{4.37}$$

According to Eq. (4.6), considering zero angular moment of the motion, $\boldsymbol{\tau}_c = \mathbf{0}$, and $\mathbf{f} = m(\ddot{\mathbf{c}} - \mathbf{g})$ in dynamic motions, the inequality Eq. (4.37) becomes:

$$m\mathbf{a}_c.\ddot{\mathbf{c}} - m\mathbf{a}_c.g + r_{cwc} \left\| \mathbf{A}_{O,i} \right\| \leqslant \mathbf{0} \tag{4.38}$$

Assuming $\sigma_{\hat{a}} = -a_{Oz} + a_y c^x - a_x c^y$, we can re-write the equation as:

$$m\mathbf{a}_c.\ddot{\mathbf{c}} - mg\sigma_{\hat{a}} + r_{cwc} \left\| \mathbf{A}_{O,i} \right\| \leqslant \mathbf{0} \tag{4.39}$$

Note that $\sigma_{\hat{a}}$ includes position of CoM which we consider it as *constant variable* at each iteration as specified in Section 4.2.1 and Eq. (4.9). The term $\mathbf{a}_c.\ddot{\mathbf{c}}$ is calculated as

$$\begin{aligned} \mathbf{a}_c.\ddot{\mathbf{c}} &= \phi\ddot{c}^x + \varphi\ddot{c}^y - \sigma_{\hat{a}}\ddot{c}^z \\ \phi &= -a_z c^y + a_y c^z + a_{Ox} \\ \varphi &= +a_z c^x - a_x c^z + a_{Oz}. \end{aligned}$$

By assuming $\left\| \mathbf{A}_{O,i} \right\| = 1$ without loss of generality, the inequality becomes:

$$\phi\ddot{c}^x + \varphi\ddot{c}^y - \sigma_{\hat{a}}\ddot{c}^z - g\sigma_{\hat{a}} \leqslant -\frac{r_{cwc}}{m} \tag{4.40}$$

Considering slackness of the inequality as

$$\sigma_{acc} = -\phi\ddot{c}^x - \varphi\ddot{c}^y + \sigma_{\hat{a}}(\ddot{c}^z + g)$$

which is the half-space representation of the CoM acceleration region for any $\ddot{z}_G \geqslant -g$, we have:

$$\sigma_{acc} \geqslant \frac{r_{cwc}}{m}. \tag{4.41}$$

The above equation indicates that in the respective configuration, the CoM of the robot can generate a minimum acceleration of $\frac{r_{cwc}}{m}$ in every desired direction for maintaining the balance.

4.3.4 Whole-body Controller Framework

The planned motions and scenarios need to be implemented and executed on the robot. For this purpose, a controller needs to be employed that controls all robot joints based on the desired tasks. However, most of the time, multiple tasks need to be executed simultaneously on the robot (e.g., locomotion of the robot and manipulation of objects). Approaching various tasks is also the responsibility of the whole-body controller.

We base our framework on top of the whole-body controller introduced in Bouyarmane et al. (2019b). Additionally, the proposed strategy will contain a *region-free* and *online* balance controller thanks to the implementation of the Chebyshev center method. We address the objectives of this controller as a QP problem in task-space by

- steering the task $\mathbf{t}_j$ around a set-point, as CoM and configuration tasks, or
- directing the task from an initial value to a target, such as end-effector or CoM trajectory tasks.

We aim to reach the desired motions ($\mathbf{t}_j^{des}$) in the whole-body controller by task-space formulation and maximizing the Chebyshev radius. In the current implementation, we consider a independent Chebyshev radii ($r_{c,i}$) for each contact. Therefore, we introduce the Chebyshev radius vector containing all radii as $\mathbf{r}_c = [r_{c,1}, \ldots, r_{c,i}]^T$. Consequently, we can formulate the unified QP scheme as follows:

$$\min_{\ddot{\mathbf{q}}^a, \mathbf{w}, \boldsymbol{\tau}^a, \mathbf{r}_c} \; -\sum_i r_{c,i} + \sum_j \mathbf{w}_j \left\| \ddot{\mathbf{t}}_j - \ddot{\mathbf{t}}_j^{des} \right\|^2 \tag{4.42}$$

$$\text{s.t. } Eq.\ (4.9), Eq.\ (4.20), Eq.\ (4.24),\ Eq.\ (4.25),\ Eq.\ (4.26),\ Eq.\ (4.29c),\ \text{and } Eq.\ (4.31).$$

where $\mathbf{w}_j$ denotes the weight of which assigned to each motion task. Fig. 4.2 demonstrates the schematic of the integrated framework which comparable with the presented schematics in previous chapters (Fig. 2.3 and Fig. 3.5). In this framework, the motion states are directed to the controller. In order to be able to implement the additional decision variables ($\mathbf{r}_c$) to the classical approach within the `mc_rtc` framework, we utilized a recently developed library named `TVM` for formulating the quadratic problems which is addressed in Section 1.6.4.

4.4 Simulations and Results

In the last section, we expressed the structure of the unified framework as the whole-body controller. This schematic licenses the humanoid robot to traverse the scenarios under active dynamic balance. The principal contribution of the current chapter concerning the previous one is implementing the online balance strategy within the controller rather than the separate planner. By the proposed formation, all real-time motion tasks are involved in the robot's balance.

In this section, we are investigating the capacities of the unified framework through pushing and wiping scenarios. The simulations are carried out by the whole-body

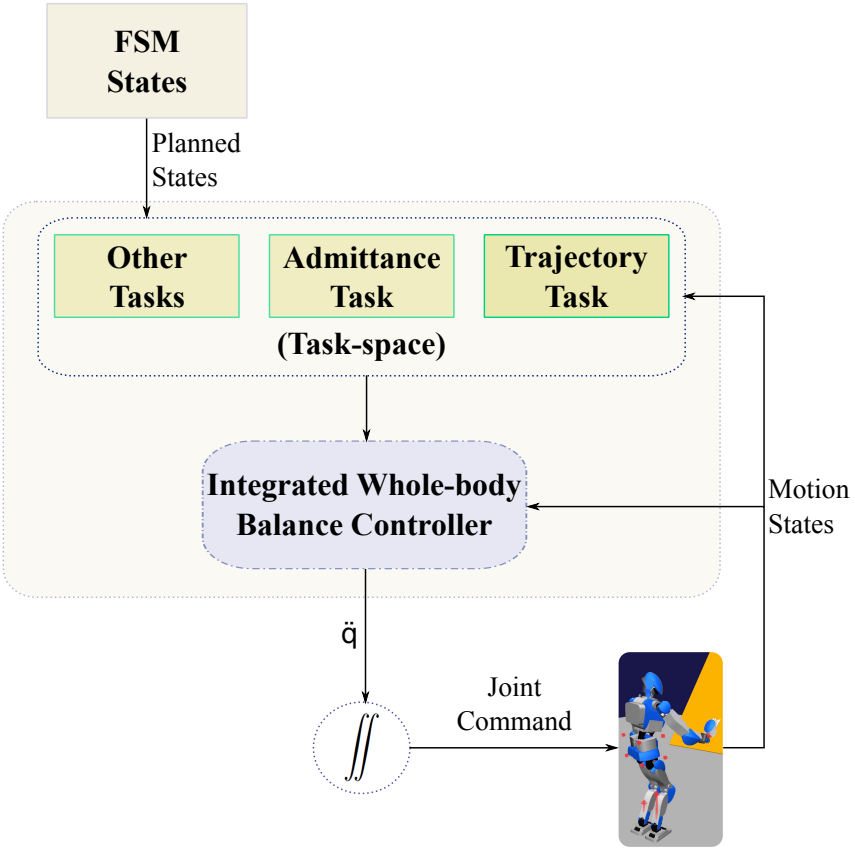

FIGURE 4.2 – *Schematic of the integrated whole-body balance controller framework.*

controller and consist of numerous motion tasks. In the following, we examine the designed plans while pushing and wiping motions of the robot.

4.4.1 Pushing Against the Board

The framework has no limitation on the configuration of contacts. Therefore, we can design scenarios with random contact positions and orientations such as tilted boards. Here, we use a panel with an angle of $\approx 50°$. The scenario starts by moving the hand towards the tilted board by executing an end-effector trajectory task within the FSM planner. Then the robot continues his motion to make contact with the board. The completion criterion of this state is based on the force-sensing of the relevant end-effector. So, the movement stops after sensing the small quantity of force (around 5 N of normal force).

To continue, we aim for controlling the force of the end-effector using the admittance force control within the force task. The user can define the force target within the FSM. We regulate the pressure to raise up to 15 N and then release it to zero. Fig. 4.4 showes the normal force tracking of the right-hand while pushing against the panel.

The following figures demonstrate the CoM of the robot and its derivatives during the whole motion. The Fig. 4.5(a) is the CoM position of the robot in X and Y directions of the global frame. The Fig. 4.5(b) is extracted from the performance of the same

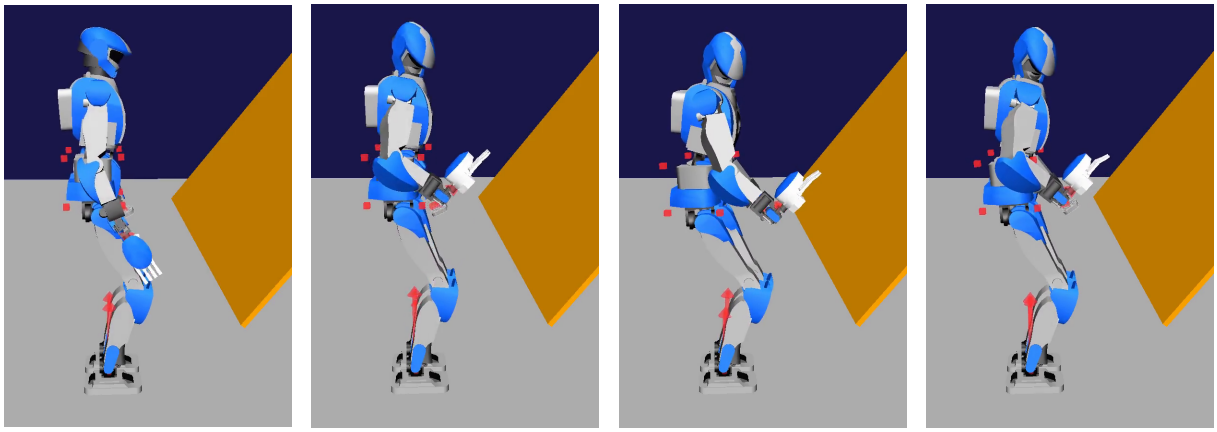

FIGURE 4.3 – *Simulation of Pushing against a tilted board.*

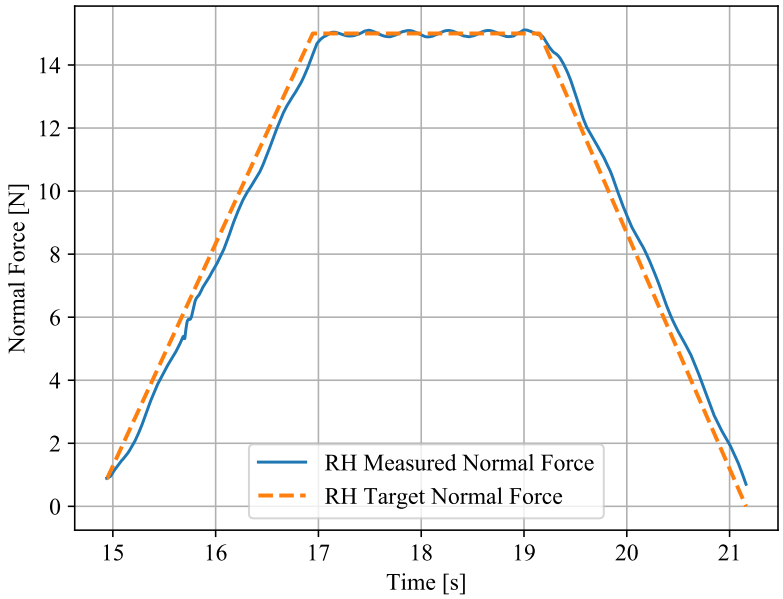

FIGURE 4.4 – *Normal force tracking of the HRP-4 humanoid robot with the contacting end-effector.*

scenario using the proposed method in the previous chapter, which can be compared with Fig. 4.5(a).

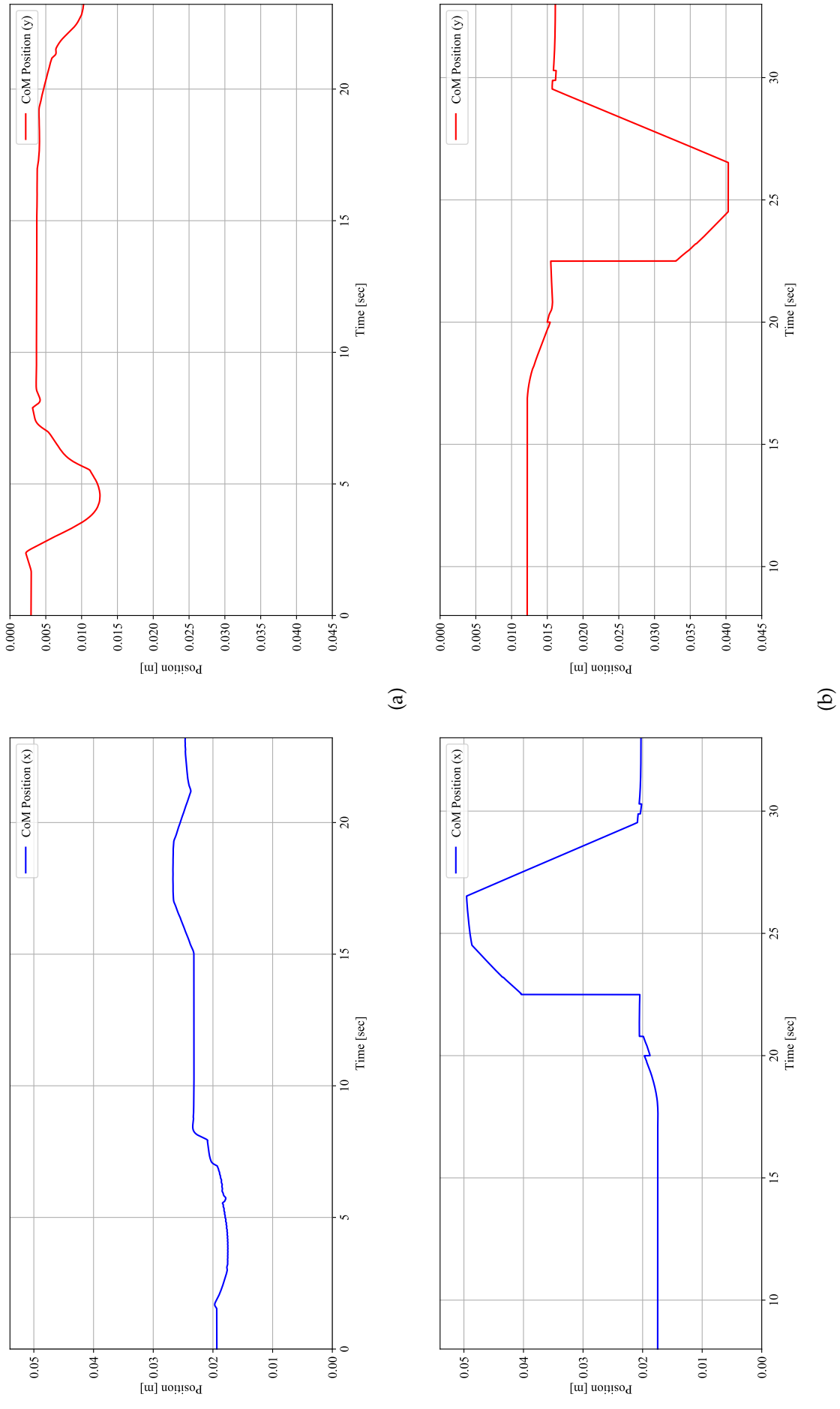

FIGURE 4.5 – *CoM profile of the HRP-4 humanoid robot while execution of pushing experiment with (a) integrated whole-body framework, and (b) the proposed approach in Chapter 3.*

In the current chapter, we are considering the dynamic balance of the robot that contains the CoM acceleration within its calculation. Fig. 4.6 and Fig. 4.7 show the CoM velocity and acceleration trajectories of the robot during the pushing scenario.

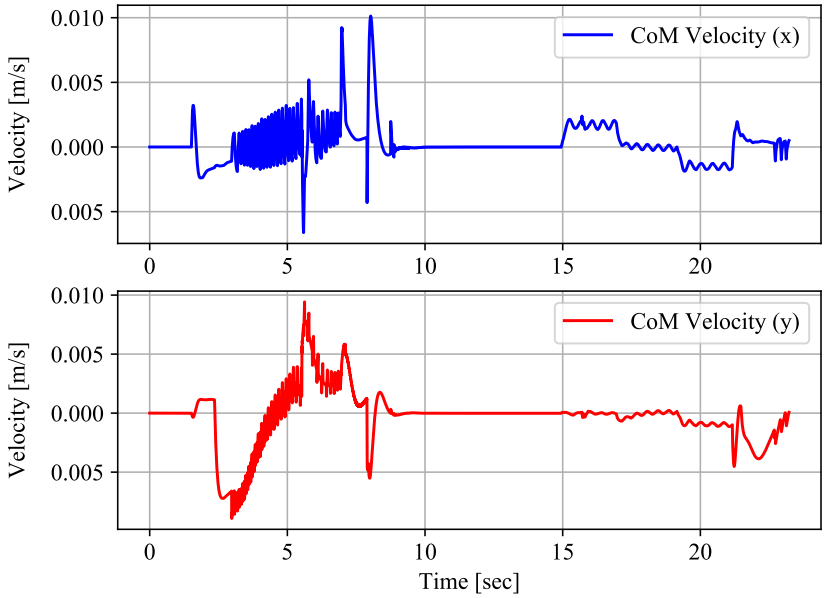

FIGURE 4.6 – *CoM Velocity profile of the HRP-4 humanoid robot while execution of pushing experiment.*

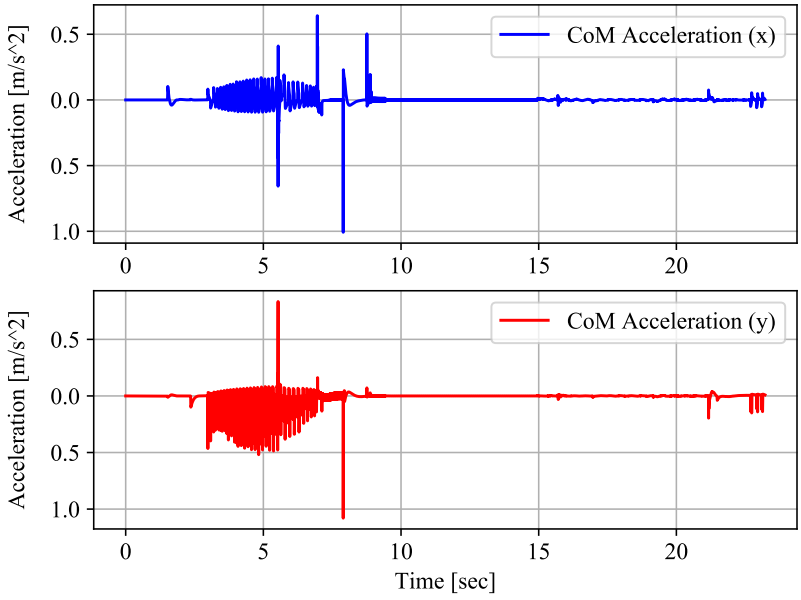

FIGURE 4.7 – *CoM Acceleration profile of the HRP-4 humanoid robot while execution of pushing experiment.*

The robot keeps his balance due throughout the scenario without adding any balance-related tasks such as a CoM task. In the following, we extend the application to the sliding methods and investigate the controller's capabilities through a wiping scenario.

4.4.2 Wiping the Tilted Board

After accomplishing the pushing task leveraging the unified structure, we aim for the wiping motion of the robot. For this purpose, we re-do the steps up to pushing the wall with 15 N. Afterwards, we begin a wiping scenario and the end-effector of the robot draws a circle of 10 cm on the same tilted board. By starting the sliding motion, the whole-body controller considers the contact as a sliding contact due to its tangential velocity and uses the corresponding contact equations within the constraints.

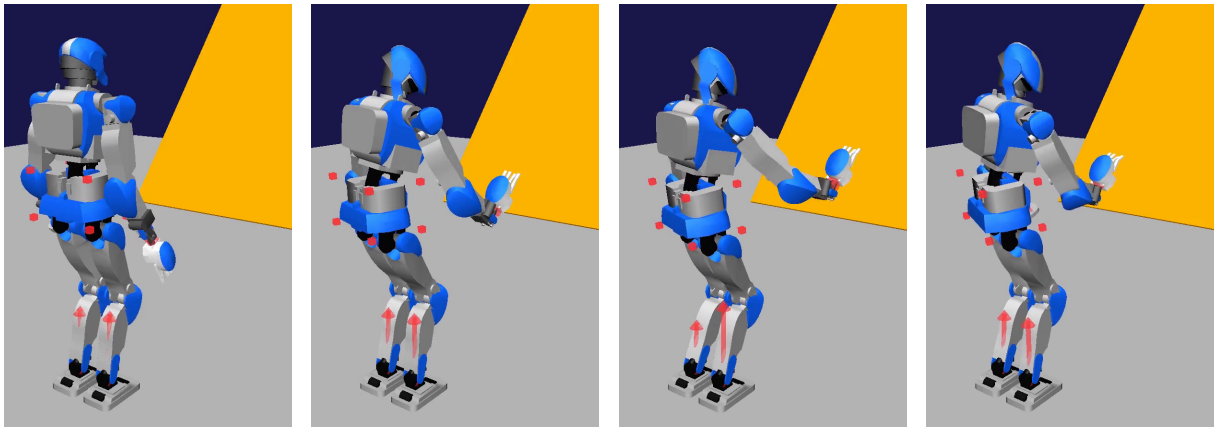

FIGURE 4.8 – *Simulation of wiping a tilted board.*

Fig. 4.9 illustrates the target (user-defined value) and measured force of the sliding end-effector in the normal direction of the board.

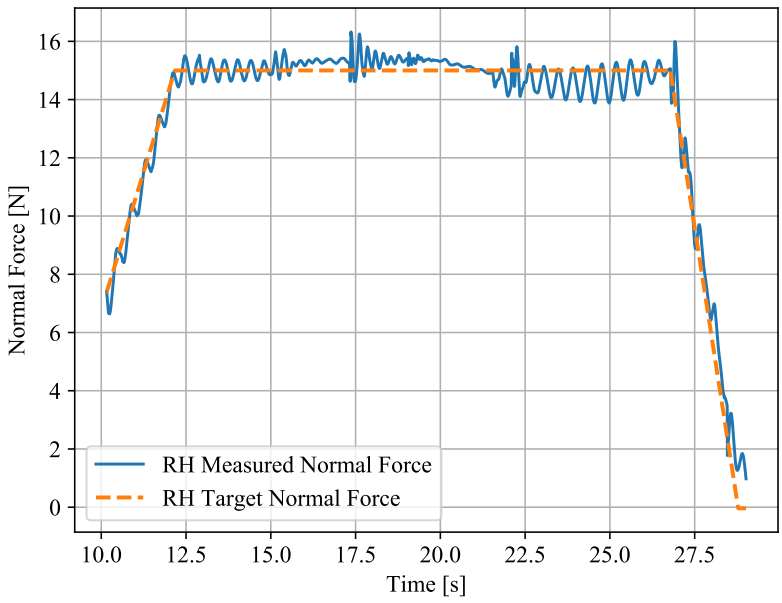

FIGURE 4.9 – *Normal force tracking of the HRP-4 humanoid robot with the contacting end-effector while wiping the tilted board.*

Moreover, Fig. 2.11 shows the CoM of the robot, which is calculated as the output of the whole-body QP. By execution of the same scenario using the proposed method

of the previous chapter (region-free approach within the planner), the CoM position as the output of the planner QP is demonstrated in Fig. 4.10(b) which can be compared with Fig. 2.11.

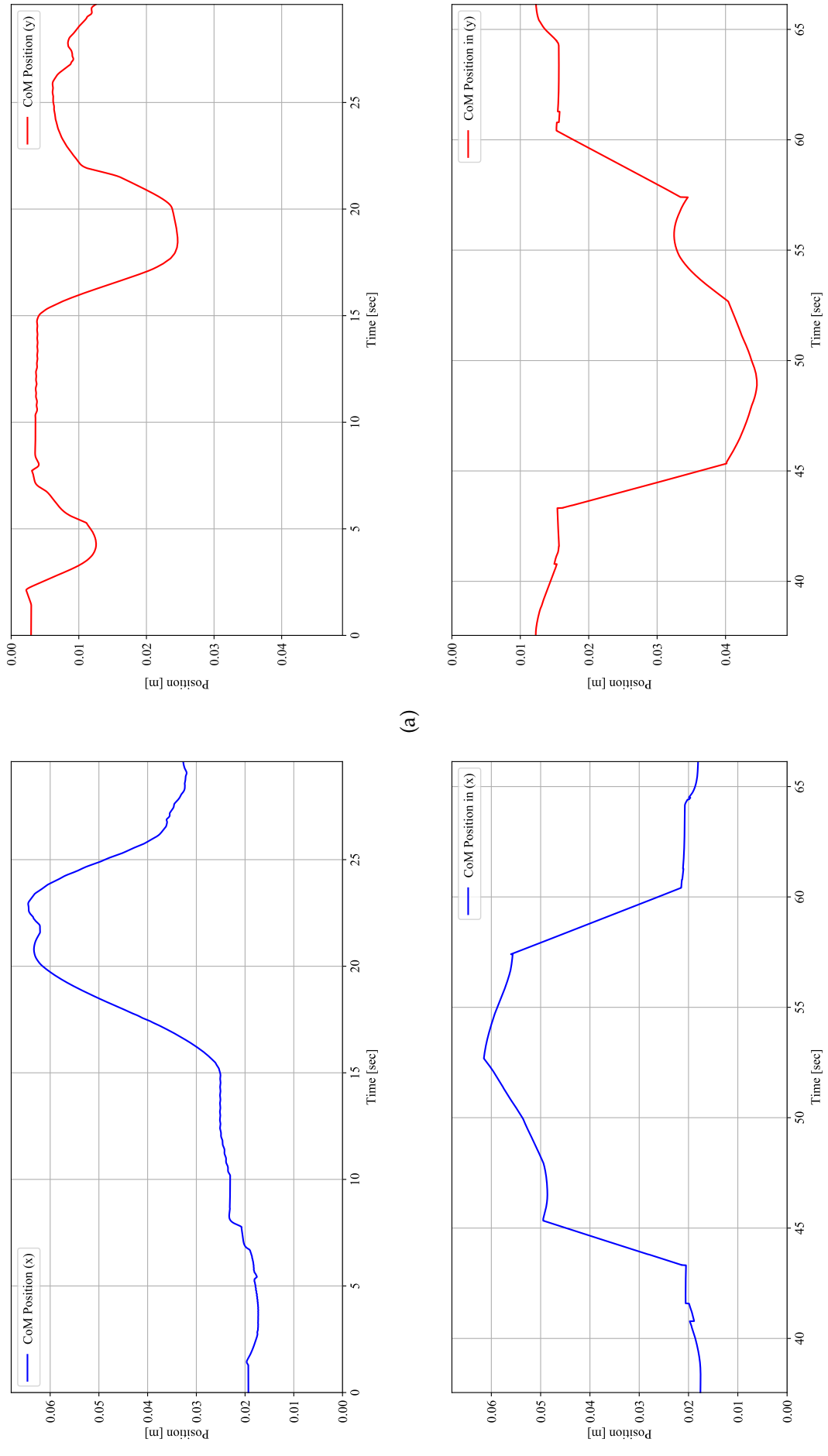

FIGURE 4.10 – *CoM profile of the HRP-4 humanoid robot while execution of wiping experiment with (a) integrated whole-body framework, and (b) the proposed approach in Chapter 3.*

Also, the following figures illustrate the range of the CoM velocity and acceleration profiles of the wiping scenario.

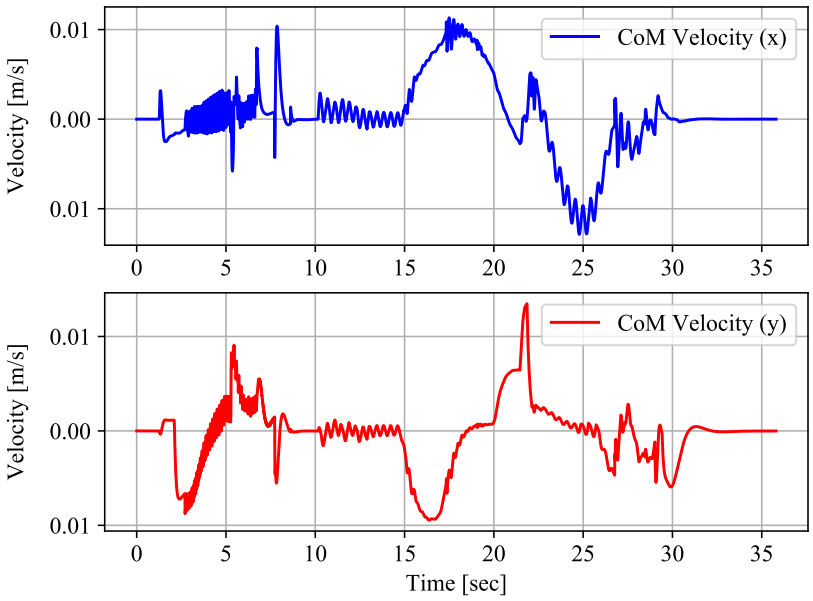

FIGURE 4.11 – *CoM Velocity profile of the HRP-4 humanoid robot while execution of wiping experiment.*

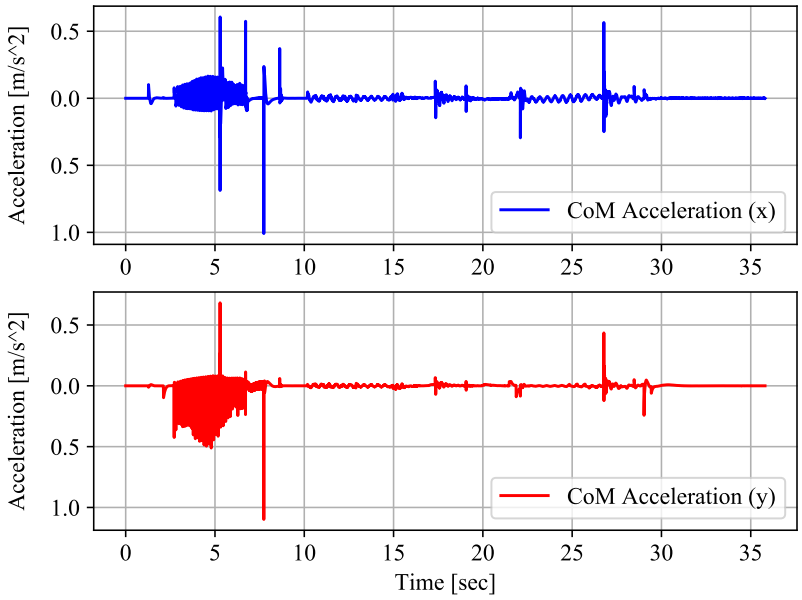

FIGURE 4.12 – *CoM Acceleration profile of the HRP-4 humanoid robot while execution of wiping experiment.*

The execution of the scenarios mentioned above shows the current structure's capabilities in executing the whole-body generated motions accompanied by an online

balance control. A video of the respective simulations are available online [2]. However, several aspects need to be investigated and extended to reach a fully automatic whole-body balance controller, which will be addressed in the next chapter as future works.

4.5 Conclusion

Previously, in Chapter 3, we introduced a region-free approach that enables the online implementation of the balance controller without any configuration limitations addressed in Chapter 2. This method is fast as it does not need the geometric computation of the balance region. In this chapter, we picked another step towards the online balance of the robot by introducing a unified structure for the robot's motion.

While executing the motion tasks, such as end-effector tasks, the balance controller established within the planner has no sense of the robot's configuration. The actuator position is not considered as part of this planner. However, only the contact points and wrenches are considered to this extent after establishing the contacts. In other words, if the robot moves its free limbs without any contact as a motion task, the planner assumes no robot's motion.

In this chapter, we leveraged the region-free approach as a fast balance strategy within the whole-body controller. This controller contains all motion tasks and constraints and solves the QP problem by considering the robot's balance. Therefore, any executed tasks are considered within a unified balancing framework. To formulate the problem of whole-body structure with the additional and dynamic variables, we utilized the `TVM` library.

The capabilities of the proposed framework are investigated through pushing and wiping scenarios. The robot was able to accomplish the underlying tasks under dynamic balance. The current implementation is a road map for the future of the online balance control of humanoids. Still, multiple characteristics need to be studied and stretched. In the following chapter, we will mention the future works based on this research.

2. https://drive.google.com/file/d/1bXtqQKwfbpdcSFJQkn_h_rx0QLXJlaAy/view?usp=sharing

CONCLUSION

Performing complex scenarios is primarily available via multi-contact settings. Also, the presence of different contact modes promotes the accomplishment of these tasks. The robot's balance in multi-contact has been widely investigated through geometric construction and evaluation of the balance regions. However, the online implementation of the balance criteria is still a challenge to solve.

According to the most recent researches Caron et al. (2015a); Abi-Farraj et al. (2019), the computation of multi-contact balance regions needs to be at least calculated at each stance configuration of the robot (a configuration without change of contact modes). However, the geometric computation of multi-contact regions is a time-consuming process that prohibits real-time controller implementation. Moreover, exploring other contact modes than the fixed one results in a change in stance configuration and, subsequently, an increase in computational time.

In this thesis, we investigated the balance control of the humanoid robots in multi-contact settings. Also, we tackled the challenge of real-time implementation of the balance control strategies. We introduced two main strategies for solving the online implementation issue, which are

- constructing the CoM-support area using an analytical solution, and
- introducing a fast-computed QP formulation for balance control.

The first strategy aims to form and calculate the balance region in 2D (balance area) under mathematical assumptions for the analytical solution. However, the mentioned assumptions reduce the range of use cases that can leverage from this method. In this approach, the fixed contacts are assumed to be coplanar, and this is not the case in many scenarios unless we fix the feet on the ground and execute manipulation and wiping tasks using the hands.

The second approach solved the addressed mathematical limitation by proposing a QP formulation based on the region-free method. In this method, there is no need for explicit geometrical representation of the balance regions. The corresponding inequalities are involved in the QP, and the balance is guaranteed with the cost of conservativeness. So, using this strategy, not only the implementation of the balance controller is available online without any restrictions and computational limitations, but also different contact modes can be simultaneously involved in the scenario as executed in the experiments of the third chapter.

As a final step of this thesis towards the balance control of the humanoid robots,

we integrate the online balancing structure within the whole-body controller rather than the planner. The balance criterion is based on the proposed region-free approach, which enables real-time implementation. Leveraging this unified framework, all motion tasks and constraints are considered within the robot's balance, which was not the case for planners. Additionally, by holding the centroidal and actuated dynamics of the robot, we are able to generate the whole-body motions under active balance. The capabilities of the proposed strategy are evaluated through pushing and wiping scenarios in simulations.

The current study is an initiative at the future of balance control in humanoids, and there exist several aspects to investigate and accomplish. As short-term aspirations for continuing this research direction, we can consider the extension of contact modes to soft and rolling contacts. This helps the robot to execute more generic scenarios as well as keep the balance in real-time. Moreover, the conservativeness of the approach can be reduced by further evaluation and analysis of the region-free method.

Producing the planned and challenging outlines by the current or modified version of the balance controller can be counted as a mid-term intent for the future. The scenarios which contain the contact plannings and need switches between contact modes can be executed under balance. For this circumstance, a considerable case study could be accessing narrow spaces and generating the crawling motion pattern, which contains more contacts than hands and feet (additional contacts as knees and elbows).

Finally, the extension of the approach for multi-contact locomotion and loco-manipulation tasks can be considered a long-term objective for the current study. Many challenges in humanoid robotics, such as stair and ladder climbing, multi-contact travel,..., can be adequately addressed by an efficient balance control strategy. Implementing the planning methods for executing such tasks and their compatibility with the whole-body balance controller can result in impressive scenarios.

BIBLIOGRAPHIE

Abe, Y., Da Silva, M., and Popović, J. (2007). Multiobjective control with frictional contacts. In *ACM SIGGRAPH/Eurographics symposium on Computer animation*, pages 249–258. Citeseer. 18

Abi-Farraj, F., Henze, B., Ott, C., Giordano, P. R., and Roa, M. A. (2019). Torque-Based Balancing for a Humanoid Robot Performing High-Force Interaction Tasks. *IEEE Robotics and Automation Letters*, 4(2):2023–2030. 19, 22, 52, 53, 59, 99

Amir, D. (1984). Best simultaneous approximation (chebyshev centers). In *Parametric Optimization and Approximation*, pages 19–35. Springer. 57, 84

Audren, H. and Kheddar, A. (2017). Model-predictive control in multi-contact based on stability polyhedrons. In *IEEE-RAS International Conference on Humanoid Robotics*, pages 631–636. 21

Audren, H. and Kheddar, A. (2018). 3-D Robust Stability Polyhedron in Multicontact. *IEEE Transactions on Robotics*, 34(2):388–403. 21, 33, 34, 52, 53, 85

Audren, H., Kheddar, A., and Gergondet, P. (2016). Stability polygons reshaping and morphing for smooth multi-contact transitions and force control of humanoid robots. In *IEEE-RAS International Conference on Humanoid Robots*, pages 1037–1044. 53

Audren, H., Vaillant, J., Kheddar, A., Escande, A., Kaneko, K., and Yoshida, E. (2014). Model preview control in multi-contact motion-application to a humanoid robot. In *IEEE/RSJ International Conference on Intelligent Robots and Systems*, pages 4030–4035. 9

Azad, M., Ortenzi, V., Lin, H. C., Rueckert, E., and Mistry, M. (2016). Model estimation and control of compliant contact normal force. In *IEEE-RAS International Conference on Humanoid Robots*, pages 442–447. 23

Balkcom, D. J. and Trinkle, J. (2002). Computing wrench cones for planar rigid body contact tasks. *The International Journal of Robotics Research*, 21(12):1053–1066. 13

Beck, A. and Eldar, Y. C. (2007). Regularization in regression with bounded noise: A Chebyshev center approach. *SIAM Journal on Matrix Analysis and Applications*, 29(2):606–625. 56

Bevly, D., Farritor, S., and Dubowsky, S. (2000). Action module planning and its application to an experimental climbing robot. In *IEEE International Conference on Robotics and Automation*, volume 4, pages 4009–4014 vol.4. 10

Bicchi, A. (1994). On the problem of decomposing grasp and manipulation forces in multiple whole-limb manipulation. *Robotics and Autonomous Systems*, 13(2):127–147. 14

Bolotnikova, A., Courtois, S., and Kheddar, A. (2020). Multi-contact planning on humans for physical assistance by humanoid. *IEEE Robotics and Automation Letters*, 5(1):135–142. 24, 73

Bolotnikova, A., Gergondet, P., Tanguy, A., Courtois, S., and Kheddar, A. (2021). Task-Space Control Interface for SoftBank Humanoid Robots and its Human-Robot Interaction Applications. In *2021 IEEE/SICE International Symposium on System Integration, SII 2021*, pages 560–565. 24, 25

Bouyarmane, K., Caron, S., Escande, A., and Kheddar, A. (2019a). *Multi-contact Motion Planning and Control*, pages 1763–1804. Springer Netherlands, Dordrecht. 12, 21, 37

Bouyarmane, K., Chappellet, K., Vaillant, J., and Kheddar, A. (2019b). Quadratic Programming for Multirobot and Task-Space Force Control. *IEEE Transactions on Robotics*, 35(1):64–77. 19, 20, 42, 56, 68, 70, 82, 89

Bouyarmane, K. and Kheddar, A. (2011a). Multi-contact stances planning for multiple agents. In *IEEE International Conference on Robotics and Automation*, pages 5246–5253. 18, 19, 28

Bouyarmane, K. and Kheddar, A. (2011b). Using a multi-objective controller to synthesize simulated humanoid robot motion with changing contact configurations. In *IEEE International Conference on Intelligent Robots and Systems*, pages 4414–4419. 21

Bouyarmane, K. and Kheddar, A. (2012). Humanoid robot locomotion and manipulation step planning. *Advanced Robotics*, 26(10):1099–1126. 19

Boyd, S. and Vandenberghe, L. (2004). *Convex optimization*. Cambridge university press. 84, 85

Brasseur, C., Sherikov, A., Collette, C., Dimitrov, D., and Wieber, P. B. (2015). A robust linear MPC approach to online generation of 3d biped walking motion. In *IEEE-RAS International Conference on Humanoid Robots*, pages 595–601. 52

Bretl, T. and Lall, S. (2008). Testing static equilibrium for legged robots. *IEEE Transactions on Robotics*, 24(4):794–807. 21, 33, 85

Caron, S. (2015). *Computational Foundation for Planner-in-the-Loop Multi-Contact Whole-Body Control of Humanoid Robots*. PhD thesis, University of Tokyo. 14, 38, 55, 63, 81

Caron, S. and Kheddar, A. (2016). Multi-contact walking pattern generation based on model preview control of 3d com accelerations. In *IEEE-RAS International Conference on Humanoid Robots*, pages 550–557. 52, 67, 88

Caron, S., Kheddar, A., and Tempier, O. (2019). Stair climbing stabilization of the HRP-4 humanoid robot using whole-body admittance control. In *IEEE International Conference on Robotics and Automation*. 8, 25, 26

Caron, S., Pham, Q. C., and Nakamura, Y. (2015a). Leveraging cone double description for multi-contact stability of humanoids with applications to statics and dynamics. In *Robotics: Science and Systems*. 22, 52, 64, 78, 85, 99

Caron, S., Pham, Q. C., and Nakamura, Y. (2015b). Stability of surface contacts for humanoid robots: Closed-form formulae of the Contact Wrench Cone for rectangular support areas. In *IEEE International Conference on Robotics and Automation*, pages 5107–5112. 22, 34

Caron, S., Pham, Q. C., and Nakamura, Y. (2017). ZMP support areas for multicontact mobility under frictional constraints. *IEEE Transactions on Robotics*, 33(1):67–80. 22

Carpentier, J., Budhiraja, R., and Mansard, N. (2017). Learning Feasibility Constraints for Multi-contact Locomotion of Legged Robots. In *Robotics: Science and Systems*, volume Porceedings of Robotics Science and Systems, page 9p., Cambridge, MA, United States. 21

Chestnutt, J., Kuffner, J., Nishiwaki, K., and Kagami, S. (2003). Planning biped navigation strategies in complex environments. In *IEEE-RAS International Conference on Humanoid Robots*. 8

Chung, S.-Y. and Khatib, O. (2015). Contact-consistent elastic strips for multi-contact locomotion planning of humanoid robots. In *IEEE International Conference on Robotics and Automation*, pages 6289–6294. 8

Collette, C., Micaelli, A., Andriot, C., and Lemerle, P. (2007). Dynamic balance control of humanoids for multiple grasps and non coplanar frictional contacts. In *IEEE-RAS International Conference on Humanoid Robots*, pages 81–88. 18, 21, 36, 56

Collette, C., Micaelli, A., Andriot, C., and Lemerle, P. (2008). Robust balance optimization control of humanoid robots with multiple non coplanar grasps and frictional contacts. In *IEEE International Conference on Robotics and Automation*, pages 3187–3193. 8

Dai, H., Valenzuela, A., and Tedrake, R. (2014). Whole-body motion planning with centroidal dynamics and full kinematics. In *IEEE-RAS International Conference on Humanoid Robots*, pages 295–302. IEEE. 20, 21

Dandekar, K. and Srinivasan, M. A. (1995). 3 dimensional finite element model of the monkey fingertip for predicting responses of slowly adapting mechanoreceptors. In *American Society of Mechanical Engineers, Bioengineering Division (Publication) BED*, volume 29, pages 257–258. 15

De Lasa, M., Mordatch, I., and Hertzmann, A. (2010). Feature-based locomotion controllers. *ACM Transactions on Graphics*, 29(4):1–10. 20

Defense Advanced Research Projects Agency (2018). About DARPA. 6

Del Prete, A., Romano, F., Natale, L., Metta, G., Sandini, G., and Nori, F. (2014). Prioritized optimal control. In *IEEE International Conference on Robotics and Automation*, pages 2540–2545. IEEE. 18

Del Prete, A., Tonneau, S., and Mansard, N. (2016). Fast algorithms to test robust static equilibrium for legged robots. In *IEEE International Conference on Robotics and Automation*, pages 1601–1607. IEEE. 16, 21

Escande, A., Kheddar, A., and Miossec, S. (2013). Planning contact points for humanoid robots. *Robotics and Autonomous Systems*, 61(5):428–442. 8, 11, 12

Escande, A., Mansard, N., and Wieber, P.-B. (2014). Hierarchical quadratic programming: Fast online humanoid-robot motion generation. *The International Journal of Robotics Research*, 33(7):1006–1028. 17, 18

Farnioli, E., Gabiccini, M., and Bicchi, A. (2015). Optimal contact force distribution for compliant humanoid robots in whole-body loco-manipulation tasks. In *IEEE International Conference on Robotics and Automation*, pages 5675–5681. 9

Featherstone, R. (2014). *Rigid body dynamics algorithms*. Springer. 51, 88

Fernbach, P., Tonneau, S., Stasse, O., Carpentier, J., and Taïx, M. (2020). C-croc: Continuous and convex resolution of centroidal dynamic trajectories for legged robots in multicontact scenarios. *IEEE Transactions on Robotics*, 36(3):676–691. 23

Fernbach, P., Tonneau, S., and Taïx, M. (2018). Croc: Convex resolution of centroidal dynamics trajectories to provide a feasibility criterion for the multi contact planning problem. In *IEEE/RSJ International Conference on Intelligent Robots and Systems*, pages 1–9. 21

Frank, A. A. (1968). *Control Systems for Legged Locmotion Machines*. PhD thesis, University of Southern California, Los Angeles, USA. 6

Fujii, S., Inoue, K., Takubo, T., Mae, Y., and Arai, T. (2008). Ladder climbing control for limb mechanism robot "asterisk". In *IEEE International Conference on Robotics and Automation*, pages 3052–3057. 10

Fukuda, K. et al. (2004). Frequently asked questions in polyhedral computation. *ETH, Zurich, Switzerland*. 85

Garcia-Haro, J. M., Henze, B., Mesesan, G., Martinez, S., and Ott, C. (2019). Integration of dual-Arm manipulation in a passivity based whole-body controller for torque-controlled humanoid robots. In *IEEE-RAS International Conference on Humanoid Robots*, pages 644–650. 8

Garkavi, A. L. (1964). On the Chebyshev center and convex hull of a set. *Uspekhi Matematicheskikh Nauk*, 19(6):139–145. 84

Greenwood, J. and Williamson, J. (1966). Contact of nominally flat surfaces. *Proceedings of the Royal Society A. Mathematical, Physical and Engineering Sciences*, 295(1442):300–319. 61

Harada, K., Kajita, S., Kanehiro, F., Fujiwara, K., Kaneko, K., Yokoi, K., and Hirukawa, H. (2007). Real-time planning of humanoid robot's gait for force-controlled manipulation. *IEEE/ASME Transactions on Mechatronics*, 12(1):53–62. 8

Harada, K., Kajita, S., Kaneko, K., and Hirukawa, H. (2003). Zmp analysis for arm/leg coordination. In *IEEE/RSJ International Conference on Intelligent Robots and Systems*, volume 1, pages 75–81 vol.1. 6

Harada, K., Kajita, S., Kaneko, K., and Hirukawa, H. (2006). Dynamics and balance of a humanoid robot during manipulation tasks. *IEEE Transactions on Robotics*, 22(3):568–575. 22

Harada, K., Kaneko, M., and Tsujii, T. (2000). Rolling-based manipulation for multiple objects. *IEEE Transactions on Robotics and Automation*, 16(5):457–468. 14

Hashimoto, K., Yoshimura, Y., Kondo, H., Lim, H. O., and Takanishi, A. (2011). Realization of quick turn of biped humanoid robot by using slipping motion with both feet. In *IEEE International Conference on Robotics and Automation*, pages 2041–2046. 23

Hauser, K. (2014). Fast interpolation and time-optimization with contact. *The International Journal of Robotics Research*, 33(9):1231–1250. 16

Henze, B., Dietrich, A., Roa, M. A., and Ott, C. (2017). Multi-contact balancing of humanoid robots in confined spaces: Utilizing knee contacts. In *IEEE/RSJ International Conference on Intelligent Robots and Systems*, pages 697–704. 8

Henze, B., Ott, C., and Roa, M. A. (2014). Posture and balance control for humanoid robots in multi-contact scenarios based on Model Predictive Control. In *IEEE International Conference on Intelligent Robots and Systems*, pages 3253–3258. 19, 21, 22

Henze, B., Roa, M. A., and Ott, C. (2016). Passivity-based whole-body balancing for torque-controlled humanoid robots in multi-contact scenarios. *The International Journal of Robotics Research*, 35(12):1522–1543. 19, 20, 24, 25, 26

Herzog, A., Righetti, L., Grimminger, F., Pastor, P., and Schaal, S. (2014). Balancing experiments on a torque-controlled humanoid with hierarchical inverse dynamics. In *IEEE/RSJ International Conference on Intelligent Robots and Systems*, pages 981–988. IEEE. 20

Herzog, A., Schaal, S., and Righetti, L. (2016). Structured contact force optimization for kino-dynamic motion generation. In *IEEE/RSJ International Conference on Intelligent Robots and Systems*, pages 2703–2710. IEEE. 20

Hiraoka, N., Murooka, M., Noda, S., Okada, K., and Inaba, M. (2021). Online generation and control of quasi-static multi-contact motion by pwt jacobian matrix with contact wrench estimation and joint load reduction*. *Advanced Robotics*, 35(1):48–63. 8, 9, 20

Hirukawa, H., Hattori, S., Harada, K., Kajita, S., Kaneko, K., Kanehiro, F., Fujiwara, K., and Morisawa, M. (2006). A universal stability criterion of the foot contact of legged robots - Adios ZMP. *IEEE International Conference on Robotics and Automation*, pages 1976–1983. 64, 85

Hyon, S.-H., Hale, J. G., and Cheng, G. (2007). Full-body compliant human–humanoid interaction: Balancing in the presence of unknown external forces. *IEEE Transactions on Robotics*, 23(5):884–898. 6

Ibanez, A., Bidaud, P., and Padois, V. (2012). Unified preview control for humanoid postural stability and upper-limb interaction adaptation. In *IEEE/RSJ International Conference on Intelligent Robots and Systems*, pages 1801–1808. 22

Iida, H., Hozumi, H., and Nakayama, R. (1989). Development of ladder climbing robot lcr-1. *Journal of Robotics and Mechatronics*, 1(4):311–316. 10

Joh, J. and Lipkin, H. (1991). Lagrangian wrench distribution for cooperating robotic mechanisms. In *IEEE International Conference on Robotics and Automation*, pages 224–229 vol.1. 7

Kajita, S., Asano, F., Moriswa, M., Miura, K., Kaneko, K., Kanehiro, F., and Yokoi, K. (2013). Vertical vibration suppression for a position controlled biped robot. In *IEEE International Conference on Robotics and Automation*, pages 1637–1642. 42

Kajita, S., Kaneko, K., Harada, K., Kanehiro, F., Fujiwara, K., and Hirukawa, H. (2004). Biped walking on a low friction floor. In *IEEE/RSJ International Conference on Intelligent Robots and Systems*, pages 3546–3552. 23

Kajita, S., Morisawa, M., Miura, K., Nakaoka, S., Harada, K., Kaneko, K., Kanehiro, F., and Yokoi, K. (2010). Biped walking stabilization based on linear inverted pendulum tracking. In *IEEE/RSJ International Conference on Intelligent Robots and Systems*, pages 4489–4496. 8, 42

Kanajar, P., Caldwell, D. G., and Kormushev, P. (2017). Climbing over large obstacles with a humanoid robot via multi-contact motion planning. In *IEEE International Symposium on Robot and Human Interactive Communication*, pages 1202–1209. 8, 11, 12

Kanehiro, F., Yoshimi, T., Kajita, S., Morisawa, M., Fujiwara, K., Harada, K., Kaneko, K., Hirukawa, H., and Tomita, F. (2005). Whole body locomotion planning of humanoid robots based on a 3d grid map. In *IEEE International Conference on Robotics and Automation*, pages 1072–1078. 11, 12

Kaneko, K., Kanehiro, F., Kajita, S., Morisawa, M., Fujiwara, K., Harada, K., and Hirukawa, H. (2005). Slip observer for walking on a low friction floor. In *IEEE/RSJ International Conference on Intelligent Robots and Systems*, pages 1457–1463. 23

Kanoun, O., Lamiraux, F., and Wieber, P.-B. (2011). Kinematic control of redundant manipulators: Generalizing the task-priority framework to inequality task. *IEEE Transactions on Robotics*, 27(4):785–792. 17

Keith, F., Wieber, P.-B., Mansard, N., and Kheddar, A. (2011). Analysis of the discontinuities in prioritized tasks-space control under discreet task scheduling operations. In *IEEE/RSJ International Conference on Intelligent Robots and Systems*, pages 3887–3892. IEEE. 18

Khatib, O. (1980). *Commande dynamique dans l'espace opérationnel des robots manipulateurs en présence d'obstacles*. PhD thesis, Institut Supérieur de l'Aéronautique et de l'Espace, Toulouse, France. 7

Kheddar, A., Caron, S., Gergondet, P., Comport, A., Tanguy, A., Ott, C., Henze, B., Mesesan, G., Englsberger, J., Roa, M. A., Wieber, P., Chaumette, F., Spindler, F., Oriolo, G., Lanari, L., Escande, A., Chappellet, K., Kanehiro, F., and Rabaté, P. (2019). Humanoid robots in aircraft manufacturing: The airbus use cases. *IEEE Robotics Automation Magazine*, 26(4):30–45. 8, 9, 25, 26, 51, 70, 73

Kim, D., Lee, J., Ahn, J., Campbell, O., Hwang, H., and Sentis, L. (2018). Computationally-robust and efficient prioritized whole-body controller with contact constraints. In *IEEE/RSJ International Conference on Intelligent Robots and Systems*, pages 1–8. 17

Kim, J. T. and Park, J. H. (2011). Quick change of walking direction of biped robot with foot slip in single-support phase. In *IEEE-RAS International Conference on Humanoid Robots*, pages 339–344. 23

Knitter, W. (1988). The informing vision of the practical: the concepts of character, virtue, vice and privation. *Journal of Curriculum Studies*, 20(6):483–492. 57

Koeda, M. and Sugimoto, D. (2018). Load Gradient Model in Foot Soles for Non-Parallel Shuffling Humanoid Walk. In *AMS 2017 - Asia Modelling Symposium 2017 and 11th International Conference on Mathematical Modelling and Computer Simulation*, pages 71–76. IEEE. 25

Koeda, M., Uda, Y., Sugiyama, S., and Yoshikawa, T. (2011). Shuffle turn and translation of humanoid robots. In *IEEE International Conference on Robotics and Automation*, pages 593–598. 23, 25

Kojima, K., Ishiguro, Y., Sugai, F., Nozawa, S., Kakiuchi, Y., Okada, K., and Inaba, M. (2017). Rotational sliding motion generation for humanoid robot by force distribution in each contact face. *IEEE Robotics and Automation Letters*, 2(4):2088–2095. 23, 25

Kojima, K., Nozawa, S., Okada, K., and Inaba, M. (2015). Shuffle motion for humanoid robot by sole load distribution and foot force control. In *IEEE International Conference on Intelligent Robots and Systems*, pages 2187–2194. 23, 25

Komvopoulos, K. and Choi, D.-H. (1992). Elastic finite element analysis of multi-asperity contacts. *Journal of Tribology*. 15

Koptev, M., Figueroa, N., and Billard, A. (2021). Real-time self-collision avoidance in joint space for humanoid robots. *IEEE Robotics and Automation Letters*, 6(2):1240–1247. 8

Kuffner, J., Nishiwaki, K., Kagami, S., Inaba, M., and Inoue, H. (2001). Footstep planning among obstacles for biped robots. In *IEEE/RSJ International Conference on Intelligent Robots and Systems*, volume 1, pages 500–505 vol.1. 8

Kuffner, J. J., Kagami, S., Nishiwaki, K., Inaba, M., and Inoue, H. (2002). Dynamically-stable motion planning for humanoid robots. *Autonomous Robots*, 12(1):105–118. 8

Kuindersma, S., Permenter, F., and Tedrake, R. (2014). An efficiently solvable quadratic program for stabilizing dynamic locomotion. In *IEEE International Conference on Robotics and Automation*, pages 2589–2594. IEEE. 17

Kumagai, I., Morisawa, M., Benallegue, M., and Kanehiro, F. (2019). Bipedal locomotion planning for a humanoid robot supported by arm contacts based on geometrical feasibility. In *IEEE-RAS International Conference on Humanoid Robots*, pages 132–139. 8

Kumagai, I., Morisawa, M., Hattori, S., Benallegue, M., and Kanehiro, F. (2020). Multi-contact locomotion planning for humanoid robot based on sustainable contact graph with local contact modification. *IEEE Robotics and Automation Letters*, 5(4):6379–6387. 10

Kumagai, I., Murooka, M., Morisawa, M., and Kanehiro, F. (2021). Multi-contact locomotion planning with bilateral contact forces considering kinematics and statics during contact transition. *IEEE Robotics and Automation Letters*, 6(4):6654–6661. 10

Kumar, V. and Waldron, K. (1988). Force distribution in closed kinematic chains. In *IEEE International Conference on Robotics and Automation*, pages 114–119 vol.1. 7

Laurenzi, A., Hoffman, E. M., Polverini, M. P., and Tsagarakis, N. G. (2018). Balancing control through post-optimization of contact forces. In *IEEE-RAS International Conference on Humanoid Robots*, pages 320–326. IEEE. 20

Lee, S.-H. and Goswami, A. (2010). Ground reaction force control at each foot: A momentum-based humanoid balance controller for non-level and non-stationary ground. In *IEEE/RSJ International Conference on Intelligent Robots and Systems*, pages 3157–3162. 19

Lee, Y., Hwang, S., and Park, J. (2016). Balancing of humanoid robot using contact force/moment control by task-oriented whole body control framework. *Autonomous Robots*, 40(3):457–472. 21

Lee, Y., Kim, S., Park, J., Tsagarakis, N., and Lee, J. (2021). A whole-body control framework based on the operational space formulation under inequality constraints via task-oriented optimization. *IEEE Access*, 9:39813–39826. 19

Leidner, D. S. (2019). *Cognitive Reasoning for Compliant Robot Manipulation*. Springer. 23

Lin, Q., Burdick, J., and Rimon, E. (2000). A stiffness-based quality measure for compliant grasps and fixtures. *IEEE Transactions on Robotics and Automation*, 16(6):675–688. 14

Liu, M., Lober, R., and Padois, V. (2016). Whole-body hierarchical motion and force control for humanoid robots. *Autonomous Robots*, 40(3):493–504. 18

Liu, M., Micaelli, A., Evrard, P., Escande, A., and Andriot, C. (2011). Interactive dynamics and balance of a virtual character during manipulation tasks. In *IEEE International Conference on Robotics and Automation*, pages 1676–1682. IEEE. 18

Lu, Z., Aoyama, T., Sekiyama, K., Hasegawa, Y., and Fukuda, T. (2010). Walk-to-brachiate transfer of multi-locomotion robot with error recovery. In *IEEE/RSJ International Conference on Intelligent Robots and Systems*, pages 166–171. 11

Luo, J., Zhang, Y., Hauser, K., Park, H. A., Paldhe, M., Lee, C. S. G., Grey, M., Stilman, M., Oh, J. H., Lee, J., Kim, I., and Oh, P. (2014). Robust ladder-climbing with a humanoid robot with application to the darpa robotics challenge. In *IEEE International Conference on Robotics and Automation*, pages 2792–2798. 10, 11

Lötstedt, P. (1982). Mechanical systems of rigid bodies subject to unilateral constraints. *SIAM Journal on Applied Mathematics*, 42(2):281–296. 14

Macchietto, A., Zordan, V., and Shelton, C. R. (2009). Momentum control for balance. In *ACM SIGGRAPH 2009 Papers*, SIGGRAPH '09, New York, NY, USA. Association for Computing Machinery. 20

Mansard, N., Khatib, O., and Kheddar, A. (2009). A unified approach to integrate unilateral constraints in the stack of tasks. *IEEE Transactions on Robotics*, 25(3):670–685. 17

Mason, S., Rotella, N., Schaal, S., and Righetti, L. (2018). An mpc walking framework with external contact forces. In *IEEE International Conference on Robotics and Automation*, pages 1785–1790. 8

Merkt, W., Ivan, V., and Vijayakumar, S. (2019). Continuous-time collision avoidance for trajectory optimization in dynamic environments. In *IEEE/RSJ International Conference on Intelligent Robots and Systems*, pages 7248–7255. 8

Mirjalili, R., Yousefi-Korna, A., Shirazi, F. A., Nikkhah, A., Nazemi, F., and Khadiv, M. (2018). A whole-body model predictive control scheme including external contact forces and com height variations. In *2018 IEEE-RAS 18th International Conference on Humanoid Robots (Humanoids)*, pages 1–6. 8, 9

Miura, K., Kanehiro, F., Kaneko, K., Kajita, S., and Yokoi, K. (2013). Slip-turn for biped robots. *IEEE Transactions on Robotics*, 29(4):875–887. 23, 25

Modugno, V., Nava, G., Pucci, D., Nori, F., Oriolo, G., and Ivaldi, S. (2017). Safe trajectory optimization for whole-body motion of humanoids. In *IEEE-RAS International Conference on Humanoid Robotics*, pages 763–770. 18

Moore, J. (2021). Varignon's Theorem. [Online; accessed 2021-09-30]. 88

Morisawa, M., Benallegue, M., Cisneros, R., Kumagai, I., Escande, A., Kaneko, K., and Kanehiro, F. (2019). Multi-Contact Stabilization of a Humanoid Robot for Realizing Dynamic Contact Transitions on Non-coplanar Surfaces. In *IEEE International Conference on Intelligent Robots and Systems*. 8, 9

Morisawa, M., Cisneros, R., Benallegue, M., Kumagai, I., Escande, A., and Kanehiro, F. (2018). Online 3D CoM Trajectory Generation for Multi-Contact Locomotion Synchronizing Contact. In *IEEE-RAS International Conference on Humanoid Robots*. 8, 10

Murooka, M., Kumagai, I., Morisawa, M., Kanehiro, F., and Kheddar, A. (2021). Humanoid loco-manipulation planning based on graph search and reachability maps. *IEEE Robotics and Automation Letters*, 6(2):1840–1847. 9, 10

Murooka, M., Noda, S., Nozawa, S., Kakiuchi, Y., Okada, K., and Inaba, M. (2014). Manipulation strategy decision and execution based on strategy proving operation for carrying large and heavy objects. In *IEEE International Conference on Robotics and Automation*, pages 3425–3432. 9, 10

Murooka, M., Nozawa, S., Kakiuchi, Y., Okada, K., and Inaba, M. (2015). Whole-body pushing manipulation with contact posture planning of large and heavy object for humanoid robot. In *IEEE International Conference on Robotics and Automation*, pages 5682–5689. 8

Nakai, H., Kuniyoshi, Y., Inaba, M., and Inoue, H. (2002). Metamorphic robot made of low melting point alloy. In *International Conference on Intelligent Robots and Systems*, volume 2, pages 2025–2030 vol.2. 10

Neunert, M., Stäuble, M., Giftthaler, M., Bellicoso, C. D., Carius, J., Gehring, C., Hutter, M., and Buchli, J. (2018). Whole-body nonlinear model predictive control through contacts for quadrupeds. *IEEE Robotics and Automation Letters*, 3(3):1458–1465. 20

Nishiwaki, K., Yoon, W.-k., and Kagami, S. (2006). Motion control system that realizes physical interaction between robot's hands and environment during walk. In *IEEE-RAS International Conference on Humanoid Robots*, pages 542–547. 9

Noda, S., Murooka, M., Nozawa, S., Kakiuchi, Y., Okada, K., and Inaba, M. (2014). Generating whole-body motion keep away from joint torque, contact force, contact moment limitations enabling steep climbing with a real humanoid robot. In *IEEE International Conference on Robotics and Automation*, pages 1775–1781. 10, 11

Nozawa, S., Kanazawa, M., Kakiuchi, Y., Okada, K., Yoshiike, T., and Inaba, M. (2016). Three-dimensional humanoid motion planning using COM feasible region and its application to ladder climbing tasks. In *IEEE-RAS International Conference on Humanoid Robots*, pages 49–56. 21

Or, Y. and Ames, A. D. (2019). Dynamic walking on slippery surfaces: Demonstrating stable bipedal gaits with planned ground slippage. In *IEEE International Conference on Robotics and Automation*, pages 3705–3711. 23

Orin, D. E., Goswami, A., and Lee, S.-H. (2013). Centroidal dynamics of a humanoid robot. *Autonomous robots*, 35(2):161–176. 20, 21, 78

Orsolino, R., Focchi, M., Caron, S., Raiola, G., Barasuol, V., Caldwell, D. G., and Semini, C. (2020). Feasible region: An actuation-aware extension of the support region. *IEEE Transactions on Robotics*, 36(4):1239–1255. 21

Ott, C., Henze, B., and Lee, D. (2013). Kinesthetic teaching of humanoid motion based on whole-body compliance control with interaction-aware balancing. In *IEEE/RSJ International Conference on Intelligent Robots and Systems*, pages 4615–4621. 22

Ott, C., Roa, M. A., and Hirzinger, G. (2011). Posture and balance control for biped robots based on contact force optimization. In *IEEE-RAS International Conference on Humanoid Robots*, pages 26–33. 19

Padois, V., Ivaldi, S., Babič, J., Mistry, M., Peters, J., and Nori, F. (2017). Whole-body multi-contact motion in humans and humanoids: Advances of the codyco european project. *Robotics and Autonomous Systems*, 90:97–117. Special Issue on New Research Frontiers for Intelligent Autonomous Systems. 21

Pang, J. S. and Trinkle, J. (2000). Stability characterizations of rigid body contact problems with Coulomb friction. *ZAMM Zeitschrift fur Angewandte Mathematik und Mechanik*, 80(10):643–663. 13, 63, 85

Petrič, T. and Žlajpah, L. (2013). Smooth continuous transition between tasks on a kinematic control level: Obstacle avoidance as a control problem. *Robotics and Autonomous Systems*, 61(9):948–959. 18

Pham, H. and Pham, Q. C. (2020). Convex Controller Synthesis for Robot Contact. *IEEE Robotics and Automation Letters*, 5(2):3330–3337. 73

Polverini, M. P., Laurenzi, A., Hoffman, E. M., Ruscelli, F., and Tsagarakis, N. G. (2020). Multi-contact heavy object pushing with a centaur-type humanoid robot: Planning and control for a real demonstrator. *IEEE Robotics and Automation Letters*, 5(2):859–866. 9, 20

Posa, M., Cantu, C., and Tedrake, R. (2014). A direct method for trajectory optimization of rigid bodies through contact. *The International Journal of Robotics Research*, 33(1):69–81. 20, 23

Posa, M., Kuindersma, S., and Tedrake, R. (2016). Optimization and stabilization of trajectories for constrained dynamical systems. In *IEEE International Conference on Robotics and Automation*, pages 1366–1373. IEEE. 20

Quiroz-Omaña, J. J. and Adorno, B. V. (2019). Whole-body control with (self) collision avoidance using vector field inequalities. *IEEE Robotics and Automation Letters*, 4(4):4048–4053. 8

Raibert, M. H. and Craig, J. J. (1981). Hybrid Position/Force Control of Manipulators. *Journal of Dynamic Systems, Measurement, and Control*, 103(2):126–133. 7

Reher, J. P., Hereid, A., Kolathaya, S., Hubicki, C. M., and Ames, A. D. (2020). Algorithmic foundations of realizing multi-contact locomotion on the humanoid robot DURUS. *Springer*, pages 400–415. 8

Righetti, L., Buchli, J., Mistry, M., Kalakrishnan, M., and Schaal, S. (2013). Optimal distribution of contact forces with inverse-dynamics control. *The International Journal of Robotics Research*, 32(3):280–298. 17, 18

Ruscelli, F., Polverini, M. P., Laurenzi, A., Hoffman, E. M., and Tsagarakis, N. G. (2020). A multi-contact motion planning and control strategy for physical interaction tasks using a humanoid robot. In *IEEE/RSJ International Conference on Intelligent Robots and Systems*, pages 3869–3876. 8, 20, 21

Saab, L., Mansard, N., Keith, F., Fourquet, J.-Y., and Souères, P. (2011). Generation of dynamic motion for anthropomorphic systems under prioritized equality and inequality constraints. In *IEEE International Conference on Robotics and Automation*, pages 1091–1096. IEEE. 18

Saab, L., Ramos, O. E., Keith, F., Mansard, N., Souères, P., and Fourquet, J.-Y. (2013). Dynamic whole-body motion generation under rigid contacts and other unilateral constraints. *IEEE Transactions on Robotics*, 29(2):346–362. 17, 20

Salini, J., Barthélemy, S., and Bidaud, P. (2010). Lqp-based controller design for humanoid whole-body motion. In Lenarcic, J. and Stanisic, M. M., editors, *Advances in Robot Kinematics: Motion in Man and Machine*, pages 177–184, Dordrecht. Springer Netherlands. 18

Samadi, S., Caron, S., Tanguy, A., and Kheddar, A. (2020). Balance of humanoid robots in a mix of fixed and sliding multi-contact scenarios. In *IEEE International Conference on Robotics and Automation*, pages 6590–6596. 24, 53, 54, 56, 79, 84

Samadi, S., Roux, J., Tanguy, A., Caron, S., and Kheddar, A. (2021). Humanoid control under interchangeable fixed and sliding unilateral contacts. *IEEE Robotics and Automation Letters*, 6(2):4032–4039. 7, 79, 84, 87

Samson, C. and Espiau, B. (1990). Application of the task-function approach to sensor-based control of robot manipulators. *IFAC Proceedings Volumes*, 23(8, Part 5):269–274. 11th IFAC World Congress on Automatic Control, Tallinn, 1990 - Volume 5, Tallinn, Finland. 17

Senoo, T. and Ishikawa, M. (2017). Analysis of sliding behavior of a biped robot in centroid acceleration space. *Robotica*, 35(3):636–653. 52

Sentis, L. (2010). Compliant control of whole-body multi-contact behaviors in humanoid robots. *IEEE Transactions on Robotics*, 26(3):29–66. 7, 17, 21, 53

Sherikov, A., Dimitrov, D., and Wieber, P.-B. (2015). Balancing a humanoid robot with a prioritized contact force distribution. In *International Conference on Humanoid Robots*, pages 223–228. IEEE. 18

Shi, J., Woodruff, J. Z., Umbanhowar, P. B., and Lynch, K. M. (2017). Dynamic In-Hand Sliding Manipulation. *IEEE Transactions on Robotics*, 33(4):778–795. 12

Siciliano, B. and Slotine, J.-J. (1991). A general framework for managing multiple tasks in highly redundant robotic systems. In *International Conference on Advanced Robotics' Robots in Unstructured Environments*, pages 1211–1216. IEEE. 17

Sinha, P. and Abel, J. (1992). A contact stress model for multifingered grasps of rough objects. *IEEE Transactions on Robotics and Automation*, 8(1):7–22. 7

Stephens, B. J. and Atkeson, C. G. (2010). Dynamic balance force control for compliant humanoid robots. In *IEEE/RSJ international conference on intelligent robots and systems*, pages 1248–1255. IEEE. 19

Stilman, M., Nishiwaki, K., and Kagami, S. (2008). Humanoid teleoperation for whole body manipulation. In *IEEE International Conference on Robotics and Automation*, pages 3175–3180. 9

Takasugi, N., Kojima, K., Nozawa, S., Kakiuchi, Y., Okada, K., and Inaba, M. (2016). Real-time skating motion control of humanoid robots for acceleration and balancing. In *2016 IEEE/RSJ International Conference on Intelligent Robots and Systems (IROS)*, pages 1356–1363. 25

Takasugi, N., Kojima, K., Nozawa, S., Sugai, F., Yohei, K., Okada, K., and Inaba, M. (2019). Extended three-dimensional walking and skating motion generation for multiple noncoplanar contacts with anisotropic friction: Application to walk and skateboard and roller skate. *IEEE Robotics and Automation Letters*, 4(1):9–16. 25

Tenek, L. T. and Argyris, J. (1997). *Finite element analysis for composite structures*, volume 59. Springer Science & Business Media. 15

Tonneau, S., Del Prete, A., Pettré, J., Park, C., Manocha, D., and Mansard, N. (2018). An efficient acyclic contact planner for multiped robots. *IEEE Transactions on Robotics*, 34(3):586–601. 23

Trinkle, J. C., Pang, J. S., Sudarsky, S., and Lo, G. (1997). On dynamic multi-rigid-body contact problems with coulomb friction. *ZAMM Zeitschrift fur Angewandte Mathematik und Mechanik*, 77(4):267–279. 24

Vahrenkamp, N., Berenson, D., Asfour, T., Kuffner, J., and Dillmann, R. (2009). Humanoid motion planning for dual-arm manipulation and re-grasping tasks. In *IEEE/RSJ International Conference on Intelligent Robots and Systems*, pages 2464–2470. 24, 26

Vaillant, J., Kheddar, A., Audren, H., Keith, F., Brossette, S., Escande, A., Bouyarmane, K., Kaneko, K., Morisawa, M., Gergondet, P., Yoshida, E., Kajita, S., and Kanehiro, F. (2016). Multi-contact vertical ladder climbing with an HRP-2 humanoid. *Autonomous Robots*, 40(3):561–580. 8, 10, 11

Vázquez, J. A. and Velasco-Villa, M. (2013). Experimental estimation of slipping in the supporting point of a biped robot. *Journal of Applied Research and Technology*, 11(3):348–359. 23

Verrelst, B., Stasse, O., Yokoi, K., and Vanderborght, B. (2006). Dynamically stepping over obstacles by the humanoid robot hrp-2. In *IEEE-RAS International Conference on Humanoid Robots*, pages 117–123. 11

Vukobratović, M. and Borovac, B. (2004). Zero-Moment Point — Thirty Five Years of Its Life. *International Journal of Humanoid Robotics*, 01(01):157–173. 6

Wang, Y.-T., Kumar, R. V., and Abel, J. (1991). Dynamics of rigid bodies undergoing multiple frictional contacts. *Technical Reports (CIS)*, page 424. 14

Wensing, P. M., Bin Hammam, G., Dariush, B., and Orin, D. E. (2013). Optimizing foot centers of pressure through force distribution in a humanoid robot. *International Journal of Humanoid Robotics*, 10(03):1350027. 18

Werner, A., Henze, B., Rodriguez, D. A., Gabaret, J., Porges, O., and Roa, M. A. (2016). Multi-contact planning and control for a torque-controlled humanoid robot. In *IEEE/RSJ International Conference on Intelligent Robots and Systems*, pages 5708–5715. IEEE. 20

Wieber, P. B. (2006). Trajectory free linear model predictive control for stable walking in the presence of strong perturbations. In *IEEE-RAS International Conference on Humanoid Robots*, pages 137–142. 52

Winkler, A. W., Bellicoso, C. D., Hutter, M., and Buchli, J. (2018). Gait and trajectory optimization for legged systems through phase-based end-effector parameterization. *IEEE Robotics and Automation Letters*, 3(3):1560–1567. 20

Xydas, N., Bhagavat, M., and Kao, I. (2000). Study of soft-finger contact mechanics using finite elements analysis and experiments. In *IEEE International Conference on Robotics and Automation*, volume 3, pages 2179–2184. IEEE. 15

Yamane, K., Kuffner, J. J., and Hodgins, J. K. (2004). Synthesizing animations of human manipulation tasks. In *ACM SIGGRAPH 2004 Papers*, SIGGRAPH '04, page 532–539, New York, NY, USA. Association for Computing Machinery. 8

Yokoi, K., Yoshida, E., and Sanada, H. (2009). Unified motion planning of passing under obstacles with humanoid robots. In *IEEE International Conference on Robotics and Automation*, pages 1185–1190. 11

Yoneda, H., Sekiyama, K., Hasegawa, Y., and Fukuda, T. (2008). Vertical ladder climbing motion with posture control for multi-locomotion robot. In *IEEE/RSJ International Conference on Intelligent Robots and Systems*, pages 3579–3584. 10

Yoshida, E., Esteves, C., Belousov, I., Laumond, J.-P., Sakaguchi, T., and Yokoi, K. (2008). Planning 3-d collision-free dynamic robotic motion through iterative reshaping. *IEEE Transactions on Robotics*, 24(5):1186–1198. 8

Yoshida, E., Poirier, M., Laumond, J. P., Kanoun, O., Lamiraux, F., Alami, R., and Yokoi, K. (2010). Pivoting based manipulation by a humanoid robot. *Autonomous Robots*, 28(1):77–88. 9

Yun, X. (1991). Coordination of two-arm pushing. In *IEEE International Conference on Robotics and Automation*, pages 182–187 vol.1. 7

Zhang, Y., Luo, J., Hauser, K., Ellenberg, R., Oh, P., Park, H. A., Paldhe, M., and Lee, C. G. (2013). Motion planning of ladder climbing for humanoid robots. In *IEEE Conference on Technologies for Practical Robot Applications*, pages 1–6. 10

Zheng, Y. F. and S. Luh, J. Y. (1986). Joint torques for control of two coordinate moving robots. In *IEEE International Conference on Robotics and Automation*, pages 1375–1380. 7

Zhou, Q., Yu, Z., Zhang, S., Chen, X., Qin, M., Zhang, W., and Huang, Q. (2018). Simultaneous prevention of rotational and translational slip for a humanoid robot. *Applied Sciences (Switzerland)*, 8(9). 23